Intravascular Ultrasound and Magnetic Resonance Imaging of Atherosclerosis and Assessment of Endothelial Function

Lachlan Frost

Discipline of Medicine, School of Medicine

The University of Adelaide

&

Cardiovascular Research Centre

Royal Adelaide Hospital

April 2015

Submitted in the total fulfilment of the requirements

for the degree of Doctor of Philosophy

THESIS DECLARATION

I certify that this work contains no material which has been accepted for the award of any other degree or diploma in any university or other tertiary institution and, to the best of my knowledge and belief, contains no material previously published or written by another person, except where due reference has been made in the text. In addition, I certify that no part of this work will, in the future, be used in a submission for any other degree or diploma in any university or other tertiary institution without the prior approval of the University of Adelaide and where applicable, any partner institution responsible for the joint-award of this degree.

I give consent to this copy of my thesis when deposited in the University Library, being made available for loan and photocopying, subject to the provisions of the Copyright Act 1968.

I also give permission for the digital version of my thesis to be made available on the web, via the University's digital research repository, the Library Search and also through web search engines, unless permission has been granted by the University to restrict access for a period of time.

Signed,

Lachlan Frost

University of Adelaide

THESIS RELATED ABSTRACTS

Frost L, Richardson J, Carbone A, Puri R, Nelson A, Sidhartha S, Worthley M, Worthley S. Geometric Accuracy of Mechanical and Phased-Array Intravascular Ultrasound Catheters: A Phantom Study. *60th Scientific Sessions of the Cardiac Society of Australia and New Zealand.* Brisbane 2012. http://dx.doi.org/10.1016/j.hlc.2012.05.510

Frost L, Richardson J, Carbone A, Bertaso A, Puri R, Nelson A, Sidhartha S, Worthley M, Worthley S. Rabbit Aortic Vasodilation Assessment by 1.5T Magnetic Resonance Imaging and Intravascular Ultrasound. *60th Scientific Sessions of the Cardiac Society of Australia and New Zealand*. Brisbane 2012. http://dx.doi.org/10.1016/j.hlc.2012.05.587

Frost L, Richardson J, Carbone A, Worthley M, Worthley S. Progressive Endothelial Dysfunction is Related to Plaque Burden in an Experimental Model of Atherosclerosis. *University of Adelaide, Faculty of Health Science Postgraduate Research Conference* (2013).

Sidharta S, Puri R, **Frost L**, Kataoka Y, Carbone A, Willoughby S, Nelson A, Nicholls S, Worthley S, Worthley M. The Impact of Lumen Size and Microvascular Resistance on Fourier-Domain Optical Coherence Tomography (FD-OCT) Coronary Measurements. *International Journal of Cardiology*. (2014) 174:210-211

Frost L, Carbone A, Worthley M, Worthely S. In-vivo and In-vitro Variability in Cross Sectional Measurements with IVUS Catheters. *University of Adelaide, Faculty of Health Science Postgraduate Research Conference* (2014).

TABLE OF CONTENTS

ACKNOWLEDGEMENTS

I am sincerely grateful to the following people for their support and assistance as this thesis would not have been possible without their combined efforts.

Firstly, I would like to acknowledge my supervisor Professor Stephen Worthley for allowing me the opportunity to undertake this research. I would also like to acknowledge my co-supervisors, Associate Professor Matthew Worthley and Dr Karen Teo, for their contributions in the production of this thesis.

I would also like to acknowledge the Florey Medical Research Foundation for the generous provision of a scholarship which has enabled me to undertake this work.

I must thank the staff at Large Animal Research and Imaging Facility (LARIF), now known as the Preclinical, Imaging and Research Laboratories (PIRL), for providing an accommodating, nurturing and professional environment in which to conduct this study. In particular, I would like to convey my deepest gratitude to Loren Matthews, Briony Overall and Dr Tim Kuchel for their invaluable advice and assistance over the years.

I would also like to thank Dr James Richardson for contributing his time and knowledge in refining the rabbit IVUS procedure, Kerry Williams for her expertise in performing the MRI scans for this study, Jim Manavis and Dr John Finnie for their expert assistance in providing histological preparations and interpretations for the study.

In particular, I must acknowledge Angelo Carbone who is both colleague and friend. His steadfast support as well as technical assistance during every MRI scan and IVUS procedure has been immeasurable. Without his help, this thesis would not have been possible.

To my parents Malcolm and Ros. I would like to thank them for their unwavering love and support throughout my life. Above all I would like to thank my beautiful wife Joanne for her constant love and support.

COMMON ABBREVIATIONS

ACh	Acetylcholine
CAD	Coronary Artery Disease
CSA	Cross Sectional Area
CVD	Cardiovascular Disease
ECG	Electrocardiogram
ED	End Diastole
EEM	External Elastic Membrane
eNOS	Endothelial Nitric Oxide Synthase
FLASH	Fast Low Angle Shot
FOV	Field of View
GTN	Glyceryl Trinitrate
ICC	Intra Class Coefficient
IVUS	Intravascular Ultrasound
MHz	Megahertz
MIP	Maximum Intensity Projection
MRI/MR	Magnetic Resonance Imaging/Magnetic Resonance
NC	Necrotic Core
NO	Nitric Oxide

NURD	Non Uniform Rotational Distortion
NZW	New Zealand White
PAV	Percentage Atheroma Volume
PDW	Proton Density Weighted
RF	Radio Frequency
ROI	Region of Interest
SNR	Signal to Noise Ration
T	Tesla
TCFA	Thin-Cap Fibroatheroma
TM	Tissue Map
TOF	Time of Flight
VH	Virtual Histology
VSM	Vascular Smooth Muscle
VWA	Vessel Wall Area

THESIS SYNOPSIS

In this thesis we aimed to investigate the application of IVUS and MRI in assessing plaque and endothelial function in the experimental rabbit model of atherosclerosis.

The first experimental chapter focussed on validating the accuracy and reproducibility of mechanical and phased-array IVUS catheter designs in an in-vivo and ex-vivo setting.

The second experimental chapter sought to investigate the plaque characterisation technologies of iMAP and VH-IVUS. This was the first time that the two systems had been compared head to head in the experimental rabbit model. The results provided significant and systematic variability in plaque composition analysis with both systems.

The third experimental chapter describes an in-vivo investigation between serial endothelial function and vascular remodelling. We have documented that progressive endothelial dysfunction occurs with increasing plaque burden and observed that vascular remodelling in the rabbit experimental model occurs in a way analogous to clinical positive remodelling.

In the fourth experimental chapter we described a novel MRI application for the assessment of endothelial function. The MRI endothelial function results were compared against those obtained using IVUS. We have shown MRI to be a viable non-invasive modality for assessing luminal CSA changes in very small calibre vessels in response to vasoactive drugs.

The final experimental chapter describes the comparison between MRI and IVUS serial quantifying plaque burden. We concluded that MRI is a feasible non-invasive alternative for imaging atherosclerosis in the experimental rabbit model.

Chapter 1:

INTRODUCTION

TABLE OF CONTENTS

BACKGROUND

Atherosclerosis is the main underlying contributor to cardiovascular disease, a condition that remains the leading cause of death and disability in Australia, responsible for 35% of all deaths in 2008[1]. Atherosclerotic plaque rupture and subsequent thrombosis is responsible for 75% of fatal acute myocardial infarctions and sudden cardiac death [2,3] The accurate identification and management of atherosclerotic lesions prior to causing ACS remains a significant challenge. The inability of coronary angiography to image the vessel wall has led to the development of technologies such as intravascular ultrasound and the application of MRI. An accurate in-vivo identification of high risk or vulnerable plaque would therefore allow early management strategies to be implemented to prevent future coronary events.

Atherosclerosis

Atherosclerosis is a progressive, diffuse systemic disease process that is the result of a complex interaction between blood elements, disturbed blood flow, and vessel wall abnormality, involving several pathological processes: inflammation, with increased endothelial permeability, endothelial activation, leukocyte and smooth muscle cell proliferation, lipid accumulation, necrosis and calcification[4,5]. It is now largely considered as a chronic inflammatory disease that may eventually lead to plaque rupture, thrombosis and acute myocardial infarction or ischaemic stroke[6,7].

Atherosclerotic lesions occur in large and medium-sized elastic and muscular arteries. Atherosclerosis process begins in early childhood[8] and progresses slowly throughout life. It is important to note that the most extensive and detailed knowledge of the natural history of atherosclerosis is the result of human autopsy studies with additional data gathered from atherectomy of coronary arteries and endarterectomy of carotid arteries.

The first observation of this disease process is the adaptive intimal thickening (AHA* Type I) due to smooth muscle cell (SMC) proliferation; this is thought to be a physiological response to haemodynamic stress[9]. This non-atherosclerotic lesion is only visible microscopically and consists of isolated groups of macrophages and monocytes within the sub-endothelial space.

Intimal thickening can progress to a fatty streak or xanthoma (AHA Type II) which is the further accumulation of cholesterol engorged macrophages called foam cells with some T-Cells and is macroscopically visible and is raised[9]. Fatty streaks are asymptomatic and are prevalent, being found in 85% of 21-39 year olds[10]. The

formation of fatty streak lesion is a reversible process; however progression of disease is associated with the appearance of extracellular lipid forming a more pronounced intimal layer, known as pathologic intimal thickening (PIT, AHA Type III). PIT is a progressive lesion characterised by layers of SMC in a proteoglycan extracellular matrix near the lumen with an underlying lipid pool. Importantly there is evidence of macrophage infiltration near the lumen[11]. PIT is the precursor lesion to the fibroatheroma.

The Fibroatheroma (AHA Type IV) lesion consists of an acellular necrotic core, which is different to the lipid pool of the PIT due to the presence of cellular debris and no matrix. The necrotic core is surrounded by an overlying layer of fibrous tissue composed of collagen, proteoglycan and intersperse SMC. This fibrous cap is subject to thinning, resulting in the thin-cap fibroatheroma (TCFA) or vulnerable plaque.

*American Heart Association: Coronary plaque classification[12].

Vulnerable plaque

A “vulnerable” plaque is an atherosclerotic plaque that has a high short-term risk of rupture causing a cardiac event. The concept of a vulnerable plaque has constantly been modified since it was first postulated in 1992 by Muller et al[13], initially it was introduced as an attempt to understand which lesions are likely to rupture. Libby[14] adapted this idea to include morphology, characterising the vulnerable lesion as being composed of a lipid rich core with many lipid laden macrophages and monocytes centrally located in an eccentric plaque with a thin friable fibrous cap. Burke et al[15] further adapted the classification of the thin cap as being <65µm thick and infiltrated with macrophages. The cap thickness of <65µm was postulated as a marker of vulnerability from their autopsy studies of men with CVD that had suddenly died, out of the 41 hearts that had acute thrombosis due to rupture the mean cap thickness of culprit lesions was 23±19 µm and 95% had a cap thickness of <65µm.

Currently vulnerable plaques are referred to as thin-capped fibro-atheroma (TCFA) have a lipid-rich core with an overlying thin fibrous cap (<65µm)[16]. These lesions are associated with positive remodelling[17], typically eccentric and mildly stenosed, the average degree of stenosis in culprit lesions is less than 50%[18-20].

THE ENDOTHELIUM

The endothelium is a monolayer lining of cells on the luminal surface of the vasculature. It influences vasomotion and thereby haemodynamics by regulating the activity of the underlying vascular smooth muscle (VSM). The endothelium responds to changes in blood pressure, flow, oxygen tension and metabolites by releasing vasodilators including nitric oxide and prostaglandins and vasoconstrictors such as endothelin-1.

The importance of the endothelium as a regulator of smooth muscle was realised in a series of experiments by Furchgott and Zawadzki[21,22]. They first observed that acetylcholine (ACh) a known in-vivo vasodilator, caused constriction in some preparations of isolated rabbit aortic strips. They demonstrated that gentle rubbing of the intimal surface whilst preparing the strips resulted in a loss of the relaxation response to ACh. This was the result of the mechanical removal of the endothelial cells as the relaxation response was preserved when care was taken not to rub the intimal surface.

In a series of ‘sandwich’ experiments they demonstrated that pre-constricted strips without endothelium could be made to relax in response to ACh when an additional endothelial-intact strip was mounted in the same bath with the endothelial surface placed on the endothelial-free surface of the initial strip.

They hypothesised that ACh was acting on muscarinic receptors on endothelial cells stimulating them to release a non-prostanoid substance that diffuses to the smooth muscle layer causing relaxation. They termed the substance endothelial-derived relaxing factor (EDRF)[23]. It was later elucidated that EDRF was in fact the diffusible membrane permeant gas Nitric Oxide (NO)[24].

The normal endothelium is responsible for vascular haemostasis, the control vascular relaxation and contraction, thrombogenesis and fibrinolysis, platelet activation and inhibition. The endothelium also exerts vasoprotective effects, vasodilatation, suppression of smooth muscle cell growth and inhibition of inflammatory responses[25]. These processes are largely mediated by the endothelium derived nitric oxide (NO).[26]

NO is synthesised from L-Arginine by the enzyme endothelial nitric oxide synthase (eNOS) in the presence of cofactors such as Tetrahydrobiopterin (BH_4) in the endothelium where it is constitutively expressed[27]. NO diffuses to the vascular smooth muscle cells activating guanylate cyclase causing cGMP mediated relaxation and subsequent vasodilatation. There is evidence of reduced expression of eNOS in carotid artery atherosclerosis[28].

Endothelial Dysfunction

Endothelial dysfunction is a characteristic feature of patients at risk of developing coronary atherosclerosis. Endothelial dysfunction results in increased endothelial permeability, platelet aggregation, leukocyte adhesion and cytokine production[25]. Endothelial dysfunction is associated with a decreased production or bioavailability of NO and therefore the impairment of NO-mediated vasomotor and anti-thrombotic effects[29]. Endothelial dysfunction is a systemic process that has been shown to be an independent predictor of major cardiac events[30].

Endothelial dysfunction is considered to be a key factor in the initiation and development of atherosclerosis. Initial clinical studies by Ludmer et al. [31] had provided mechanistic associations between endothelial dysfunction and atherogenesis. Endothelial dysfunction is assumed to equate to endothelial activation and is present in the preclinical stage of atherosclerosis and therefore appears to be an early and reliable marker for the presence of atherogenic risk factors[32 33].

Recent studies have shown that endothelial dysfunction may be reversible in coronary arteries in response to novel treatments such as cholesterol lowering therapies and angiotensin-converting enzyme inhibitors[34].

INVASIVE IMAGING OF ATHEROSCLEROSIS

Angiography

Contrast angiography has remained the most common diagnostic method of coronary imaging for the past 50 years despite its many problems[42]. Angiography can only detect a 2D silhouette (two surfaces) of the contrast filled lumen. It describes lesion severity in terms of per cent reduction of luminal diameter within the lesion compared to a disease free segment. However atherosclerosis is a diffuse disease with no truly normal segment, an IVUS study has shown that out of 884 "normal" angiographic reference segments only 60 (6.8%) were truly disease free [43]. Angiography is also confounded by the process of positive remodelling, where the external elastic membrane expands to prevent luminal loss[44], resulting in significant underestimation of coronary atherosclerosis during the early stage of CAD[45]. The assessment of CAD by angiography does not predict the severity of atherosclerosis in terms of clinical outcome [46] or vessel physiology[47]. Coronary angiography is subject to significant intraobserver and interobserver variability, raising the issue regarding its accuracy and reproducibility in assessing the extent of coronary artery disease[48-51]. In fact, major discrepancies between angiographic visual estimation of lesion severity and post mortem examination had been reported previously[48,52,53].

Intravascular Ultrasound

Intravascular ultrasound (IVUS) is an imaging modality that provides high resolution, cross-sectional topographic images of the vessel lumen and wall.

In 1971 Bom et al developed the first catheter based technology that provided real-time intra-cardiac imaging[54]. They developed a 32 element phased-array ultrasound transducers on a 9Fr catheter that could be advanced within the cardiac chambers demonstrating that ultrasound imaging could be used to produce high-resolution images of cardiac structures[36]. This technology was further advanced in 1988 by Yock et al with the miniaturisation of a single-element system that enabled transducer placement within coronary arteries[55]. Technological advances including further reduction in ultrasound transducer size (0.87-1.17mm), increased core frequencies (30-45 MHz) and low profile catheters have resulted in the ability to generate high resolution, intravascular ultrasound images of the coronary arteries.

Early clinical use of IVUS involved facilitating percutaneous coronary interventions (PCI)[56]. IVUS has been utilised in the guidance and optimal placement of stents[57], improving clinical outcomes[58,59]. Serial IVUS studies have been utilised to evaluate new intracoronary devices[60]. In addition to its clinical usefulness IVUS has proven itself as an effective tool for researching the natural history of atherosclerosis[61,62].

Basic principles of Intravascular Ultrasound

Ultrasonic signals are generated when an electric current is applied to a piezoelectric transducer causing rapid expansion and contraction producing sound waves. There are two distinct IVUS catheter designs; the mechanical single element rotating system and the electronic phased array system. The mechanical system rotates a single transducer on a driveshaft at 1800rpm; this design is available commercially as the 40MHz iCross or Atlantis SR Pro catheters (Boston Scientific, Santa Clara, California) and the Revolution 45MHz catheter (Volcano Therapeutics, Rancho Cordova, California). In comparison, the phased array system uses 64 stationary transducers that are sequentially activated; this is available commercially as the 20MHz Eagle Eye catheter (Volcano Therapeutics, Rancho Cordova, California).

When an ultrasound wave meets a tissue boundary it is either partially reflected or transmitted. The degree of reflection depends on the difference in the acoustic impedance of the two tissues[63]. The returning ultrasound signal in turn acts on the transducer causing it to expand and contract producing an electric current. The flux from the returning signal and therefore current is interpreted by the console as a radiofrequency signal. Greyscale images are generated from analysis of the amplitude of this radiofrequency signal. Visual interpretation of these images allow for quantification of individual plaque components as the amplitude within an overall signal varies according to the reflected tissue characteristics; lipidic lesions appear hypoechoic, fibromuscular as low intensity echoes and calcified tissue as relatively echogenic[63]. However some components have similar echo reflections, hence a dense fibrotic area may look analogous to a calcified region therefore limiting interpretation. Though analysis of IVUS images has been shown to

correlate well with histology[64] it is highly dependent on the experience of the interpreter[65]. Generally IVUS transducers (20-40 MHz), have an axial resolution of approximately 150-200μm and lateral resolution of 200-250μm with >5mm depth of penetration[66].

IVUS catheter designs

There are two distinct IVUS catheter designs that are commercially available; the mechanical single element rotating system and the electronic phased array system. The mechanical system rotates a single transducer on a driveshaft at 1800rpm. The mechanical catheters utilise a transducer with a core frequency between 30-50MHz. This design is available commercially as the 40MHz iCross or Atlantis SR Pro catheters (Boston Scientific, Santa Clara, California) and the Revolution 45MHz catheter (Volcano Therapeutics, Rancho Cordova, California). The imaging core is fixed to the driveshaft and is housed within a telescopic section which is filled with saline, when a pullback is performed the core is retracted within the housing avoiding any friction with the vessel wall. In comparison, the phased array system uses 64 stationary transducers that are sequentially activated; this is available commercially as the 20MHz Eagle Eye Gold/Platinum catheter (Volcano Therapeutics, Rancho Cordova, California).

Mechanical transducers have a higher resolution due to the increased frequency (smaller wavelength) and increased acoustic power as the mechanical transducer transmits all energy in the same direction producing greater tissue penetration this may improve resolution but increases signal noise.

Mechanical catheters are subject to non-uniform rotational distortion (NURD) resulting from an uneven rotation of the driveshaft when the catheter has acute bends or when imaging tortuous vessels[67]. Phased array catheters transmits its energy in multiple directions,

Emerging designs such as micro-motor catheters have the benefits of mechanical transducer such as having a single element with greater acoustic power and resolution but without the limitations inherent to utilising a driveshaft such as NURD and guidewire artefact[68,69]. Micro-motor catheters are not currently available commercially.

Principles of tissue characterisation systems

To counter the limitations of accurate visual analysis of grey scale IVUS images, radiofrequency-based tissue characterisation was developed. This technique employs specific methods of post-processing analysis of the radiofrequency signal in order to estimate plaque composition. Three platforms have been developed and are commercially available through Virtual Histology-IVUS (Volcano Therapeutics, Rancho Cordova, California), iMap (Boston Scientific, Santa Clara, California) and Integrated Backscatter-IVUS (YD Co., Nara, Japan). Although all three systems have been validated, the VH-IVUS system is the most widely distributed[70].

Tissue characterisation is based on the concept that the differing properties of plaque constituents will alter the spectrum of the radiofrequency signal, allowing for in-vivo plaque analysis. Each system assesses different spectral parameters including y-intercept, minimum/maximum power, mid-band fit, frequency at minimum/maximum power and slope using different approaches[71]. These systems present the information as a two-dimensional colour coded “tissue-map” providing more information than isolated interpretation of unprocessed images.

Virtual Histology

Virtual Histology (VH-IVUS) was the first commercially available radiofrequency (RF) based tissue characterisation platform. At present VH-IVUS is only available with the phased-array 20MHz Eagle Eye catheter and the s5/s5i imaging systems (Volcano Therapeutics, Rancho Cordova, California). The classification tree for the 45MHz Revolution catheter (Volcano Therapeutics, Rancho Cordova, California) is not currently available for commercial use.

The proprietary algorithm uses autoregressive analysis of the radiofrequency signal to quantify individual plaque components[72]. It was developed using explanted coronary arteries obtained at autopsy and RF data was acquired from sections homologous for particular plaque components (fibrous, fibrolipidic, necrotic and calcified)[71]. Autoregressive modelling was applied to the raw RF data producing a power spectrum which can be allocated using a statistical classification tree into one of the four plaque components[73,74]. Therefore, when confronted with an unknown sample, VH-IVUS will classify the constituent to its closest match and generate a colour coded "tissue map" for specific plaque components; fibrous (green), fibrolipidic (green-yellow), necrotic (red) and calcified (white). The VH-IVUS system has been shown to have sensitivities and specificities ranging from 72–99% [72,75,76] with high predictive accuracy; 93.4% fibrous, 94.6% fibrolipidic, 95.1% necrotic and 96.8% dense calcium in ex-vivo coronary arteries[76]. The system has also been validated in atherectomy samples[77] and experimental models of atherosclerosis[78,79].

The VH-IVUS systems are gated to the R-wave of the electrocardiogram (ECG) signal and will not perform VH analysis unless the data is acquired with an ECG signal. Though ECG-gating has been shown to be beneficial for accurate volumetric analysis[80] it may introduce a source of error in serial imaging studies where co-registration of VH-IVUS images is crucial. This limitation can be overcome by using an ECG simulator to provide a uniform rate during pullback, with the number of VH-IVUS frames acquired directly proportional to the rate selected.

Notably, the VH-IVUS system has been used in the PROSPECT (Providing Regional Observations to Study Predictors of Events in the Coronary Tree) study[61]. The PROSPECT study was the first clinical prospective study to examine the natural history of atherosclerosis in the acute coronary syndrome patients. Investigators observed a significant association between the VH-IVUS derived plaque characteristics and the development of future coronary events, although this was not significantly greater than more standard assessment and quantification of plaque volume via grey scale IVUS. They also identified that culprit plaques become voluminous before causing an event in contrast to the current concept that mildly stenotic plaques cause disruption. Comparable findings were also noted in the VIVA (Virtual Histology in Vulnerable Atherosclerosis) study[81].

iMap

The iMap (Boston Scientific, Santa Clara, California) system is the latest commercially available RF-based tissue characterisation platform. Utilising a spectral similarity approach, iMap converts RF data into a frequency spectrum and compares this against a histology-derived database in order to characterise the tissue. It then applies pattern recognition analysis obtained by fast-fourier transformation. This approach uses the full RF spectrum (0-100MHz) which involves more calculations than VH-IVUS (which uses reduced/summarised data), potentially enhancing the probability of correct classification of plaque constituents[82].

In comparison to VH-IVUS, iMap applies a different colour tissue map to classify fibrotic (light green), lipidic (yellow), necrotic (pink) and calcified (blue) plaque[83]. Recent ex-vivo validation of saline-infused human coronary arteries at autopsy demonstrated predictive accuracies of 97% necrotic, 98% lipidic, 95% fibrotic and 98% calcified[82]. Unlike VH-IVUS, iMap analysis does not require ECG-gating and acquires data continuously, with RF analysis on every fourth frame, thereby providing more detailed information on plaque composition. The iMap system does not assume any intima media area when performing analysis, in contrast to VH-IVUS which imposes a medial layer (<250μm). This appears as a gray band positioned just inside of the outer vessel contour[84] potentially permitting iMap to analyse the earliest structural changes in atherosclerosis development.

The iMap system utilises mechanical catheter designs (iCross/Atlantis) where the guidewire is adjacent to the transducer resulting in a characteristic narrow-angle shadow which is not present in the phased array design utilised by VH-IVUS as the

guidewire passes through the annular transducer array. The iMap classifies the guidewire artefact as necrotic tissue and one study comparing VH-IVUS and iMap observed that iMap recorded a necrotic core size 15.5% greater than VH-IVUS, an observation due to guidewire artefact[83].

At present, iMap is available with the mechanical 40MHz Atlantis SR Pro catheter and the iLab console (Boston Scientific, Santa Clara, California). The higher frequency and acoustic power of the single transducer design used by the iMap system may provide superior resolution and therefore plaque characterisation than the phased array system of VH-IVUS. However to date no study has directly assessed the relative characterisation abilities of iMap and VH-IVUS against histology.

Assessment of Endothelial Function

Endothelial dysfunction was first assessed clinically by intracoronary infusions of Acetylcholine (ACh) and Glyceryl Trinitrate (GTN). ACh causes direct muscarinic receptor mediated vasoconstriction and endothelium derived NO vasodilation. Coronary artery diameter was measured by qualitative coronary angiography (QCA) before and after administration of ACh and GTN.[31,34]. Other agents have been used to assess the coronary vasomotion including bradykinin, substance P, serotonin and salbutamol[35,36].

Normal epicardial segments dilate, mildly diseased and stenotic segments constrict after ACh infusion [37]. Previous studies have demonstrated a vasoconstrictor response in epicardial arteries after ACh infusion in angiographically normal arteries. However endothelial dysfunction has been shown to occur in patients with an absence of atherosclerosis angiographic or ultrasound[33]. It has also been observed in asymptomatic children and young adults with predisposing risk factors to atherosclerosis (hypercholesterolemia and smoking)[38].

As endothelial dysfunction occurs in coronary circulation concurrently and in the peripheral circulation an assessment of peripheral endothelial function can be used as a surrogate for assessing coronary endothelial dysfunction[39,40].

Non-invasive assessment of endothelial function is currently limited to the peripheral circulation[41], such as flow mediated dilation (FMD) which utilises ultrasound to measure the diameter of the brachial artery before and after increasing shear stress induced by reactive hyperaemia[39].

Integrated Backscatter (IB-IVUS)

Integrated backscatter Intravascular Ultrasound (IB-IVUS) (YD Co., Nara, Japan) utilises an analytical approach which was initially developed to characterise interstitial fibrosis in myocardial tissue[85]. IB-IVUS relies more on detailed quantification of the radiofrequency signal rather than the alteration in frequency used by VH-IVUS and iMap[86]. At present, the IB-IVUS system is only available for clinical use in Japan.

The IB-IVUS system uses an analogue to digital converter to digitise the signal acquired by the ClearView platform (Boston Scientific, Santa Clara, California) and is stored on a PC for analysis. This method applies a windowed fast-fourier transformation of the RF component and calculates the average power of the signal, measured in decibels. The IB-IVUS generates colour coded “tissue maps” fibrous (green), dense fibrous (yellow) lipid pool (blue) and calcification (red). Ex-vivo validation of coronary artery obtained at autopsy demonstrated predictive accuracies of 93% fibrous, 90% lipid-rich and 96% fibrocalcific components[87].

A comparison of IB-IVUS against VH-IVUS at characterising ex-vivo human coronary artery tissue, showed IB-IVUS had a slightly higher diagnostic accuracy (Cohens kappa 0.83 for IB-IVUS compared to 0.73 for VH-IVUS)[88]. A disadvantage of IB-IVUS is that analysis can only be performed offline, whereas both VH-IVUS and iMap both provide real-time analysis. Additionally, IB-IVUS IVUS and iMap can be analysed using either their respective console software or with independent software packages like EchoPlaque (INDEC Systems Inc., Mountain View, California).

	VH-IVUS	**iMap**	**IB-IVUS**
Manufacturer	Volcano Therapeutics, Rancho Cordova, California	Boston Scientific, Santa Clara, California	YD Co., Nara, Japan
Catheter Design	Phased Array and Mechanical	Mechanical	Mechanical
Transducer Frequency	20MHz, 45MHz	40Mhz	40MHz
Data Acquisition	ECG-gated	Continuous	Continuous
Algorithm	Autoregressive	Fast-Fourier Pattern Recognition	Fast-Fourier Integrated-Backscatter
"Tissue Map"	Fibrous: Green Fibrolipidic: Green-Yellow Necrotic: Red Calcified: White	Fibrous: Green Lipidic: Yellow Necrotic: Pink Calcified: Blue	Fibrous: Green Dense Fibrous: Yellow Lipid Pool: Blue Calcified: Red
Predictive accuracies	Fibrous: 93.4% Fibrolipidic: 94.6% Necrotic: 95.1% Calcified: 96.8%[76]	Fibrous: 95% Lipidic: 98% Necrotic: 97% Calcified: 98%[82]	Fibrous: 93% Lipid Pool: 90% Fibrocalcific: 96%[87]

Table 1) Comparison of plaque characterisation platforms

Optical Coherence Tomography

Optical Coherence Tomography (OCT) is a technique analogous to IVUS but analyses backscattered infrared light instead of ultrasound in order to provide high-resolution images. OCT uses light, which is >190,000 times faster than sound and cannot therefore be directly measured and requires the use of an interferometer, which splits the light source into two "arms" – a reference arm and a sample arm which is directed into the tissue[89]. The reflected signal from both arms is recombined and a photo-detector is used to detect the interference fringes to construct the image.

OCT uses light with a wavelength of 1250-1350nm, providing superior axial and lateral (12-18µm, 20-90µm) resolution compared to IVUS (axial 150-200µm, lateral 150-300µm). This permits the resolution of thin fibrous caps, macrophages and the necrotic core,[90] although the true ability for the OCT technology to effectively evaluate plaque characterisation, remains debatable.

A technical challenge associated with OCT imaging is the requirement for a blood-free environment as blood cells result in signal attenuation and consequently image degradation. To avoid this there are two methods to displace blood during image acquisition. The occlusive approach involves inflating a balloon proximal to the imaging wire and flushing the coronary artery with a solution (usually saline or Ringer's lactate) This method however is no longer used due to associated side effects of the temporary arterial occlusion which include chest discomfort, brady/tachycardia, and ECG changes. The non-occlusive approach developed with the frequency domain (FD)-OCT system and its accelerated pullback rate requires only a single high rate bolus injection of contrast (~4mls/s) through the guiding

catheter[91]. The FD-OCT (also known as swept source OCT) system also utilises a swept frequency laser as light source rather than a broadband light source as in conventional OCT system.

The ability of OCT to characterise plaque components is restricted to visual interpretation of the false colour images; currently no quantitative algorithm exists. There has also been reports of incorrect classification between calcium deposits and lipid pools compared with histology[92]. The use of OCT for plaque characterisation is also limited by its small depth of penetration (1-3mm) compared to IVUS (>5mm) and therefore does not provide imaging beyond the internal elastic lamina.

Near-Infrared Spectroscopy

Near-infrared spectroscopy (NIRS) has been used routinely in science and industry to determine chemical composition of unknown substances and has now been applied to assessing the chemical composition of atherosclerotic plaque. The NIRS system was developed exclusively to detect lipid core plaque (LCP) which is rich in cholesterol monohydrate and cholesterol ester, a signature of necrotic core[93]. It relies on the concept that molecular structures absorb and scatter near-infrared light differently at varying wavelengths. This NIRS measurement of the probability of LCP present within the scanned arterial segment is displayed in a colour map called chemogram. The interpretation can be further enhanced by computing a block chemogram, a summary metric of LCP probability in each 2mm block of arterial segment. Based on the NIRS algorithm, an LCP is considered to be present if at least 1 2-mm segment in block chemogram displays a strong positive signal.
The spectroscopic information for each pixel is transformed into a probability of lipid core which is presented as a red to yellow colour scale, the low probability of lipid is shown as red and high probability of lipid shown as yellow.

The NIRS system is composed of a scanning near-infrared laser and a fibre optic catheter, coupled with an automated pullback and rotation device. Unlike IVUS and OCT, NIRS directly identifies lipid pools. The Spectroscopic Assessment of Coronary Lipid (SPECTACL) trial was the first study comparing the spectra obtained from the patients undergoing percutaneous coronary intervention to previously validated autopsy spectra, and demonstrated that NIRS data could be safely acquired in patients and the spectra obtained in-vivo were comparable to autopsy specimens[94]. The main disadvantage of NIRS is that it only provides chemical information on the lipid component of the plaque without structural data.

This limitation has directed the development of the LipiScan Coronary Imaging System (InfraReDx Inc., Burlington, Massachusetts) which combines both 40MHz rotational IVUS imaging system with co-registered NIRS chemogram. This device is comprised of a scanning near-infrared laser and a fiber-optic catheter similar in size and use to an IVUS catheter[95].

NON-INVASIVE IMAGING OF ATHEROSCLEROSIS

Cardiac Magnetic Resonance (CMR)

Although IVUS is highly reproducible and provides a tomographic assessment of the vessel wall it is an invasive procedure. Cardiac magnetic resonance (CMR) imaging is advantageous in that it permits serial imaging of the same atherosclerotic lesion whilst being completely non-invasive[96]. CMR is a unique imaging modality that provide contrast between soft tissue structures, that doesn't use ionising radiation and provides high spatial and temporal resolution about cardiac anatomy function and viability[97]. Recent advances in CMR had led to the possibility of in-vivo atheroma imaging.

Basic principles of MRI

When a person is placed in the external magnetic field becomes partially magnetised this is largely due to the hydrogen ions or protons that compose water and fat within the body. By creating subsequent magnetic fields perpendicular to the original magnetic field, the vector of magnetisation can be changed. As a magnetic field changes it produces a radiofrequency wave. These RF waves are detected by receiver coils that are analysed and a MRI image is generated

MRI has been used to study atherosclerotic lesions longitudinally has been used to document atherosclerotic burden in human and animal models of atherosclerosis and has been validated as a new tool for the documentation of arterial remodelling [98]. It has also been used to quantify all major carotid plaque components in-vivo: Lipid rich/necrotic core, calcification, loose matrix and haemorrhage. The identification of plaque components was based on the signal intensity relative to

the adjacent muscle in human endarterectomy patients. Results showed high sensitivity 79%-95% and moderate to high specificity 76%-91% in plaque components greater than $2mm^2$ [99]

Other studies have used CMR to identify fibrotic and calcified regions in atherosclerotic plaque in the coronary arteries of an experimental porcine model[100], and to differentiate between lipidic and fibrotic using T2W imaging sequences with lipidic areas appearing brighter and fibrotic areas appearing darker. This study also revealed that T2W images showed greater contrast than PDW images. These studies have shown that CMR has the capacity to noninvasively detect and quantify fibrous and lipid components[101].

This study will determine if CMR is a viable non-invasive alternative to assessing atherosclerosis**.** CMR will be used to image the rabbit abdominal aorta using CINE and PDW sequences. Results of plaque quantification will be compared against IVUS to test the agreement between the two modalities.

REFERENCES

1. Australian Institute of Health and Welfare 2011. Cardiovascular Disease: Australian Facts 2011. Cardiovascular Disease Series 2011.

2. Shah P, Forrester J. Pathophysiology of Acute Coronary Syndromes. The American Journal of Cardiology 1991;68:16-23.

3. Falk E, Shah P, Fuster V. Coronary Plaque Disruption. Circulation 1995;92:657-71.

4. Hansson G. Inflammation, Atherosclerosis, and Coronary Artery Disease. New England Journal of Medicine 2005;352:1685-95.

5. Skålén K, Gustafsson M, Rydberg E, et al. Subendothelial Retention of Atherogenic Lipoproteins in Early Atherosclerosis. Nature 2002;417:750-4.

6. Ross R. Atherosclerosis - An Inflammatory Disease. New England Journal of Medicine 1999;340:115-26.

7. Libby P, Ridker P, Maseri A. Inflammation and Atherosclerosis. Circulation 2002;105:1135-43.

8. Stary H. Evolution and Progression of Atherosclerotic Lesions in Coronary Arteries of Children and Young Adults. Arteriosclerosis 1989;9:19-32.

9. Stary H, Chandler B, Glagov S, et al. A Defintion of Initial, Fatty Streak, and Intermediate Lesions of Atherosclerosis. A Report from the Comittee on Vascular

Lesions of the Council on Atherosclerosis, American Heart Association. Arteriosclerosis, Thrombosis, and Vascular Biology 1994;14:840-56.

10. Berenson GS, S, Bao W, Newman W, Tracy R, Wattigney W. Association Between Multiple Cardiovascular Risk Factors and Atherosclerosis in Children and Young Adults. New England Journal of Medicine 1998;338:1650-6.

11. Kolodgie F, Burke A, Nakazawa G, Virmani R. Is Pathological Intimal Thickening the Key to Understanding Early Plaque Progression in Human Atherosclerotic Disease. Arteriosclerosis, Thrombosis, and Vascular Biology 2007;27:986-9.

12. Stary H, Chandler B, Dinsmore R, et al. A Definition of Advanced Types of Atherosclerotic Lesions and a Histological Classification of Atherosclerosis. Circulation 1995;92:1355-74.

13. Muller J, Tofler G. Triggering and Hourly Variation of Onset of Arterial Thrombosis. Annals of Epidemiology 1992;2:393-405.

14. Libby P. Molecular Basis of the Acute Coronary Syndromes. Circulation 1995;91:2844-50.

15. Burke A, Farb A, Malcolm G, Liang Y, Smialek J, Virmani R. Coronary Risk Factors and Plaque Morphology in Men with Coronary Disease who Died Suddenly. The New England Journal of Medicine 1997;336:1276-82.

16. Yamagishi M, Terashima M, Awano K, et al. Morphology of Vulnerable Coronary Plaque: Insights from Follow-Up of Patients Examined by Intravascular Ultrasound Before an Acute Coronary Syndrome. Journal of the American College of Cardiology 1999;35:16-111.

17. Birgelen C, Klinkhart W, Mintz G, et al. Plaque Distribution and Vascular Remodeling of Ruptured and Nonruptured Coronary Plaques in the Same Vessel: An Intravascular Ultrasound In Vivo. Journal of the American College of Cardiology 2001;37:1864-70.

18. Giroud D, Li J, Urban P, Meier B, Rutishauser W. Relation of the Site of Acute Myocardial Infarction to the Most Severe Coronary Arterial Stenosis at Prior Angiography. American Journal of Cardiology 1992;69:729-32.

19. Little W, Constantinescu M, Applegate R, et al. Can Coronary Angiography Predict the Site of a Subsequent Myocardial Infarction in Patients with Mild to Moderate Coronary Artery Disease. Circulation 1988;78:1157-66.

20. Ambrose J, Tannenbaum M, Alexopoulos D, et al. Angiographic Progression of Coronary Artery Disease and the Development of Myocardial Infarction. Journal of the American College of Cardiology 1988;12:56-62.

21. Furchgott R, Zawadzki J. The Obligatory Role of Endothelial Cells in the Relaxation of Arterial Smooth Muscle by Acetylcholine. Nature 1980;288:373-6.

22. Furchgott R. Role of Endothelium in Responses of Vascular Smooth Muscle. Circulation Research 1983;53:557-73.

23. Furchgott R. Endothelium-Derived Relaxing Factor: Discovery, Early Studies, and Identification as Nitric Oxide. Bioscience Reports 1998;19:235-51.

24. Palmer R, Ferrige G, Moncada S. Nitric Oxide Release Accounts for the Biological Activity of Endothelium-Derived Relaxing Factor. Nature 1987;327:524-6.

25. Davignon J, Ganz P. Role of Endothelial Dysfunction in Atherosclerosis. Circulation 2004;109:27-32.

26. Luscher T, Barton M. Biology of the Endothelium. Clinical Cardiology 1997;20:3-10.

27. Palmer R, Ashton D, Moncada S. Vascular Endothelial Cells Synthesise Nitric Oxide from L-Arginine. Nature 1988;333:664-6.

28. Oemar B, Tschudi M, Godoy N, Brovkovich V, Malinski T, Luscher T. Reduced Endothelial Nitric Oxide Synthanse Expression and Production in Human Atherosclerosis. Circulation 1998;97:2494-948.

29. Verma S, Anderson T. Fundamentals of Endothelail Function for the Clinical Cardiologist. Circulation 2011;105:546-9.

30. Schächinger V, Britten M, Zeiher A. Prognostic Impact of Coronary Vasodilator Dysfunction on Adverse Long-Term Outcome of Coronary Heart Disease. Circulation 2000;101:1899-906.

31. Ludmer P, Selwyn A, Shook T, et al. Paradoxical Vasoconstriction Induced by Acetylcholine in Atherosclerotic Coronary Arteries. New England Journal of Medicine 1986;17:1046-51.

32. Drolet M, Plante E, Battistini B, Couet J, Arenault M. Early Endothelial Dysfunction in Cholesterol-Fed Rabbits: A Non-Invasive In Vivo Ultrasound Study. Cardiovascular Ultrasound 2004;1:1-8.

33. Reddy K, Nair R, Sheehan H, Hodgson J. Evidence that Selective Endothelial Dysfunction may Occur in the Absence of Angiographic or Ultrasound Atherosclerosis in Patients with Risk Factors for Atherosclerosis. Journal of the American College of Cardiology 1994;4:833-43.

34. Celermajer D. Endothelial Dysfunction: Does it Matter? Is it Reversible? Journal of the American College of Cardiology 1997;30:325-33.

35. Puri R, Liew G, Nicholls S, et al. Coronary β_2-adrenoreceptors Mediate Endothelium-Dependent Vasoreactivity in Humans: Novel Insights From an In Vivo Intravascular Ultrasound Study. European Heart Journal 2011;33:495-504.

36. Farouque O, Meredith I. The Assessment of Endothelial Function in Humans. Coronary Artery Disease 2001;12:445-54.

37. Hodgson J, Marshall J. Direct Vasoconstriction and Endothelium: Dependent Vasodilation Mechanisms of Acetylcholine Effects on Coronary Flow and Arterial Diameter in Patients with Nonstenotic Coronary Arteries. Circulation 1989;79:1043-51.

38. Celermajer D, Sorensen K, Gooch V, et al. Non-Invasive Detection of Endothelial Dysfunction in Children and Adults at Risk of Atherosclerosis. The Lancet 1992;340:1111-5.

39. Anderson T, Uehata A, Gerhard M, et al. Close Relation of Endothelial Function in the Human Coronary and Peripheral Circulations. Journal of the American College of Cardiology 1995;26:1235-41.

40. Kuvin J, Patel A, Sliney K, et al. Peripheral Vascular Endothelial Function Testing as a Noninvasive Indicator of Coronary Artery Disease. Journal of the American College of Cardiology 2001;38:1843-9.

41. Tousoulis D, Antoniades C, Stefanadis C. Evaluating Endothelial Function in Humans: A Guide to Invasive and Non-Invasive Techniques. Heart 2005;91:553-8.

42. Topol E, Nissen S. Our Preoccupation with Coronary Luminology: The Dissociation Between Angiographic Findings in Ischemic Heart Disease. Circulation 1995;92:2333-42.

43. Mintz G, Painter J, Pichard A, et al. Atherosclerosis in Angiographically "Normal" Coronary Artery Reference Segments: An Ultrasound Study with Clinical Correlations. Journal of the American College of Cardiology 1995;25:1479-85.

44. Glagov S, Weinsberg E, Zarins C, Stankunavicius R, Kolettis G. Compensatory Enlargement of Human Atherosclerotic Coronary Arteries. New England Journal of Medicine 1987;316:1371-5.

45. Hermiller J, Tenaglia A, Kisslo K, et al. In Vivo Validation of Compensatory Enlargement of Atherosclerotic Coronary Arteries. American Journal of Cardiology 1993;71:665-8.

46. Alderman E, Corley S, Fisher L, et al. Five-Year Angiographic Follow-Up of Factors Associated with Progression of Coronary Artery Disease in the Coronary Artery Surgery Study (CASS). Journal of the American College of Cardiology 1993;22.

47. White C, Wright C, Doty D, et al. Does Visual Interpretation of the Coronary Arteriogram Predict the Physiologic Importance of a Coronary Stenosis? New England Journal of England 1984;310:819-24.

48. Topol EJ, Nissen SE. Our preoccupation with coronary luminology. The dissociation between clinical and angiographic findings in ischemic heart disease. Circulation 1995;92:2333-42.

49. Zir LM, Miller SW, Dinsmore RE, Gilbert JP, Harthorne JW. Interobserver variability in coronary angiography. Circulation 1976;53:627-32.

50. Murphy ML, Galbraith JE, de Soyza N. The reliability of coronary angiogram interpretation: an angiographic-pathologic correlation with a comparison of radiographic views. Am Heart J 1979;97:578-84.

51. Galbraith JE, Murphy ML, de Soyza N. Coronary angiogram interpretation. Interobserver variability. Jama 1978;240:2053-6.

52. Roberts WC, Jones AA. Quantitation of coronary arterial narrowing at necropsy in sudden coronary death: analysis of 31 patients and comparison with 25 control subjects. Am J Cardiol 1979;44:39-45.

53. Arnett EN, Isner JM, Redwood DR, et al. Coronary artery narrowing in coronary heart disease: comparison of cineangiographic and necropsy findings. Ann Intern Med 1979;91:350-6.

54. Bom N, Lancée C, Honkoop J, Hugenholtz P. Ultrasonic Viewer for Cross-Sectional Analyses of Moving Cardiac Structures. Biomedical Engineering 1971;6:500-3.

55. Yock P, Johnson E, Linker D. Intravascular Ultrasound: Development and Clinical Potential. American Journal of Cardiac Imaging 1988;2:185-93.

56. Mintz G, Pichard A, Kovach J, et al. Impact of Preintervention Intravascular Ultrasound Imaging on Transcatheter Treatment Strategies in Coronary Artery Disease. American Journal of Cardiac Imaging 1994;73:423-30.

57. Colombo A, Hall P, Nakamura S, et al. Intracoronary Stenting Without Anticoagulation Accomplished With Intravascular Ultrasound Guidance. Circulation 1995;91:1676-88.

58. Roy P, Steinberg D, Sushinsky S, et al. The Potential Clinical Utility of Intravascular Ultrasound Guidance in Patients Undergoing Percutaneous Coronary Intervention with Drug-Eluting Stents. European Heart Journal 2008;29:1851-7.

59. López-Palop R, Pinar E, Lozano I, et al. Comparison of Intracoronary Ultrasound Expansion Parameters in Coronary Stents Implanted With or Without Balloon Predilatation. A Randomized Intravascular Ultrasound Study. Revista Espñola De Cardiologia 2004;57:403-4011.

60. Tamai H, Igaki K, Kyo E, et al. Initial and 6-Month Results of Biodegradable Poly-l-Lactic Acid Coronary Stents in Humans. Circulation 2000;102:399-404.

61. Stone G, Maehara A, Lansky A, et al. A Prospective Natural-History Study of Coronary Atherosclerosis. The New England Journal of Medicine 2011;364:226-35.

62. Koskinas K, Feldman C, Chatzizisis Y, et al. Natural History of Experimental Coronary Atherosclerosis and Vascular Remodeling in Relation to Endothelial Shear Stress: A Serial, In Vivo Intravascular Ultrasound Study. Circulation 2010;121:2092-101.

63. Mintz G, Nissen S, Anderson W, et al. American College of Cardiology Clinical Expert Consensus Document on Standards for Acquisition, Measurement and Reporting of Intravascular Ultrasound Studies (IVUS) A Report of the American College of Cardiology Task Force on Clinical Expert Consensus Documents. Journal of the American College of Cardiology 2001;37:1478-92.

64. Nishimura R, Edwards W, Warnes C, et al. Intravascularultrasound imaging: In vitro validation and pathologic correlation. Journal of the American College of Cardiology 1990;16:145-54.

65. Peters R, Kok W, Havenith M, Rijsterborgh H, Van der Wal A, Visser C. Histopathologic Validation of Intracoronary Ultrasound Imaging. Journal of the American Society of Echocardiography 1994;7:230-41.

66. Nissen SE, Yock P. Intravascular ultrasound: novel pathophysiological insights and current clinical applications. Circulation 2001;103:604-16.

67. Nissen S. Application of Intravascular Ultrasound to Characterize Coronary Artery Disease and Assess the Progression or Regression of Atherosclerosis. The American Journal of Cardiology 2002;89:24-31.

68. Wang T, Lancée C, Beurskens R, et al. Development of a High-Speed Synchronous Micro Motor and its Application in Intravascular Imaging. Sensors and Actuators 2014;218:60-8.

69. Erbel R, Roth T, Koch L, et al. IVUS of micromotors for cardiovascular imaging. Minimally Invasive Therapy & Allied Technologies 1997;6:195-8.

70. Tuzcu E, Weissman N. Imaging Coronary Artery Histology: A Virtual Pursuit? Circulation Cardiovascular Imaging 2010;3:348-50.

71. Lizzi F, Greenebaum M, Feleppa E, Elbaum M. Theoretical Framework for Spectrum Analysis in Ultrasonic Tissue Characterisation. Journal of the Acoustical Society of America 1983;73:1366-73.

72. Nair A, Kuban B, Tuzcu E, Schoenhagen P, Nissen S, Vince D. Coronary Plaque Classification with Intravscular Ultrasound Radiofrequency Data Analysis. Circulation 2002;106:2200-6.

73. Nair A, Calvetti D, Vince D. Regularized Autoregressive Analysis of Intravascular Ultrasound Backscatter: Improvement in Spatial Accuracy of Tissue Maps. IEEE Transactions on Ultrasonics Ferroelectrics and Frequency Control 2004;51:420-31.

74. Metha S, McCrary J, Frutkin A, Dolla W, Marso S. Intravascular Ultrasound Radiofrequency Analysis of Coronary Atherosclerosis: An Emerging Technology for the Assessment of Vulnerable Plaque. European Heart Journal 2007;28:1283-8.

75. Nair A, Kuban B, Obuchowski N, Vince D. Assessing Spectral Algorithms to Predict Atherosclerotic Plaque Composition with Normalized and Raw Intravascular Ultraound Data. Ultrasound in Medicine and Biology 2001;27:1319-31.

76. Nair A, Margolis P, Kuban B, Vince D. Automated Coronary Plaque Characterisation with Intravascular Ultrasound Backscatter: ex vivo Validation. EuroIntervention 2007;3:113-20.

77. Nasu K, Tsuchikane E, Katoh O, et al. Accuracy of In Vivo Coronary Plaque Morphology Assessment: A Validation Study of In Vivo Virtual Histology Compared With In Vitro Histopathology. Journal of the American College of Cardiology 2006;47:2405-12.

78. Herck J, Meyer G, Ennekens G, Herck P, Herman A, Vrints C. Validation of In Vivo Plaque Characterisation by Virtual Histology in a Rabbit Model of Atherosclerosis. EuroIntervention 2009;5:149-56.

79. Granada J, Wallace-Bradley D, Win H, et al. In Vivo Plaque Characterization Using Intravascular Ultrasound-Virtual Histology in a Procine Model of Complex Coronary Lesions. Arteriosclerosis, Thrombosis, and Vascular Biology 2007;27:387-93.

80. Bruining N, Birgelen C, Feyter P, et al. ECG-Gated Versus Nongated Three-Dimensional Intracoronary Ultrasound Analysis: Implications for Volumetric Measurements. Catheterization and Cardiovascular Diagnosis 1998;43:254-60.

81. Calvert P, Obaid D, O'Sullivan M, et al. Association Between IVUS Findings and Adverse Outcomes in Patients with Coronary Artery Disease: The VIVA (VH-IVUS in Vulnerable Atherosclerosis) Study. Journal of the American College of Cardiology: Cardiovascular Imaging 2011;8:894-901.

82. Sathyanarayana S, Carlier S, Li W, Thomas L. Characterisation of Atherosclerotic Plaque by Spectral Similarity of Radiofrequency Intravascular Ultrasound Signals. EuroIntervention 2009;5:133-9.

83. Shin E, Garcia-Garcia H, Ligthart J, et al. In Vivo Findings of Tissue Characeristics Using iMap IVUS and Virtual Histology IVUS. EuroIntervention 2011;6:1017-9.

84. Garcia-Garcia H, Gogas B, Serruys P, Bruining N. IVUS-Based Imaging Modalities for Tissue Characterization: Similarities and Differences. The International Journal of Cardiovascular Imaging 2011;27:215-24.

85. Picano EP, G, Marzilli M, Lattanzi F, Benassi A, Landini L, L'Abbate A. In Vivo Quantitative Ultrasonic Evaluation of Myocardial Fibrosis in Humans. Circulation 1990;81:58-64.

86. Kawasaki M, Takatsu H, Noda T, et al. Noninvasive Quantitative Tissue Characterization and Two-Dimensional Color-Coded Map of Human Atherosclerotic Lesions Using Ultrasound Integrated Backscatter. Journal of the American College of Cardiology 2001;38:486-92.

87. Okubo M, Kawasaki M, Ishihara Y, et al. Development of Integrated Backscatter Intravascular Ultrasound for Tissue Characterization of Coronary Plaques. Ultrasound in Medicine and Biology 2008;34:655-63.

88. Okubu M, Kawasaki M, Ishihara Y, et al. Tissue Characterization of Coronary Plaques: Comparison of Integrated Backscatter Intravascular Ultrasound with Virtual Histology Intravascular Ultrasound. Circulation Journal 2008;72:1631-9.

89. Garcia-Garcia H, Gonzalo N, Regar E, Serruys P. Virtual Histology and Optical Coherence Tomography: From Research to a Broad Clinical Application. Heart 2011;95:1362-74.

90. Prati F, Regar E, Mintz G, et al. Expert Review Document on Methodology, Terminology, and Clinical Applications of Optical Coherence Tomography:

Physical Priniciples, Methodology of Image Acquisition, and Clinical Application for Assessment of Coronary Arteries and Atherosclerosis. European Heart Journal 2010;31:401-15.

91. Bezerra H, Costa M, Guagliumi G, Rollins A, Simon D. Intracoronary Optical Coherence Tomography: A Comprehensive Review: Clinical and Research Application. Journal of the American College of Cardiology: Cardiovascular Interventions 2009;2:1035-46.

92. Regar E, Soest G, Bruining N, et al. Optical Coherence Tomography in Patients with Acute Coronary Syndrome. EuroIntervention 2010;6:G154-G60.

93. Virmani R, Kolodgie F, Burke A, Farb A, Schwartz S. Lessons from Sudden Coronary Death: A Comprehensive Morphological Classification Scheme for Atherosclerotic Lesions. Arteriosclerosis, Thrombosis, and Vascular Biology 2000;20:1262-75.

94. Waxman S, Dixon S, L'Allier P, et al. In Vivo Validation of a Catheter-Based Near-Infrared Spectroscopy System for Detection of Lipid Core Coronary Plaques: Initial Results of the SPECTACL Study. Journal of the American College of Cardiology: Cardiovascular Imaging 2009;2:858-68.

95. Garg S, Serruys P, van der Ent M, et al. First Use in Patients of a Combined Near Infra-Red Spectroscopy and Intra-vascular Ultrasound Catheter to Identify Composition and Structure of Coronary Plaque. EuroIntervention 2010;5:755-6.

96. Vancraeynest D, Pasquet A, Roelants V, Gerber B, Vanoverschelde J. Imaging the Vulnerable Plaque. Journal of the American College of Cardiology 2011;57:1961-79.

97. Ridgway J. Cardiovascular Magnetic Resonance Physics for Clinicians: Part 1. Journal of Cardiovascular Magnetic Resoance 2010;12:1-28.

98. Worthley S, Helft G, Fuster V, et al. Serial In Vivo MRI Documents Aretrial Remodeling in Experimental Atherosclerosis. Circulation 2000;101:586-9.

99. Saam T, Ferguson M, Yarnykh V, et al. Quantitative Evalutation of Carotid Plaque Composition by In Vivo MRI. Atherosclerosis, Thrombosis, and Vascular Biology 2004;25:234-9.

100. Worthley S, Helft G, Fuster V, et al. High Resolution Ex Vivo Magnetic Resonance Imaging of In Situ Coronary and Aortic Atherosclerotic Plaque in a Porcine Model. Atherosclerosis 2000;150:321-9.

101. Helft G, Worthley S, Fuster V, et al. Atherosclerosis Aortic Component Quantification by Noninvasive Magnetic Resonance Imaging: An In Vivo Study in Rabbits. Journal of the American College of Cardiology 2001;37:1149-54.

Chapter 2:

METHODS

TABLE OF CONTENTS

MAGNETIC RESONANCE IMAGING

HISTOLOGY SAMPLE PREPARATION

PHANTOM STUDY

Animal Ethics

All experiments performed for this thesis were approved by the University of Adelaide Animal Ethics Committee (M-2011-031) and the Institute of Medical and Veterinary Science (IMVS) Animal Ethics Committee (17/11). A total of 48 male, New Zealand White (NZW) rabbits were requested to conduct the proposed studies.

Rabbit model of aortic atherosclerosis

Complex atherosclerotic lesions were induced in male NZW rabbits (12 weeks 3.0-3.5kg) using a combination of an atherogenic diet and balloon denudation of the aorta[1,2]. Animals commenced an ad-libitum high cholesterol diet (0.2% cholesterol supplemented feed, Glen Forest Stock Feed, Western Australia) one week prior to baseline interventions and were continued for the duration of the study (Figure 1).

Balloon denudation of aorta

Anaesthesia was induced with 25mg/kg Ketamine (Ketamine Hydrochloride, Fort Dodge Animal Health, Fort Dodge, USA) and maintained with 1% Isoflurane in 4L/min O_2 (Isoflurane, Bomac Animal Health, NSW, Australia). Aseptic techniques were utilised to minimise post-procedural infections.

A 4cm incision was made above the femoral artery. The artery, vein and nerve were identified and separated. Proximal and distal sutures were placed around the femoral artery to aid cannulation and to minimise blood loss. The femoral artery was cannulated using a 24-gauge Jelco cannula and a 0.014" guidewire was introduced. A 4Fr Fogarty embolectomy catheter was introduced into the femoral artery and advanced under fluoroscopy (Phillips BV-24) towards the descending aortic arch before balloon inflation (10-12atm) and then withdrawn with moderate resistance to the iliac bifurcation. This was repeated three times. To prevent thrombosis post denudation Heparin (100U/kg) (Heparin Sodium, Pfizer, New York, USA) was administered via the marginal ear vein.

A second balloon denudation of the aorta was performed at the 3 month time-point for the 9 month cohort. This was performed to induce raised lesions characterised by an increase in lipid and fibrotic components as previously described[3].

INTRAVASCULAR ULTRASOUND

IVUS imaging systems

Two state-of-the-art Intravascular Ultrasound (IVUS) imaging systems were utilised during these studies (iMap and VH-IVUS). Both systems have post-processing data analysis software to facilitate plaque characterisation.

iMap IVUS

The iMap imaging system (Boston Scientific Corporation, Nattick MA, USA) consists of the iLab Ultrasound Imaging console and the commercially available single-element mechanically rotating (1800rpm) transducer Atlantis SR Pro 40MHz Coronary Imaging Catheter (3.6Fr) (Boston Scientific Corporation, Nattick MA, USA).

VH-IVUS

The Virtual Histology (VH-IVUS) imaging system (Volcano Corp, Rancho Cordova, USA) consists of the s5 imaging console and the commercially available electronic 64-element phased-array transducer Eagle Eye Platinum 20MHz Ultrasound Imaging Catheter (3.5Fr) (Volcano Corp, Rancho Cordova, USA). An external ECG simulator (60BPM) supplied the artificial ECG signal required to generate VH-IVUS images.

Baseline IVUS imaging protocol

Anaesthesia was induced with 25mg/kg Ketamine (Ketamine Hydrochloride, Fort Dodge Animal Health, Fort Dodge, USA) and maintained with 1% Isoflurane in 4L/min O_2 (Isoflurane, Bomac Animal Health, NSW, Australia). Aseptic techniques were utilised to minimise post-procedural infections.

A 4cm incision was made above the femoral artery. The artery vein and nerve were identified and separated. Proximal and distal sutures were placed around the femoral artery to aid cannulation and to minimise blood loss. The femoral artery was cannulated using a 24-gauge Jelco cannula and a 0.014” guidewire was introduced.

The VH-IVUS catheter was advanced over the guidewire and advanced under fluoroscopy (Phillips BV-24) to the level of the renal arteries; the placement was confirmed by manual IVUS imaging. Automated pullbacks were performed for both platforms at 0.5mm/s for lengths of 55-90mm. VH-IVUS pullbacks were performed by ‘piggy-backing’ the iMap pullback device. The VH-IVUS catheter was removed before introducing the iMap catheter. The imaging protocol was then repeated. The iMap catheter was left in-situ for the endothelial function assessment.

IVUS assessment of endothelial function

Endothelial function was assessed using incremental infusions of Acetylcholine (Ach), an endothelium dependent vasodilator (0.05 [low], 0.5 [mid], 2.5 [high] µg/kg/min) (Miochol-E Acetylcholine chloride, Bausch & Lomb, Auckland, New Zealand) before administration of Glyceryl Trinitrate (GTN; 3µg/kg/min), an endothelium independent by the endothelial independent vasodilator (DBL Glyceryl Trinitrate Concentrate Injection, Hospira, Victoria, Australia). ACh and GTN were administered via the marginal ear vein using a Gemini PC-2 infusion pump (IMED Corporation, San Diego, CA).

Immediately following baseline IVUS imaging, low-dose ACh was infused for 2 minutes to reach steady-state concentration and was continued whilst an automated pullback was performed (0.5mm/s) from the renal arteries to the iliac bifurcation. This was repeated for mid, high-dose ACh and GTN infusions.

Arterial Blood Sampling

Arterial blood samples (~3mls) were taken from the femoral artery at the time of cannulation. Samples were centrifuged (3000rpm, 10mins) and the supernatant was stored at -80^{o}C prior to analyses. Serum cholesterol and basic biochemical analysis were performed.

IVUS Image Analysis

All IVUS studies were exported to DVD and stored on an external hard disk drive for offline analysis using echoPlaque v.3.0.53 (Indec Systems, Santa Clara, CA, USA), except for VH-IVUS analysis which was analysed using echoPlaque v.4 (Indec Systems, Santa Clara, CA, USA). Cross sectional images representing end diastole (ED) were analysed every 30 frames (0.5mm).

The leading edge of the lumen and external elastic membrane (EEM) were traced by manual planimetry. Vessel wall area (VWA) was defined as the area occupied between luminal and EEM contours.

$VWA = EEM_{area} - Lumen_{area}$

Percentage atheroma volume [% atheroma volume (PAV)] was utilised as a marker of segmental plaque burden. This was calculated as the proportion of the entire vessel CSA occupied by atherosclerotic plaque.

$$PAV = \sum [(EEM_{area} - Lumen_{area}) / \sum EEM_{area}] \times 100$$

Vasomotor responses [% Δ segmental lumen volume (% ΔSLV)] were assessed by measuring luminal volumes at baseline and following each incremental infusion of ACh and GTN and expressed as a %Δ from baseline with a positive deviation from baseline indicated vasodilation and a negative value conversely indicated vasoconstriction.

Plaque composition analysis

Plaque composition analysis was performed for baseline images generated with both iMap and VH-IVUS systems. Tissue maps (TM) were generated using echoPlaque 4.0 (Indec Systems, Santa Clara, CA, USA) from luminal and EEM contours. Individual plaque components were represented by colour-mapping and expressed as a percentage of the VWA.

	iMap	VH-IVUS
Fibrous	Green	Green
Lipidic	Yellow	Yellow-green
Necrotic	Pink	Red
Calcified	Blue	White

Table 1) Tissue Map colour representations for iMap and VH-IVUS systems.

Co-registration of IVUS frames

To facilitate accurate comparisons between systems, co-registration between VH-IVUS and iMap frames was performed using MIB:IVUS Lab 1.46 (Indec System, Santa Clara, CA, USA).

MAGNETIC RESONANCE IMAGING

MR imaging system

MRI imaging was performed using a 1.5T Siemens MAGNETOM Sonata system and a human knee coil (Siemens Medical Solutions, Erlangen, Germany). All MR imaging during these studies was performed using this system.

MR imaging protocol

The animals were placed in the supine position in the isocentre of the scanner; anaesthesia was maintained using Isoflurane (1% in 4L/min O_2); (Isoflurane, Bomac Animal Health, NSW, Australia). A 3 lead ECG was obtained before connecting the knee coil. A foam block was positioned between the rabbit and the knee coil; to facilitate optimum contact of the ECG electrodes and the animal, and also decreased respiratory motion artefacts.

Localising sequences

Axial Time of Flight (TOF) Maximum Intensity Projection (MIP) sequences were performed in both coronal and transverse planes to localise the aorta and the position of the renal arteries. These sequences were performed in order to plan the following sequences.

White blood imaging

White blood cine imaging was used to generate diagnostic quality images of the rabbit aorta throughout the cardiac cycle. We used prospectively gated FLASH (Fast Low Angle Shot) sequences with fat saturation. Imaging parameters utilised were: Field of view (140x96mm), Phase FOV (68.8%) Slice thickness (6mm), TR (32ms), TE (4.9ms), Flip Angle (30^0), Average (3), Base resolution (256), Phase resolution (80%) Matrix (141x256), Voxel (0.7x0.5x6mm). These sequences were performed 10mm below the lowest renal artery at 5 positions 6mm apart.

Endothelial function test

ACh and GTN were administered using a Gemini PC-2 (IMED Corporation, San Diego, CA) infusion pump from the MRI control room, via a primed infusion set connected to extension tubing that was passed through the waveguide into the MRI room and connected to the ear vein cannula. Prior to connecting the infusion line to the rabbit the ear vein cannula was flushed with saline using a MR safe syringe to ensure vessel patency.

After acquiring baseline images, mid-dose ACh (0.5µg/kg/min) was infused for 2 minutes to reach steady state prior to imaging. The infusion was continued for the duration of the scan. GTN (3µg/kg/min) was then infused for 2mins and the sequences repeated.

Black blood imaging

Black blood MR imaging was utilised to generate high-resolution images of the rabbit aorta. Following the endothelial function tests, ECG independent Proton Density Weighted (PDW) sequences with fat saturation were performed. 20 sequential axial images were generated in incremental 5mm sections from the renal arteries. Imaging sequence parameters were: TR (2000ms), TE (11ms), Slice Thickness (3mm), Field of view (9x9cm), Matrix (256x256), Flip angle (180^{o}), Average (4).

MRI Image analysis

All MRI studies were exported to DVD and stored on HDD for offline analysis using QMass (Medis Medical Imaging Systems, Leiden, Netherlands). For the analysis of endothelial function (White blood CINE imaging) at each position along the aorta, phases representing end diastole (ED) and end systole (ES) were selected. Luminal contours were manually traced to determine luminal cross-sectional area (CSA). Inter-observer variability was assessed by comparing image analysis performed by two observers.

Vasomotor responses [% Δ segmental lumen volume (% ΔSLV)] were assessed by measuring luminal volumes at baseline and following each incremental infusion of ACh and GTN and expressed as a %Δ from baseline with a positive deviation from baseline indicated vasodilation and a negative value conversely indicated vasoconstriction.

MRI vessel wall analysis

The lumen and external elastic membrane (EEM) was traced using manual planimetry for the analysis of the vessel wall (Black blood PDW imaging). Vessel wall area (VWA) was defined as the area occupied between luminal and EEM contours.

$$VWA = EEM_{area} - Lumen_{area}$$

Percentage atheroma volume [% atheroma volume (PAV)] was used as a marker of segmental plaque burden. This was calculated as the proportion of the entire vessel CSA occupied by atherosclerotic plaque.

$$PAV = \sum [(EEM_{area} - Lumen_{area}) / \sum EEM_{area}] \times 100$$

HISTOLOGY SAMPLE PREPARATION

Euthanasia and specimen fixation

Upon reaching their study respective endpoints, the animals were euthanised by exsanguination under full anaesthesia after receiving heparin (100U/kg) to prevent post-mortem blood clotting. The aorta was identified and dissected before an immediate washing and flushing in Krebs* buffer (4^{o}C, pH7.4).

Abdominal aorta specimens were placed on a foam block and a Vernier calliper was used to accurately measure 5mm segments from the lowest renal artery. A pin was placed at each interval. Specimens were then stored in 10% buffered formalin prior to sectioning.

Histopathology preparation

Abdominal aorta specimens were sectioned at the marked intervals and embedded in paraffin. Sections (5µm) were stained with a combined Masson's Trichrome elastin stain and haematoxylin and eosin. A subset of abdominal aortic specimens were frozen-sectioned for Oil-Red-O staining for specific fat analysis. All sections were then digitised using a Nanozoomer photomicrograph (Hamamatsu Photonics, Hamamatsu, Japan) to facilitate morphometric and compositional analysis.

Histological analysis

All histological images were stored on HDD for offline analysis. Quantification of plaque components was performed using Image-Pro Premier v9.1 (Media Cybernetics, Rockville, MD USA). A region of interest (ROI) was created by manually tracing luminal and vessel contours before applying semi-automated thresholding to the 32-bit RGB segmented image to determine individual plaque components.

PHANTOM STUDY

Phantom imaging

A Perspex phantom was designed to assess the geometric accuracy of the phased array and mechanical catheters. It was engineered to have stepwise luminal diameters of 2, 4, 6, 8 and 10mm (tolerance +/-0.1mm). This was achieved by machining holes into a solid cylinder of Perspex with a computer controlled CNC router.

IVUS phantom protocol

The phantom was secured in a frame and immersed in a bath of 90% water and 10% ETOH to achieve the same speed of sound propagation as in blood [4]. All air bubbles were removed from the phantom lumen prior to imaging. A 0.014" guidewire was passed through the phantoms housing to ensure the IVUS catheters would remain central to the lumen during IVUS pullbacks. Pullbacks were performed with multiple catheters for both iMAP and VH-IVUS systems.

MRI phantom protocol

A second phantom was filled with agarose gel as a tissue analogue and placed in the isocentre of the scanner. The same cine sequences employed for the rabbit aorta imaging were applied at each section of the phantom. An external ECG signal was supplied in order to generate the images.

Statistical analysis

Inter/Intra observer variability was assessed using the Bland Altman[5] method as well as intraclass correlation coefficients (ICC). The ICC is a statistical method to quantify the relationship between two variables measured independently and where r=1 is a perfect correlation. For the assessment of inter-observer variability a subset of the IVUS and MRI data was analysed by two independent reviewers (LF, AC) and (LF,JDR) respectively. For the purpose of intra-observer variability a subset of both IVUS and MRI data were analysed on two separate occasions, with an interval of at least one month.

All data is presented as mean ± standard error of the mean. Statistical significance was accepted as a p value of <0.05. All statistical analysis was performed using both SPSS 20.0 (SPSS Inc, Chicago, IL, USA) and GraphPad Prism 6.0 (GraphPad Software, San Diego, CA, USA).

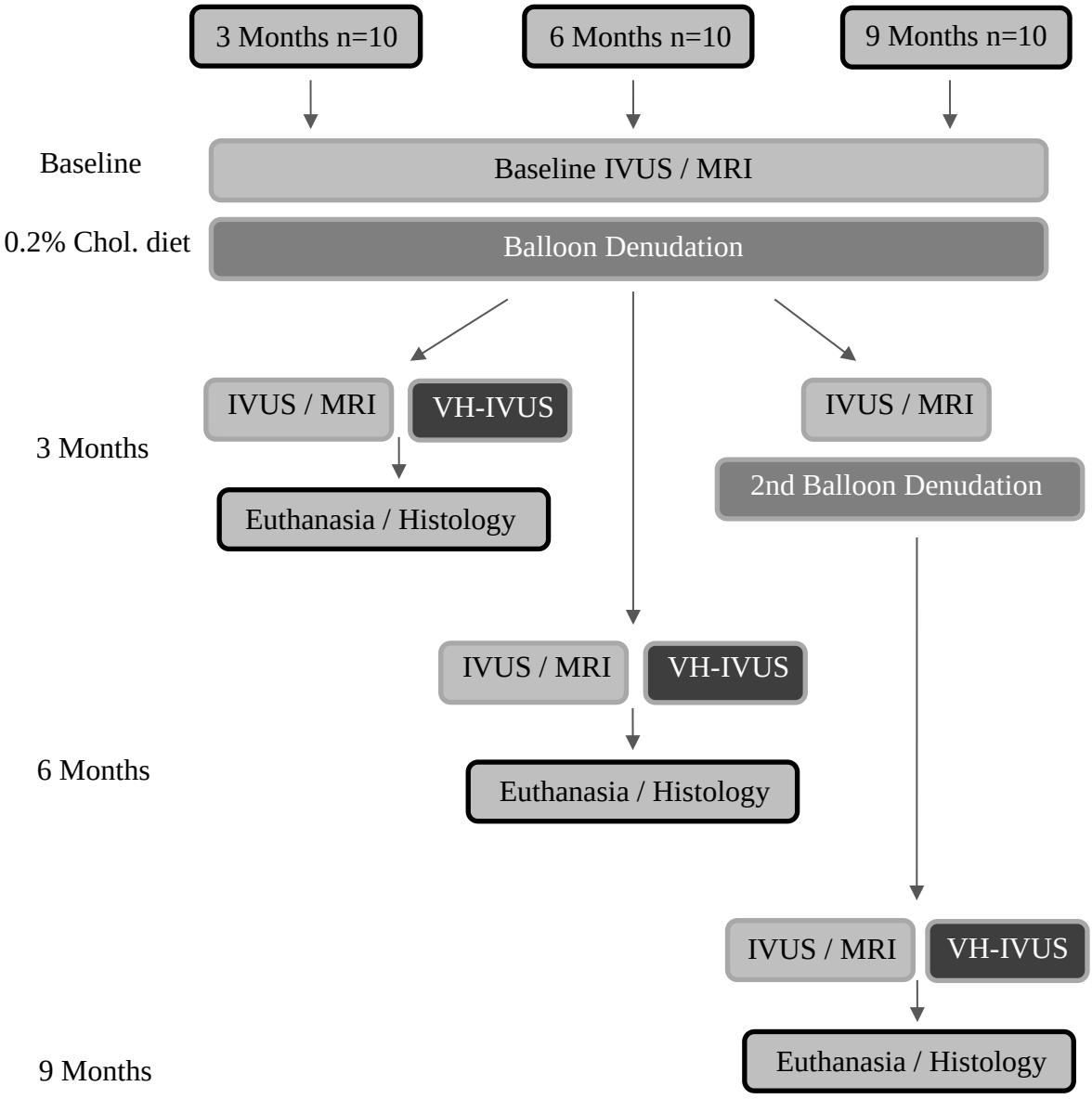

Figure 1. Flow chart of experimental timeline. IVUS = Baseline imaging/iMAP and endothelial function test, MRI = Baseline imaging and endothelial function test, VH-IVUS = Baseline imaging with VH-IVUS.

REFERENCES

1. Skinner M, Yuan C, Mitsumori L, et al. Serial Magnetic Resonance Imaging of Experimental Atherosclerosis Detects Lesion Fine Structure, Progression and Complications In Vivo. Nature 1995;1:69-73.

2. Worthley S, Helft G, Fuster V, et al. Serial In Vivo MRI Documents Aretrial Remodeling in Experimental Atherosclerosis. Circulation 2000;101:586-9.

3. Helft G, Worthley S, Fuster V, et al. Atherosclerosis Aortic Component Quantification by Noninvasive Magnetic Resonance Imaging: An In Vivo Study in Rabbits. Journal of the American College of Cardiology 2001;37:1149-54.

4. Martin K, Spinks D. Mesaurements of the Speed of Sound in Ethanol/Water Mixtures. Ultrasound in Medicine and Biology 2001;27:289-91.

5. Bland J, Altman D. Statistical Methods for Assessing Agreement Between Two Methods of Clinical Measurement. The Lancet 1986;1:307-10.

Chapter 3:

IN-VIVO AND IN-VITRO VARIABILITY IN CROSS SECTIONAL AREA MEASUREMENTS WITH PHASED ARRAY AND MECHANICAL IVUS CATHETERS

TABLE OF CONTENTS

INTRODUCTION

Intravascular ultrasound (IVUS) is routinely used in clinical and research settings, for characterization of luminal and vessel wall areas to determine the topographic and volumetric assessment of atheroma and its composition. It is performed using either mechanical or phased-array catheters which have inherent design advantages and limitations. IVUS allows an in-vivo examination of the natural history of atherosclerosis, the effect of interventions on the changes in plaque burden, as well as serving as an important adjunctive tool to guide percutaneous coronary revascularization. However the consequent impact on accuracy in determining geometric dimensions including lumen cross sectional area (CSA) is uncertain, due to limited direct in-vivo and ex-vivo comparisons.

Ultrasound signals are generated when an electric current is applied to a piezoelectric transducer, resulting in rapid expansion and contraction of the transducer which generates sound waves. The sound waves then propagate through the tissue and are subsequently reflected according to the acoustic properties of the tissue it travels through[1,2]. The final image generated is a three-layer representation of the corresponding coronary artery in alternating bright and dark echoes, with the bright echo representing the intima, a dark zone from the media, and a bright echo from the adventitia[3].

There are two distinct IVUS catheter designs, which encompass the mechanical single element rotating system and the electronic phased array system. The mechanical system comprises a single transducer rotated on a driveshaft at 1800rpm to produce a beam almost perpendicular to the catheter[2]. It is advantageous as it allows greater image resolution due to its higher operating frequency. This design is available commercially as the 40 MHz iCross or Atlantis SR Pro catheters (Boston Scientific, Santa Clara, California), the Revolution 45 MHz catheter (Volcano Corp, Rancho Cordova, California), and the 40 MHz TVC Imaging Catheter (InfraReDx Burlington, Massachusetts). Conversely, the phased-array system uses 64 stationary transducers arranged in an annular array that are sequentially activated. This is available commercially as the 20 MHz Eagle Eye catheter (Volcano Therapeutics, Rancho Cordova, California). For the IVUS transducers (20-45 MHz) currently available, the axial resolution is approximately 150-200μm while the lateral resolution is approximately 200-250μm with >5mm depth penetration.

This study aims to assess the variation of CSA measurements between three state-of-the-art commercially available IVUS catheters both in an in-vivo rabbit aorta model and an in-vitro setting using a Perspex phantom.

METHODS

Phantom design

A Perspex phantom was designed to have stepwise luminal diameters of 2, 4, 6, 8 and 10mm (tolerance +/-0.1mm) (Table 2). This was achieved by machining holes into a solid cylinder of Perspex with a computer controlled Computer Numerical Control (CNC) router. (Figure 1).

IVUS catheters

In-vitro experiments were performed using 3 catheter types including the mechanical Revolution 45 MHz catheter (3.2Fr) (Volcano Corp, Rancho Cordova, California), (n=2); the mechanical Atlantis SR Pro 40 MHz catheter (3.6Fr) (Boston Scientific, Santa Clara, California), (n=4) and the phased array 20MHz Eagle Eye Platinum catheter (3.5Fr) (Volcano Therapeutics, Rancho Cordova, California), (n=4).

In-vivo experiments were performed using 2 catheter types; the mechanical 40 MHz Atlantis SR Pro catheters (Boston Scientific, Santa Clara, California) and the phased array 20MHz Eagle Eye Platinum catheter.

IVUS consoles

The 40MHz Atlantis SR Pro catheters were used in conjunction with the iMap imaging system (Boston Scientific, Santa Clara, California). Both the 20MHz Eagle Eye Platinum and the Revolution 45 MHz catheter (Volcano Corp, Rancho Cordova, California) were used in conjunction with the s5 imaging console (Volcano Therapeutics, Rancho Cordova, California).

Catheter	Frequency (MHz)	Design	Profile (Fr)	Console	Manufacturer
Eagle Eye Platinum	20	Phased-array	3.5	s5	Volcano
Atlantis SR Pro	40	Mechanical	3.6	iLab	Boston Scientific
Revolution	45	Mechanical	3.2	s5	Volcano

Table 1. Comparison of the three IVUS catheter designs used.

In-vitro IVUS Phantom protocol

The Phantom was immersed in a solution of 90% distilled water and 10% EtOH, to replicate the speed of sound propagation as in blood (approximately 1.548 mm/μs)[4]. The phantom lumen was primed with solution prior to imaging. A 0.014" guidewire was passed through the Phantoms housing to ensure central placement of the catheters within the lumen during imaging. Automatic pullbacks were performed at a rate of 0.5mm/s and performed twice.

In-vivo IVUS imaging protocol

All procedures were approved by the University of Adelaide Animal Ethics Committee and the Institute of Medical and Veterinary Science (IMVS) Animal Ethics Committee (M-2011-031; 17/11).

20 New Zealand White (NZW) rabbits were anesthetised with Ketamine (25mg/kg) and maintained with Isoflurane (1% 4L/min O_2). The femoral artery was cannulated with a 23G Jelco cannula and a 0.014" guidewire was advanced under fluoroscopy to the descending aortic arch. The IVUS catheters were then advanced over the guidewire. IVUS imaging of the abdominal aorta was performed using automatic pullbacks (0.5m/s for 70-90mm) from the renal arteries to the iliac bifurcation. This procedure was repeated for both the mechanical 40 MHz Atlantis SR Pro catheters (Boston Scientific, Santa Clara, California) and the phased-array 20MHz Eagle Eye Platinum catheter.

Image analysis

All IVUS data analysis was performed offline using echoPlaque 3.0.53 (Indec Systems, Santa Clara, CA, USA). Co-registration between IVUS frames from the in-vivo experiments was achieved using MIB:IVUS Lab 1.46 (Indec System, Santa Clara, CA, USA).

In-vivo analysis of cross sectional IVUS images representing end diastole (ED) were analysed at every 30 frames (0.5mm) for a 15mm segment of aorta per animal.

The leading edge of the lumen and external elastic membrane (EEM) were traced by manual planimetry. Vessel wall area (VWA) was defined as the area occupied between these leading edges. Percent atheroma volume (PAV) was used as a marker of segmental plaque burden. This was calculated as the proportion of the entire vessel CSA occupied by atherosclerotic plaque. $PAV = \sum [(EEM_{area} - Lumen_{area})/ \sum EEM_{area}] \times 100$

For in-vitro analysis, 5 frames were selected for each segment of the Phantom and luminal borders were traced.

Inter- and intra-observer variability

To assess inter-observer variability a subset of the IVUS data was analysed by two independent reviewers (LF, AC). A subset of IVUS data was analysed on two separate occasions, with an interval of at least one month duration to assess intra-observer variability. This process was applied to both in-vivo and in-vitro studies.

Statistical analysis

All values are represented as mean ± standard deviation. In-vitro analysis was performed using a one way ANOVA model in conjunction with post-hoc Tukey multi-comparison test. In-vivo analysis was performed using unpaired t-tests. Correlation between in-vivo parameters (Lumen, Vessel and PAV) and intra- and inter- observer agreement were assessed using Bland-Altman, linear regression and intraclass correlation coefficients (ICC). Bland-Altman analysis was conducted with mean bias, standard deviation and 95% limits of agreement calculated. A p value <0.05 was considered statistically significant. Statistical analysis was performed with both SPSS 19.0 (SPSS Inc, Chicago, IL, USA) and GraphPad Prism 6.0 (GraphPad Software, San Diego, CA, USA).

RESULTS

In-vivo Phantom IVUS imaging

All three IVUS catheters consistently overestimated the Phantom lumen CSA. There was a significant difference in the average relative difference between the 40MHz and the 45MHz (11.31±2.94% vs 6.14±2.68%, $p<0.025$) and between the 40MHz and the 20MHz (11.31±2.94% vs 3.52±2.36%, $p<0.001$). There was no significant difference between the 45MHz and the 20MHz (6.14±2.68% vs 3.52±2.36%, $p<0.001$) (Figure 2).

In-vitro intra-observer agreement

There was a strong correlation between first and second analysis for all catheters 45MHz ($r^2=0.99$, ICC=1 $p<0.001$) 40MHz ($r^2=0.99$, ICC=1 $p<0.0001$) 20MHz ($r^2=0.98$, ICC=0.9 $p<0.0001$). Bland Altman analysis supported the high level of intra-observer agreement for all catheter types; 45MHz (bias -0.451±0.47) 40MHz (bias 0.064±0.4) 20MHz (bias -0.16±0.15) (Figure 7-9).

Phantom Diameter(mm)	Phantom CSA (mm^2)
10	78.54
8	50.27
6	28.27
4	12.57
2	3.142

Table 2. Standard diameters and corresponding Phantom CSA. CSA=Cross sectional area.

Atlantis SR Pro 40 MHz Catheter (Mechanical) (n=4)		
CSA (mm2)	**Absolute Difference (mm2)**	**Relative Difference (%)**
86.6±0.53	8.06	10.26
55.6±0.48	5.3	10.55
30.8±0.44	2.6	9.21
13.8±0.17	1.25	10.0
3.66±0.12	0.518	16.5

Table 3. In-vitro phantom IVUS measurements derived using the Atlantis SR Pro 40 MHz catheter (mechanical). CSA=Cross sectional area.

20MHz Eagle Eye Platinum Catheter (Phased-array) (n=4)		
CSA (mm2)	**Absolute Difference (mm2)**	**Relative Difference (%)**
83.1±0.38	4.52	5.75
53.3±0.39	3.08	6.12
29.2±0.22	0.915	3.23
12.7±0.09	0.125	0.99
3.09±0.12	0.01	1.49

Table 4. In-vitro phantom IVUS measurements derived using the 20MHz Eagle Eye Platinum (Phased-array). CSA=Cross sectional area.

45MHz Revolution Catheter (Mechanical) (n=2)		
CSA (mm2)	**Absolute Difference (mm2)**	**Relative Difference (%)**
84.5±0.37	6.04	7.69
54.74±0.31	4.48	8.91
30.2±0.3	2.01	7.11
13.18±0.05	0.615	4.89
3.2±0.05	0.066	2.12

Table 5. In-vitro phantom IVUS measurements derived using the 45MHz Revolution (mechanical). CSA=Cross sectional area.

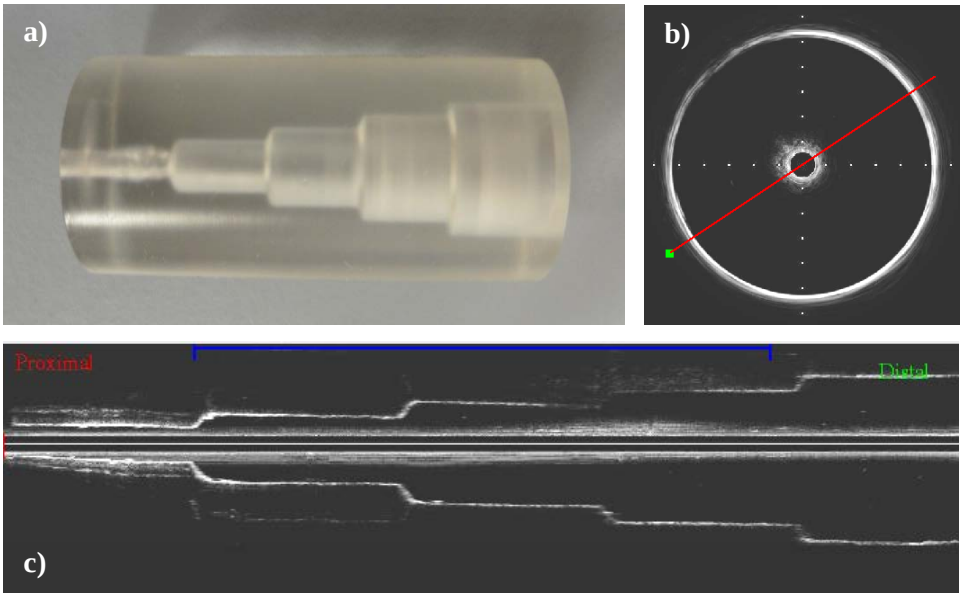

Figure 1. The Perspex phantom. a) Photo of the phantom. b) 40MHz mechanical IVUS image at 10mm. c) Longitudinal view of the Perspex phantom using 40MHz mechanical IVUS catheter.

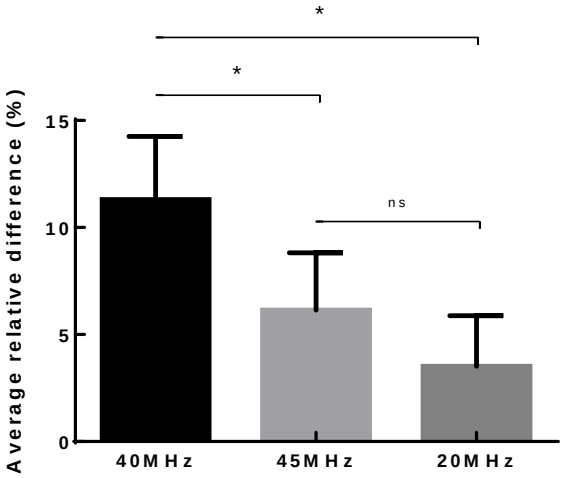

Figure 2. Comparison of relative differences between IVUS derived CSA and known phantom CSA. Data represented is pooled across all phantom diameters. There was a significant difference between the 40MHz and 45MHz catheters ($p<0.025$) and between the 40MHz and 20MHz catheters ($p<0.001$) however there was no significant difference between the 45MHz and the 20MHz ($p=0.3$).

In-Vivo IVUS imaging

IVUS imaging was performed using both 20MHz phased array and 40MHz mechanical catheters in 20 animals. Measurements of lumen and vessel CSA and the derived PAV were then compared.

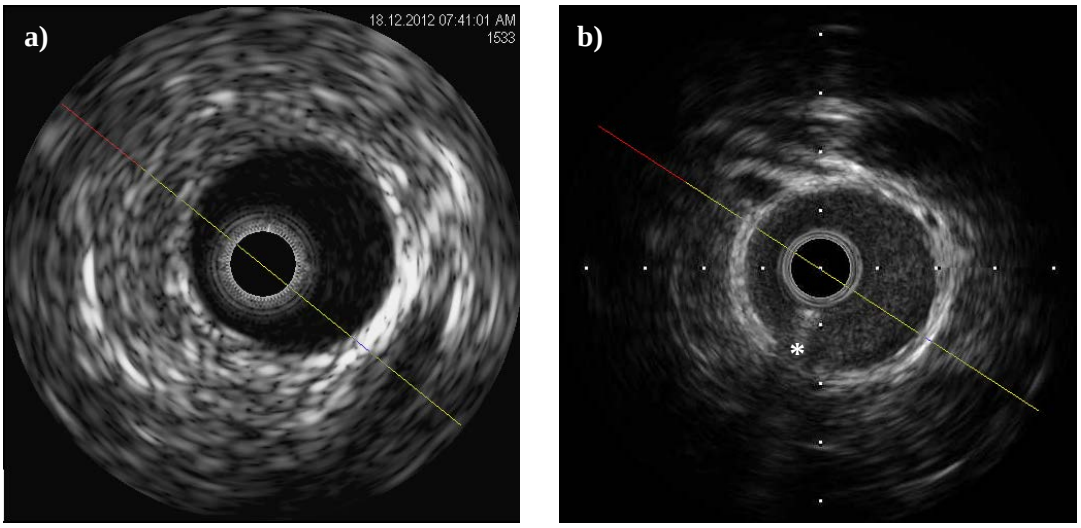

Figure 3. IVUS images of a segment of rabbit aorta. a) 20MHz Eagle Eye Platinum phased-array catheter and b) 40MHz Atlantis SR Pro mechanical catheter * denotes guidewire artefact. There is a lack of blood speckle present in a).

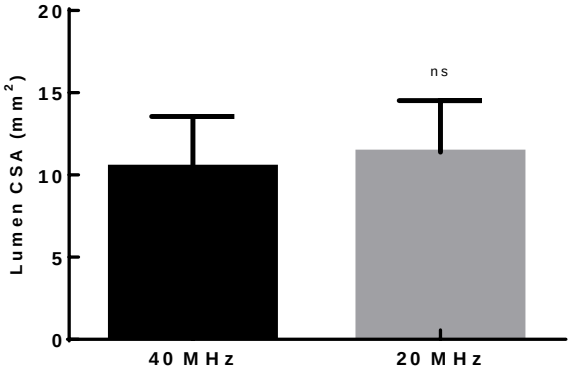

Figure 4. Mean lumen CSA measured using the 40MHz Atlantis SR PRO and the 20 MHz Eagle Eye Platinum. There was no significant difference between the 40MHz and the 20MHz catheters (p=0.35).

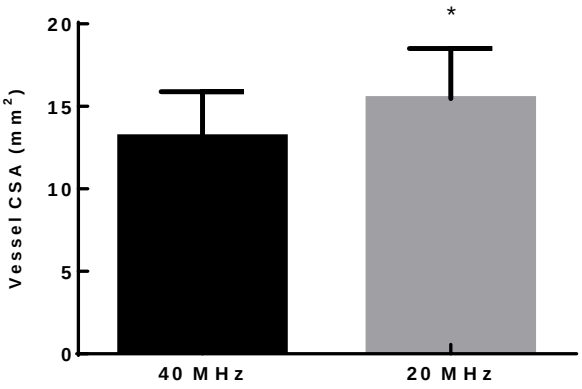

Figure 5. Mean vessel CSA measured using the 40MHz Atlantis SR PRO and the 20 MHz Eagle Eye Platinum. There was a significant difference between the 40MHz and the 20MHz catheters (p<0.01).

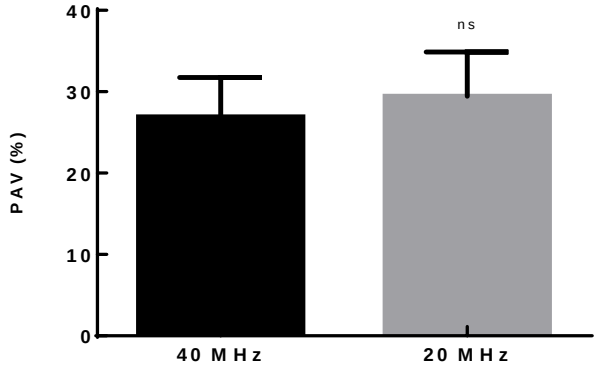

Figure 6. Mean PAV measured using the 40MHz Atlantis SR PRO and the 20 MHz Eagle Eye Platinum. There was no significant difference between the 40MHz and the 20MHz catheters ($p<0.12$).

There was no significant difference between the mean lumen CSA determined by the 40MHz and the 20MHz catheters (10.47±3.08mm^2 vs 11.38±3.14mm^2, p=0.35). The average difference was 0.91±0.73mm^2.

There was a significant difference between the mean vessel CSA determined by the 40MHz and the 20MHz catheters (13.16±2.71mm^2 vs 15.48±3.02mm^2, p<0.01). The average difference was 2.31±1.84mm^2.

There was no significant difference between the mean PAV determined by the 40MHz and the 20MHz catheters (26.9±4.85mm^2 vs 29.45±5.41mm^2, p=0.12). The average difference was 2.54±2.27m^2.

In-vivo intra-observer agreement

The absolute difference in lumen CSA between first and second analysis was 0.06±0.4mm^2 for 40MHz and 0.16±0.5mm^2 for 20MHz. For both 40 MHz and 20 MHz catheters agreement was excellent (r^2=0.99, ICC=1) and (r^2=0.98, ICC=0.9) respectively. Bland Altman analysis supported the high level of intra-observer agreement for both 40MHz and 20MHz catheters (bias 0.064±0.4) and (bias -0.16±0.15) respectively.

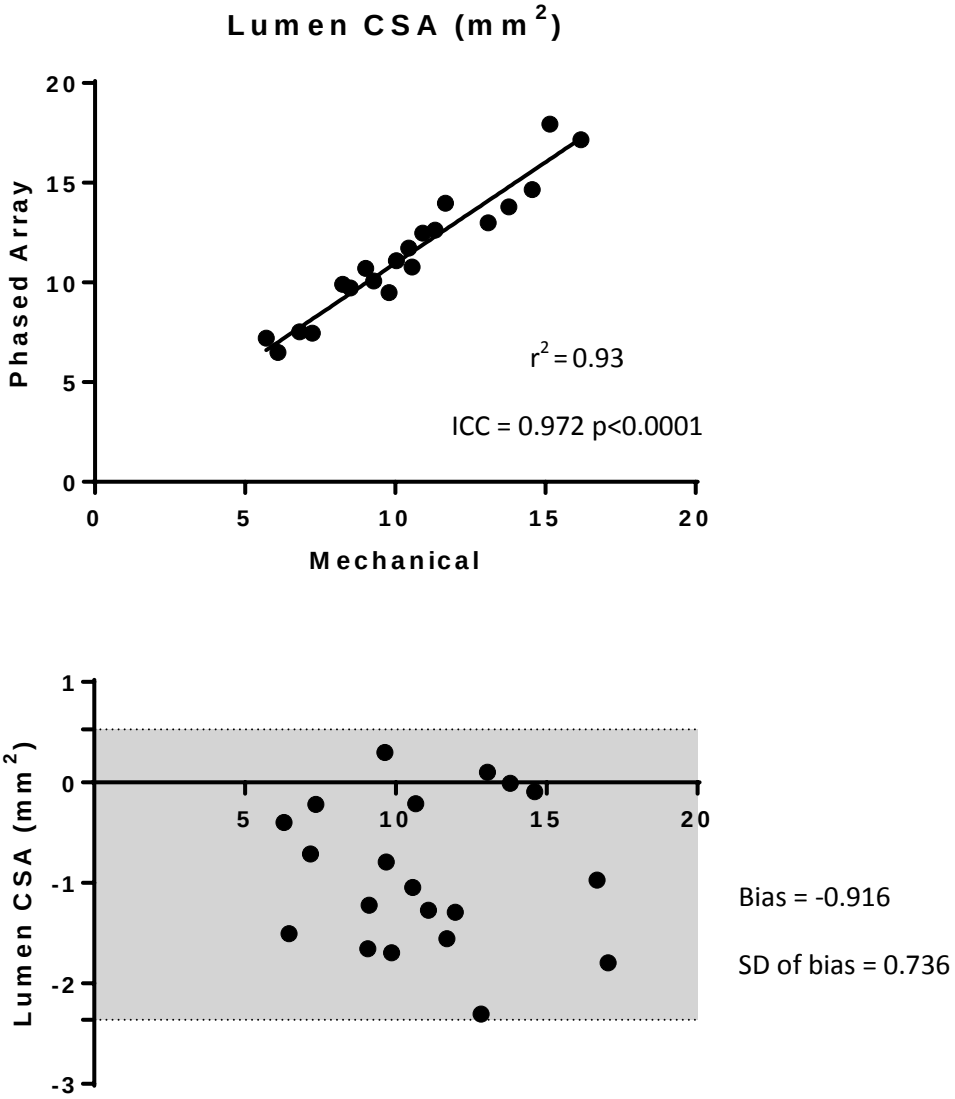

Figure 7. Mechanical vs. Phased Array catheters: Measurement of lumen CSA. Linear correlation chart with regression line and intraclass correlation coefficient (ICC). Corresponding Bland–Altman plots with mean bias, standard deviation and 95% limits of agreement displayed. (n=20)

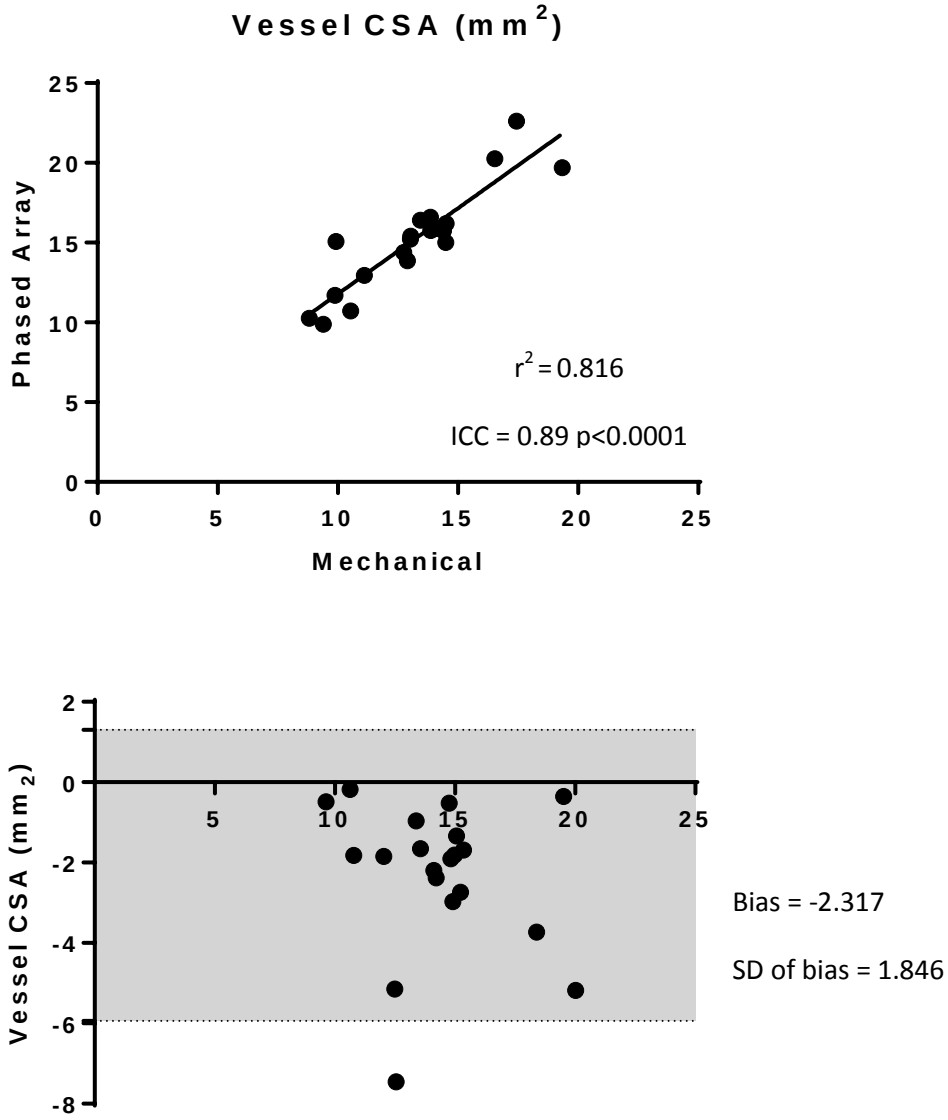

Figure 8. Mechanical vs. Phased Array catheters: Measurement of vessel CSA. Linear correlation chart with regression line and intraclass correlation coefficient (ICC). Corresponding Bland–Altman plots with mean bias, standard deviation and 95% limits of agreement displayed. (n=20)

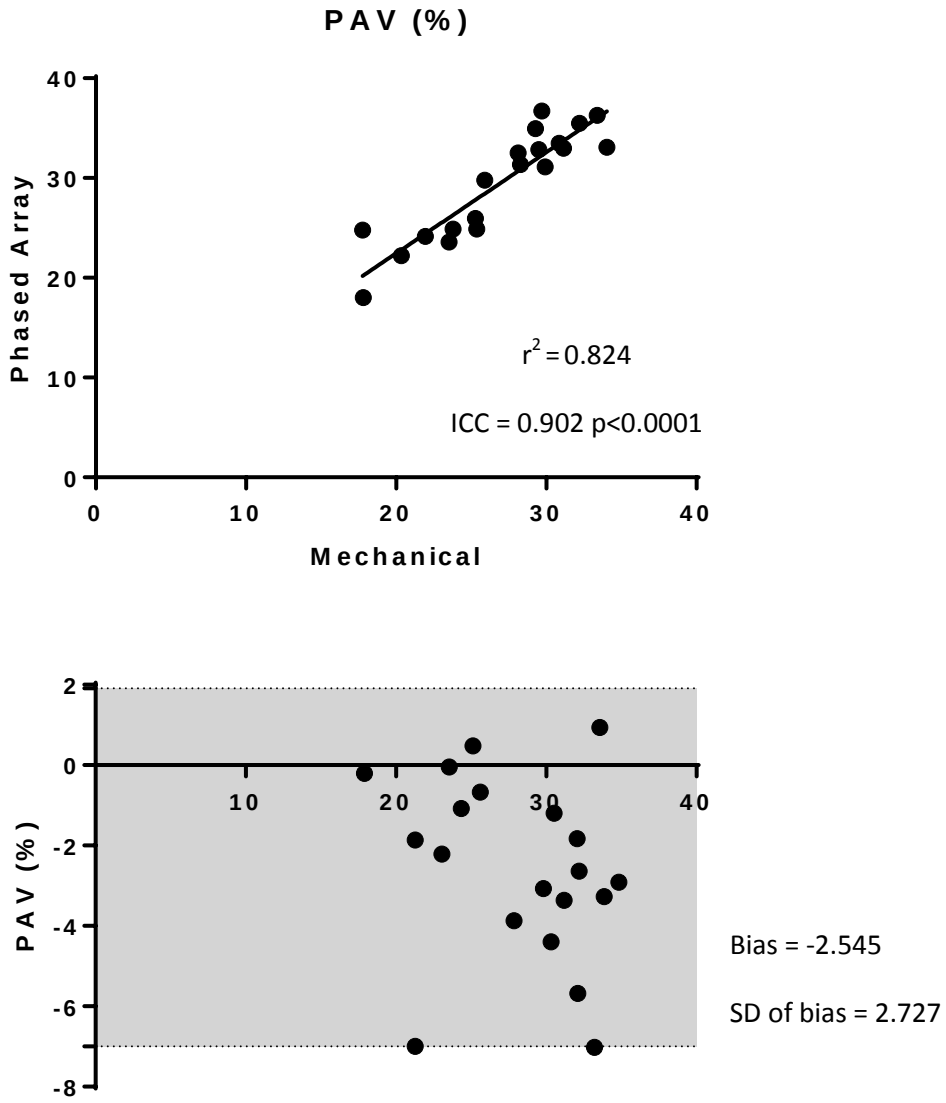

Figure 9. Mechanical vs. Phased Array catheters: Derived PAV. Linear correlation chart with regression line and intraclass correlation coefficient (ICC). Corresponding Bland–Altman plots with mean bias, standard deviation and 95% limits of agreement displayed. (n=20)

DISCUSSION

There is limited research available regarding the variability of catheter designs. It is important that despite the advances in plaque characterisation algorithms, the basic geometric accuracy of the catheters is assessed. In this study we performed a comprehensive assessment of three state-of-the-art commercially available IVUS catheters in both Phantom and in-vivo settings.

All three catheters utilised in the in-vitro study overestimated the known phantom CSA. The 20 MHz system provided the most accurate measurements, followed by the 45 MHz and the 40 MHz systems.

In the in-vivo experiments, we observed that the 20 MHz system consistently reported larger vessel CSA than the 40 MHz system. This could be attributed to the lower image quality of the 20 MHz system and a misinterpretation of the EEM when applying contours. This is consistent with the results of earlier clinical and animal studies[5,6]. It is unknown whether this difference represents an overestimation with the 20 MHz phased array or an underestimation with the 40 MHz mechanical catheters.

Mechanical and phased-array catheter systems both have specific advantages and limitations inherent to their designs. Mechanical catheters are subject to non-uniform rotational distortion (NURD) resulting from an uneven rotation of the driveshaft when the catheter has acute bends or when imaging tortuous vessels[7] However the utilisation of a single transducer enables the ultrasound signal to be transmitted in one direction, resulting in greater acoustic power and therefore a higher image resolution. In contrast, phased-array systems do not utilise a

driveshaft and therefore do not produce NURD or guidewire artefact. However the ultrasound signal is more disperse, leading to lower image resolution.

Emerging designs such as micro-motor catheters have the benefits of mechanical transducer such as having a single element with greater acoustic power and resolution but without the limitations inherent to utilising a driveshaft such as NURD and guidewire artefact[8,9]. Micro-motor catheters are not currently available commercially.

CONCLUSION

Atherosclerotic plaque burden is the most clinically important measurement and is used as a major endpoint in progression regression trials, the results of this study may have implications for serial IVUS imaging where small but possibly significant data in progression regression trials may if compromised if differing IVUS systems are ustilised in the same study.

REFERENCES

1. Mintz G, Nissen S, Anderson W, et al. American College of Cardiology Clinical Expert Consensus Document on Standards for Acquisition, Measurement and Reporting of Intravascular Ultrasound Studies (IVUS) A Report of the American College of Cardiology Task Force on Clinical Expert Consensus Documents. Journal of the American College of Cardiology 2001;37:1478-92.

2. Mintz G, Garcia-Garcia H, Nicholls S, et al. Clinical Expert Consensus Document on Standards for Acquisition, Measurement and Reporting of Intravascular Ultrasound Regression/Progression Studies. EuroIntervention 2011;6:1123-30.

3. Nishimura R, Edwards W, Warnes C, et al. Intravascularultrasound imaging: In vitro validation and pathologic correlation. Journal of the American College of Cardiology 1990;16:145-54.

4. Martin K, Spinks D. Mesaurements of the Speed of Sound in Ethanol/Water Mixtures. Ultrasound in Medicine and Biology 2001;27:289-91.

5. Rodriguez-Granillo G, Mc Fadden E, Aoki J, et al. In Vivo Variability in Quantitative Coronary Ultrasound and Tissue Characterization Measurements with Mechanical and Phased-Array Catheters. International Journal of Cardiovascular Imaging 2006:47-53.

6. Tardif J, Bertrand O, Mongrain R, et al. Reliability of Mechanical and Phased-Array Designs for Serial Intravascular Ultrasound Examinations: Animal and

Clinical Studies in Stented and Non-Stented Coronary Arteries. The International Journal of Cardiac Imaging 2000;16:365-75.

7. Nissen S. Application of Intravascular Ultrasound to Characterize Coronary Artery Disease and Assess the Progression or Regression of Atherosclerosis. The American Journal of Cardiology 2002;89:24-31.

8. Wang T, Lancée C, Beurskens R, et al. Development of a High-Speed Synchronous Micro Motor and its Application in Intravascular Imaging. Sensors and Actuators 2014;218:60-8.

9. Erbel R, Roth T, Koch L, et al. IVUS of micromotors for cardiovascular imaging. Minimally Invasive Therapy & Allied Technologies 1997;6:195-8.

Chapter 4:

A COMPARISON BETWEEN VH-IVUS AND iMAP PLAQUE CHARACTERISATION PLATFORMS

TABLE OF CONTENTS

INTRODUCTION

The propensity of atherosclerotic plaque to rupture is related to its histological composition[1-3]. Accurate in-vivo identification of vulnerable plaque therefore allows early management strategies to be implemented to prevent future coronary events[4]. Since its introduction, Intravascular Ultrasound (IVUS) has been established as the "gold standard" modality for vessel wall imaging[5] and the development of second-generation radiofrequency-based tissue characterisation platforms has altered approaches to atherosclerotic research by providing in-vivo quantification of plaque components.

Radiofrequency (RF)-based tissue characterization was developed to equalise the limitations of accurate visual analysis of greyscale IVUS images. It utilises methods of post-processing analysis of the radiofrequency signal in order to quantify plaque composition. Three such platforms have been developed and are commercially available through Virtual Histology-IVUS (Volcano Therapeutics, Rancho Cordova, California), iMap (Boston Scientific, Santa Clara, California) and Integrated Backscatter-IVUS (YD Co., Nara, Japan). Although all three systems have been validated, the VH-IVUS system is the most widely distributed[6].

Tissue characterisation is based on the concept that differing properties of plaque constituents alter the spectrum of the radiofrequency signal, thus allowing for in-vivo plaque analysis. These systems present the information as a two-dimensional colour-coded "tissue-map" providing more information than isolated interpretation of unprocessed images.

VH-IVUS uses a proprietary algorithm based on autoregressive analysis of the radiofrequency signal to quantify individual plaque components[7]. It was developed using explanted human coronary arteries obtained at autopsy and RF data was acquired from sections homologous for particular plaque components including fibrous, fibro-lipidic, necrotic and calcified[8]. Autoregressive modelling was then applied to raw RF data to produce a power spectrum which can be allocated using a statistical classification tree into one of the four plaque components[9,10]. When confronted with an unknown sample, VH-IVUS will therefore be able to classify the constituent to its closest match and generate a colour-coded "tissue map" for specific plaque components where fibrous plaque is green, fibrolipidic is green-yellow, necrotic is red and calcified plaque is white.

In comparison, iMap utilises a pattern recognition analysis obtained by fast-fourier transformation which converts RF data into a frequency spectrum and compares this against a histology-derived database to quantify plaque components. This approach uses the full RF spectrum (0-100MHz) which involves more calculations than VH-IVUS which utilises summarised data, potentially enhancing the probability of correct classification of plaque constituents[11]. iMap applies a different colour tissue map to classify plaque where fibrotic is light green, lipidic yellow, necrotic pink and calcified plaque is blue[12].

Although VH-IVUS and iMap have been validated in in-vitro[13] and ex-vivo[7,14] human coronary arteries there has been a paucity of data published on in-vivo images compared to histology. This study will for the first time provide a direct comparison between iMAP and VH-IVUS platforms in performing tissue characterisation compared to the current gold-standard of histology, in a rabbit model of atherosclerosis.

METHODS

All experiments and procedures performed were approved by the University of Adelaide Animal Ethics Committee and the Institute of Medical and Veterinary Science (IMVS) Animal Ethics Committee (M-2011-031; 17/11). Atherosclerotic lesions were generated in the rabbit abdominal aorta by a combination of a high cholesterol diet (0.2% supplemented) and balloon denudation of the endothelium in male New Zealand White rabbits (n=30, weight 3-3.5kg) as previously described. Animals were divided into 3 cohorts; 3 month (n=10), 6 month (n=10) and 9 month (n=10).

IVUS imaging protocol

Anaesthesia was induced using Ketamine (25mg/kg) and maintained with Isoflurane (1% in 4L/min O_2). The femoral artery was cannulated with a 23 gauge cannula and a 0.014" guidewire was advanced under fluoroscopy to the descending aortic arch. The IVUS catheters were then advanced over the guidewire. IVUS imaging of the abdominal aorta was performed using automatic pullbacks (0.5m/s for 70-90mm) from the renal arteries to the iliac bifurcation. This protocol was employed for both the mechanical 40 MHz Atlantis SR Pro catheters (Boston Scientific, Santa Clara, California) and the phased array 20MHz Eagle Eye Platinum catheter.

IVUS systems

iMap data was acquired using the Atlantis SR Pro 40 MHz catheter in conjunction with the iMap imaging system (3.6Fr) (Boston Scientific, Santa Clara, California). VH-IVUS data was acquired using the 20MHz Eagle Eye Platinum catheter (3.5Fr) in conjunction with the s5 imaging console (Volcano Therapeutics, Rancho Cordova, California). The VH-IVUS platform requires an ECG signal to generate the VH-IVUS frames; however the rabbit heart rate is significantly higher than the parameters of the software which is set to accepted ranges for humans. To overcome this, an ECG simulator (60BPM) was connected to the VH-IVUS console in order to supply a HR within the accepted range of the software.

All IVUS data was stored on a hard disk drive for offline analysis using echoPlaque 4.0.27 (Indec Systems, Santa Clara, CA, USA). Cross sectional images representing end diastole (ED) were analysed every 30 frames (0.5mm). Co-registration between VH-IVUS and iMAP frames was achieved by using MIB IVUS Lab 1.0.46 (Indec Systems, Santa Clara, CA, USA).

The leading edge of the lumen and external elastic membrane (EEM) were traced by manual planimetry. Vessel wall area (VWA) was defined as the area occupied between these leading edges. Tissue maps were automatically generated by the software. Individual plaque components were expressed as a percentage of the atheroma volume.

Euthanasia and sample preparation

Animals were euthanised by exsanguination under full anaesthesia after receiving heparin (100U/kg) to prevent post-mortem coagulation. The aorta was identified, dissected and immediately washed and perfused in Krebs* buffer (4^{o}C, pH7.4). Aortic specimens were carefully placed on a foam block and a Vernier calliper was used to accurately measure 5mm segments from the lowest renal artery, with a pin placed at each point. The sections were then fixed by immersion in 10% buffered formalin prior to sectioning.

*Krebs buffer solution (x10) 1.26 M NaCl, 25 mM KCl, 250 mM $NaHCO_3$, 12 mM, NaH_2PO_4, 12 mM $MgCl_2$, 25 mM $CaCl_2$. (pH 7.4)

Histopathology preparation

The abdominal aorta specimens were cut at the position of the pins and embedded in paraffin. 5µm sections were cut and stained with a combined Masson's Trichrome elastin and haematoxylin and eosin stains. A subset of aorta specimens were stained with Oil-Red-O for specific lipidic analysis (Figure 7). All sections were then digitised using a Nanozoomer photomicrograph (Hamamatsu Photonics, Hamamatsu, Japan) to allow for morphometric and compositional analysis.

Histological analysis

Quantification of plaque components was performed using Image-Pro Premier v9.1 (Media Cybernetics, Rockville, MD USA). A region of interest (ROI) was created by manually tracing luminal and vessel contours before semi-automated thresholding was applied to the 32-bit RGB segmented image.

Fibrous tissue was characterized in Masson's Trichrome stain as bundles of collagen fibers with little or no lipid accumulation. Fibrolipid tissue was characterised as loosely packed collagen bundles with interspersed extracellular lipid. Necrotic core was defined as a hypo-cellular cavity devoid of collagen and containing cellular debris and cholesterol clefts, while calcified tissue was defined as compact calcium crystals characterised by an intense staining on haematoxylin-eosin staining[15]. Individual plaque components were expressed as a percentage of plaque volume.

Statistical analysis

All values were represented as mean ± standard deviation. Analysis of plaque components reported by VH-IVUS, iMap and histology were performed using a one-way ANOVA model with post-hoc Tukey's multi-comparison test. Correlation between iMap and histology was assessed using linear regression and intraclass correlation coefficients (ICC). A p value <0.05 was considered statistically significant. Statistical analysis was performed using both SPSS 19.0 (SPSS Inc, Chicago, IL, USA) and GraphPad Prism 6.0 (GraphPad Software, San Diego, CA, USA).

RESULTS

Atherosclerotic lesions were successfully induced in the rabbit abdominal aorta by a combination of balloon denudation and high cholesterol feeding. IVUS imaging was successfully performed at 3, 6 and 9 month time-points. Analysis of iMap and VH-IVUS data was compared against ~~to~~ values obtained from histological analysis.

Histological analysis

The area of fibrosis remained unchanged across all time-points. No significant difference was observed between 3 months, 6 months and 9 months (71.62 ± 4.86%; p value; 73.48 ± 6.46%; p =0.71; 71.22 ± 5.34; p =0.5 respectively; Figure 1a).

There was a significant increase in lipid composition from 3 months to 6 months (1.32 ± 0.71% vs. 6.2±2.71%; p <0.001) and a further increase at 9 months (8.5 ± 2.74%; p <0.03; Figure 1b).

There was a significant increase in the area of necrosis from 3 months to 6 months (0.919 ± 0.52% vs. 4.79 ± 2.12%; p <0.001) but there was no further significant increase observed at 9 months (5.03 ± 2.85%; p =0.95; Figure 1c).

The area of calcification remained unchanged across all time-points. No significant difference was observed between 3 months, 6 months and 9 months (0.539 ± 0.51%; p value; 0.917 ± 0.64%; p =0.3; 0.494 ± 0.49%; p =0.11 respectively; Figure 1d).

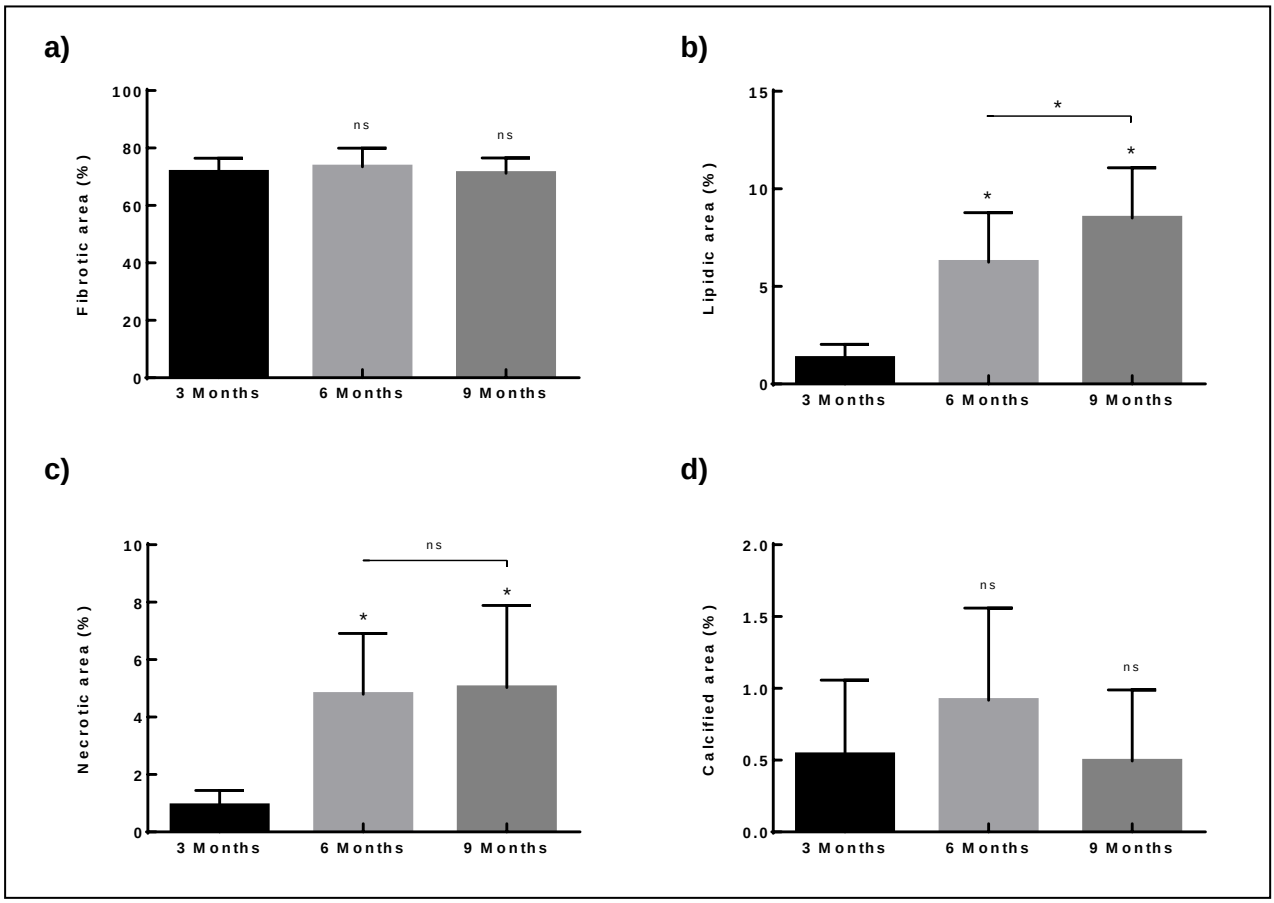

Figure 1. Histological analysis of abdominal aorta over time. 3 Months (n=10), 6 Months (n=10), 9 Months (n=10).

VH-IVUS and iMap analysis

There were no significant changes in VH-IVUS- and iMap-reported plaque component areas across all time-points. Data was therefore pooled across time-points for further analysis.

There were significant differences between all plaque components as reported by iMap and VH-IVUS. iMap analysis reported greater fibrotic areas compared to VH-IVUS (68.44 ± 7.7% vs. 27.81 ± 3.18%; $p < 0.0001$). iMap reported greater lipidic areas compared to VH-IVUS (5.18 ± 2.44% vs. 3.25 ± 4.76%; $p < 0.005$) but VH-IVUS reported greater necrotic areas compared to iMap (30.07 ± 6.26% vs. 16.18 ± 3.93%; $p < 0.0001$). VH-IVUS also reported greater calcified areas compared to iMap (37.5 ± 13.18% vs. 10.18 ± 4.97%; $p < 0.0001$). Linear regression analysis of iMap and histology measurements revealed poor correlation between both fibrotic and lipidc areas. (Figure 6)

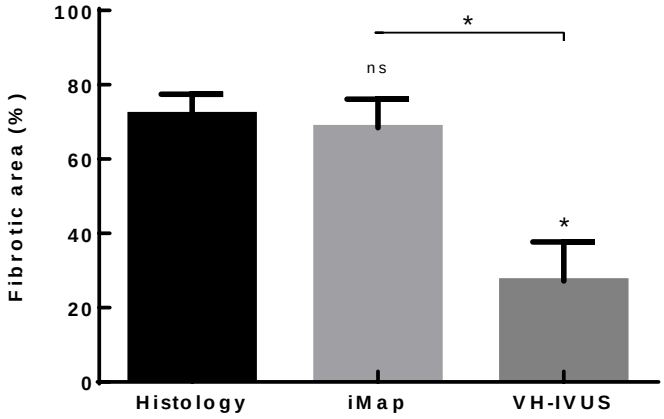

Figure 2. Pooled fibrotic areas as reported by histological analysis, iMap and VH-IVUS. There was no significant difference between iMap and histology (p =0.17). There was significant difference in fibrotic areas between VH-IVUS and histology (p <0.0001).

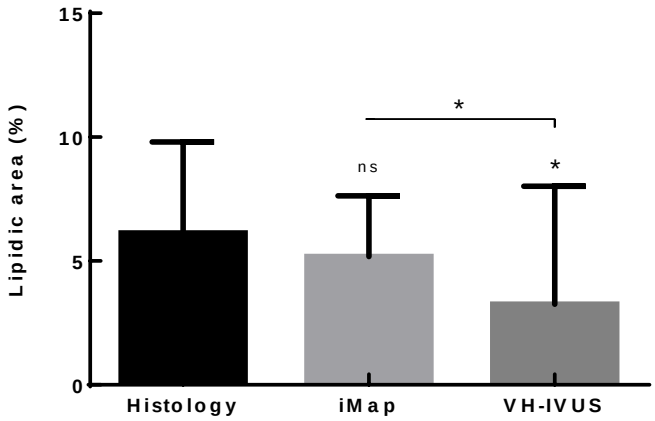

Figure 3. Pooled lipidic areas as reported by histological analysis, iMap and VH-IVUS. There was no significant difference between iMap and histology (p =0.87), however there was significant difference in lipidic areas between VH-IVUS and histology (p <0.0049).

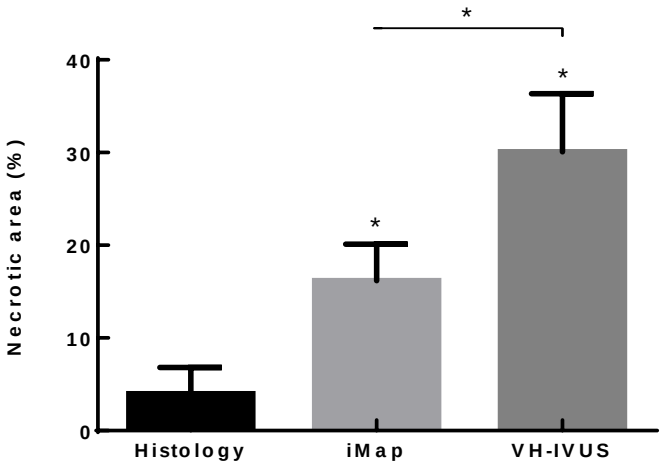

Figure 4. Pooled necrotic areas as reported by histological analysis, iMap and VH-IVUS. There was a significant difference between iMap and histology ($p < 0.0001$) as well as between VH-IVUS and histology ($p < 0.0001$).

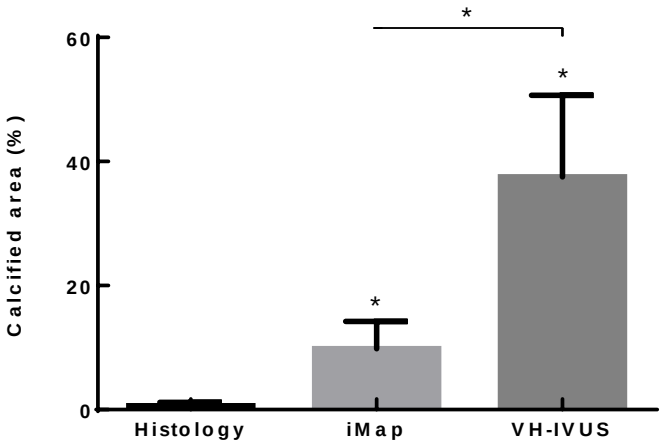

Figure 5. Pooled calcified areas as reported by histological analysis, iMap and VH-IVUS. There was a significant difference between iMap and histology ($p < 0.0001$) and also between VH-IVUS and histology ($p < 0.0001$).

Histology	Fibrotic (%)	Lipidic (%)	Necrotic (%)	Calcified (%)
3 Months	71.62 ± 4.86	1.32 ± 0.71	0.919 ± 0.52	0.539 ± 0.51
6 Months	73.48 ± 6.46	6.2 ± 2.71	4.79 ± 2.12	0.917 ± 0.64
9 Months	71.22 ± 5.34	8.5 ± 2.74	5.03 ± 2.85	0.494 ± 0.49

VH IVUS	Fibrotic (%)	Fibro-lipidic (%)	Necrotic (%)	Calcified (%)
3 Months	23.39 ± 7.4	1.50 ± 2.00	27.72 ± 4.21	45.10 ± 12.36
6 Months	30.01 ± 9	2.16 ± 3.44	32.9 ± 7.29	34.92 ± 10.17
9 Months	24.92 ± 13.22	4.59 ± 6.02	29.49 ± 6.08	35.00 ± 14.34
Pooled	27.81 ± 3.18	3.25 ± 4.76	30.07 ± 6.26	37.5 ± 13.18

iMap	Fibrotic (%)	Lipidic (%)	Necrotic (%)	Calcified (%)
3 Months	66.2 ± 4.65	4.15 ± 2.10	16.25 ± 2.21	13.35 ± 4.85
6 Months	69.77 ± 8.36	5.91 ± 3.18	16.11 ± 5.26	8.25 ± 2.87
9 Months	68.79 ± 8.67	5.27 ± 1.95	16.21 ± 3.88	9.71 ± 5.49
Pooled	68.44 ± 7.70	5.18 ± 2.44	16.18 ± 3.93	10.18 ± 4.97

Table 1. Tabular representation of individual plaque component quantification as measured by histological analysis, VH-IVUS and iMap plaque characterization platforms. 3 Months (n=10), 6 Months (n=10), 9 Months (n=10), Pooled (n=30).

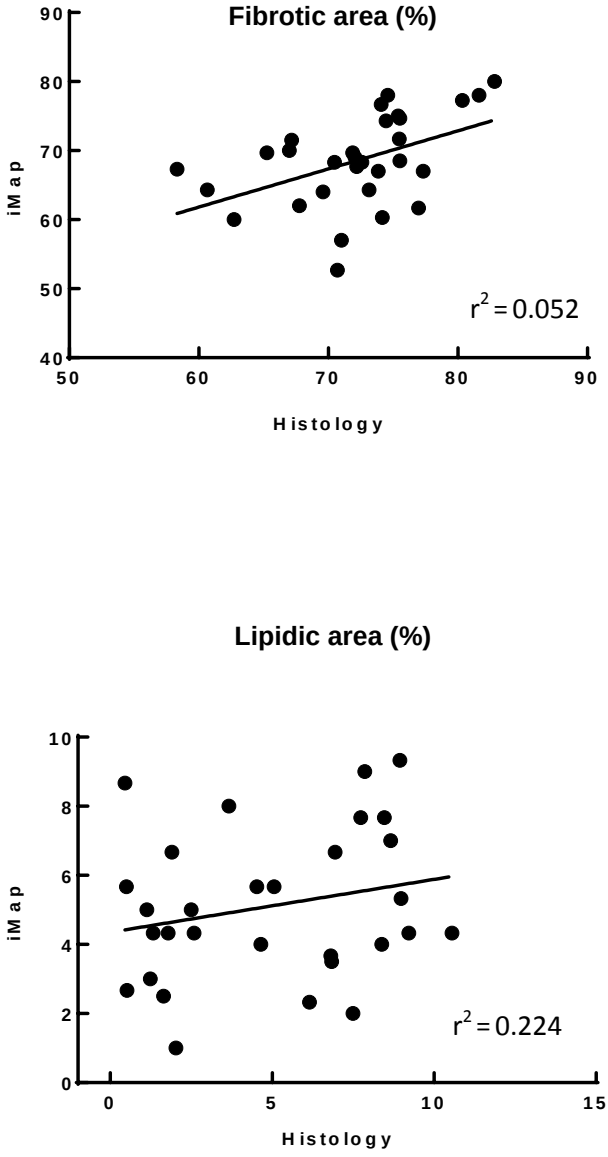

Figure 6. Percentage plaque composition comparison between iMap and histology. Linear correlation chart with regression line and intraclass correlation coefficient (ICC), (n=30).

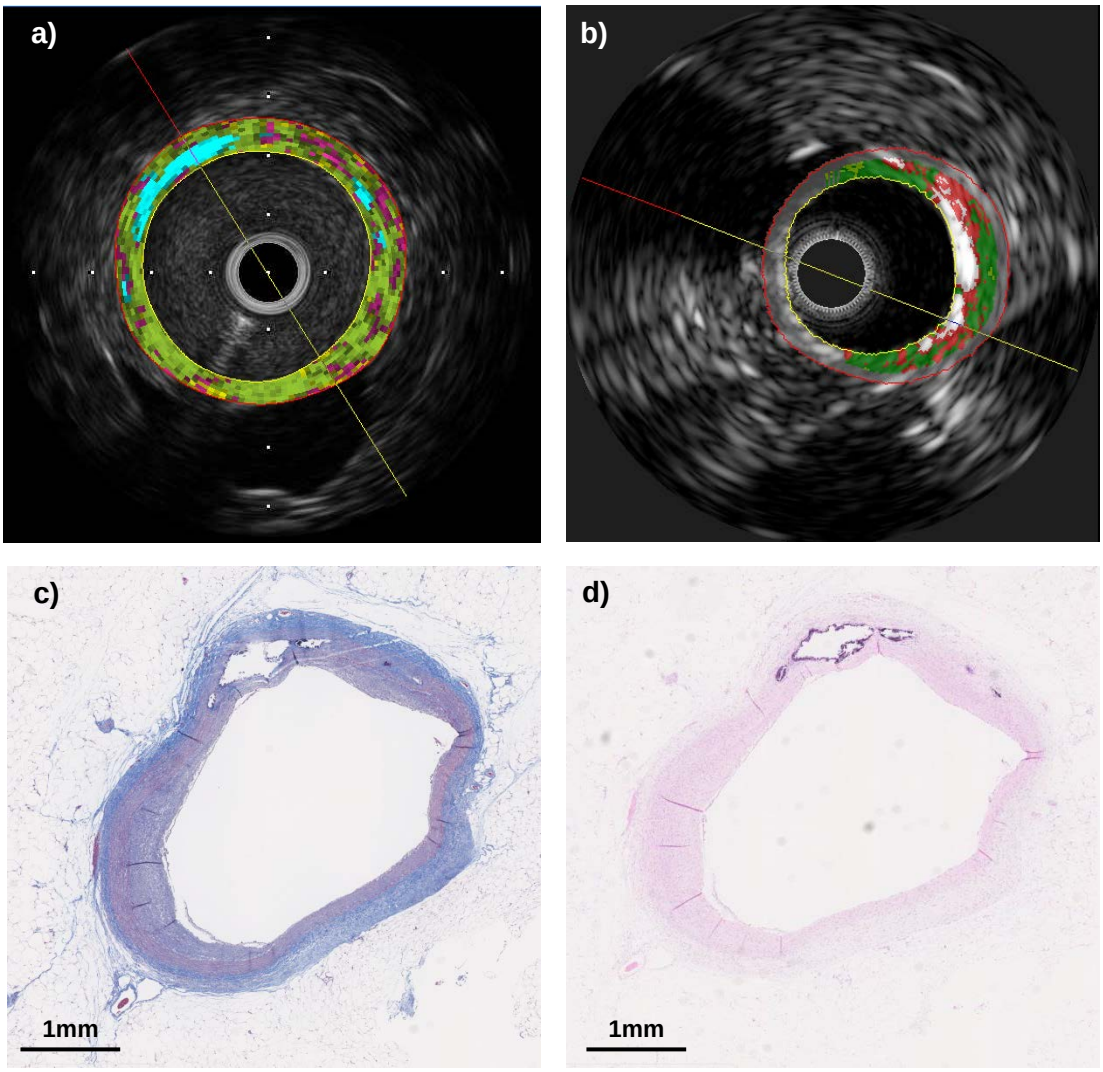

Figure 7. Plaque characterisation platform images with corresponding histological sections. a) iMap frame, b) VH-IVUS frame, c) Massons Trichrome stain, d) Haematoxylin and Eosin stain.

DISCUSSION

This study is the first to provide a direct comparison between VH-IVUS and iMap plaque characterisation platforms in conjunction with a direct comparison to plaque histology. Whilst we observed systematic differences between the two platforms for the quantification of individual plaque components, iMap reported values more congruent to histological values than VH-IVUS.

Overestimation of calcification

Both platforms overestimated calcification; VH-IVUS systematically reported higher values than iMap across all time-points. Most notably, calcification was represented by both platforms at baseline and 3-month time-points but this was not clearly observed on histological analysis and is not usually present in the rabbit model. This is most likely attributable to misinterpretation of bright reflections as calcification by both platforms, when in fact these reflections were often caused by catheter placement against the intimal surface.

Both VH-IVUS and iMap platforms assign a value for each pixel. The sum of the individual plaque components per frame must equal 100%, therefore if a region is misinterpreted (such as overestimation of calcification), values for other components are then biased. This complication is addressed in the generation of the NIRS chemogram where the algorithm assigns a non-viable pixel if there is insufficient data (such as guidewire artefact)[16].

Analysis of early plaque

VH-IVUS analysis imposes a grey medial band approximately 250μm thick in which no plaque composition analysis is performed. This was originally designed as a landmark to denote the outer edge of the vessel as it corresponds to the thickness of the media. It is however important to note that the media is frequently damaged in disease pathology including atherosclerosis[17]. The presence of this medial stripe makes analysis of early plaque composition at 3 months challenging. iMap does not impose any medial band.

Classification of guidewire artefact

The iMap system utilises a monorail catheter design where the guidewire lies adjacent to the transducer creating a narrow-angled shadow. iMap misinterprets this shadow as a necrotic region due to the low signal intensity of the shadow being interpreted as a hypo-echoic region. Given this inherent design flaw, iMap may over-represent the presence of a necrotic core which is a fundamental component of vulnerable plaque[18]. Recent advances in catheter design including the development of micro-motor catheters may minimise or even eliminate this flaw by providing the same imaging power of a mechanical catheter without the presence of guidewire artefact[19]. In contrast, the guidewire for the VH-IVUS phased-array catheter passes through the annular transducer array and therefore does not introduce a guidewire artefact.

Use in animal models

A recent study by Thim et al[20] reported no significant correlation between VH-derived necrotic core size to that measured by histology in a mini-pig model. In addition, a study by Granada et al[21] demonstrated that VH-IVUS was inaccurate in detecting the relative amount of individual plaque components within each individual corresponding histological image. It is important to note that plaque characterisation algorithms were developed using human atherosclerotic tissue therefore results obtained through use of specific animal models should be interpreted cautiously.

CONCLUSION

This novel study provides a direct comparison between iMap and VH-IVUS plaque characterisation platforms with a comparison to histology. The analysis provided significant and systematic variability in plaque composition analysis with both systems.

REFERENCES

1. Falk E, Shah P, Fuster V. Coronary Plaque Disruption. Circulation 1995;92:657-71.

2. Zaman A, Helft G, Worthley S, Badimon J. The Role of Plaque Rupture and Thrombosis in Coronary Artery Disease. Atherosclerosis 2000;149:251-66.

3. Yamagishi M, Terashima M, Awano K, et al. Morphology of Vulnerable Coronary Plaque: Insights from Follow-Up of Patients Examined by Intravascular Ultrasound Before an Acute Coronary Syndrome. Journal of the American College of Cardiology 1999;35:16-111.

4. Garcia-Garcia H, Goedhart D, Schuurbiers J, et al. Virtual Histology and Remodelling Index Allow In Vivo Identification of Allegedly High-Risk Coronary Plaques in Patients with Acute Coronary Syndromes: A Three Vessel Intravascular Radiofrequency Data Analysis. EuroIntervention 2006;2:338-44.

5. Nissen S, Gurley J, Booth D, et al. Intravascular Ultrasound Assessment of Lumen Size and Wall Morphology in Normal Subjects and Patients with Coronary Artery Disease. Circulation 1991;84:1087-99.

6. Tuzcu E, Weissman N. Imaging Coronary Artery Histology: A Virtual Pursuit? Circulation Cardiovascular Imaging 2010;3:348-50.

7. Nair A, Kuban B, Tuzcu E, Schoenhagen P, Nissen S, Vince D. Coronary Plaque Classification with Intravscular Ultrasound Radiofrequency Data Analysis. Circulation 2002;106:2200-6.

8. Lizzi F, Greenebaum M, Feleppa E, Elbaum M. Theoretical Framework for Spectrum Analysis in Ultrasonic Tissue Characterisation. Journal of the Acoustical Society of America 1983;73:1366-73.

9. Nair A, Calvetti D, Vince D. Regularized Autoregressive Analysis of Intravascular Ultrasound Backscatter: Improvement in Spatial Accuracy of Tissue Maps. IEEE Transactions on Ultrasonics Ferroelectrics and Frequency Control 2004;51:420-31.

10. Metha S, McCrary J, Frutkin A, Dolla W, Marso S. Intravascular Ultrasound Radiofrequency Analysis of Coronary Atherosclerosis: An Emerging Technology for the Assessment of Vulnerable Plaque. European Heart Journal 2007;28:1283-8.

11. Sathyanarayana S, Carlier S, Li W, Thomas L. Characterisation of Atherosclerotic Plaque by Spectral Similarity of Radiofrequency Intravascular Ultrasound Signals. EuroIntervention 2009;5:133-9.

12. Shin E, Garcia-Garcia H, Ligthart J, et al. In Vivo Findings of Tissue Characeristics Using iMap IVUS and Virtual Histology IVUS. EuroIntervention 2011;6:1017-9.

13. Nasu K, Tsuchikane E, Katoh O, et al. Accuracy of In Vivo Coronary Plaque Morphology Assessment: A Validation Study of In Vivo Virtual Histology

Compared With In Vitro Histopathology. Journal of the American College of Cardiology 2006;47:2405-12.

14. Nair A, Margolis P, Kuban B, Vince D. Automated Coronary Plaque Characterisation with Intravascular Ultrasound Backscatter: ex vivo Validation. EuroIntervention 2007;3:113-20.

15. Herck J, Meyer G, Ennekens G, Herck P, Herman A, Vrints C. Validation of In Vivo Plaque Characterisation by Virtual Histology in a Rabbit Model of Atherosclerosis. EuroIntervention 2009;5:149-56.

16. Pu J, Mintz G, Brilakis E, et al. In Vivo Characterization of Coronary Plaques: Novel Findings from Comparing Greyscale and Virtual Histology Intravascular Ultrasound and Near-Infrared Spectroscopy. European Heart Journal 2011;ehr380:1-12.

17. Garcia-Garcia H, Mintz G, Lerman A, et al. Tissue Characterisation Using Intravascular Radiofrequency Data Analysis: Recomendations for Acquisition, Analysis, Interpretation and Reporting. EuroIntervention 2009;5:177-89.

18. Vancraeynest D, Pasquet A, Roelants V, Gerber B, Vanoverschelde J. Imaging the Vulnerable Plaque. Journal of the American College of Cardiology 2011;57:1961-79.

19. Erbel R, Roth T, Koch L, et al. IVUS of micromotors for cardiovascular imaging. Minimally Invasive Therapy & Allied Technologies 1997;6:195-8.

20. Thim T, Kallestrup M, Wallace-Bradley D, et al. Unreliable Assessment of Necrotic Core by VHTM IVUS in Porcine Coronary Artery Disease. Circulation Cardiovascular Imaging 2010;3:384-91.

21. Granada J, Wallace-Bradley D, Win H, et al. In Vivo Plaque Characterization Using Intravascular Ultrasound-Virtual Histology in a Procine Model of Complex Coronary Lesions. Arteriosclerosis, Thrombosis, and Vascular Biology 2007;27:387-93.

Chapter 5:

SERIAL IVUS ANALYSIS OF ENDOTHELIAL DYSFUNCTION AND ATHEROSCLEROSIS PROGRESSION

TABLE OF CONTENTS

INTRODUCTION

Endothelial dysfunction is a systemic process associated with conditions predisposing to atherosclerosis including smoking, hypertension, hypercholesterolemia and diabetes[1]. It is believed to be the earliest precursor to atherosclerosis[2] and has been shown to be an independent predictor of cardiac events[3] however the correlation between endothelial function and regional plaque burden progression over time remains unknown. This study aimed to utilise serial Intravascular Ultrasound (IVUS) imaging to determine the in-vivo relationship between developing plaque burden and endothelial function in an experimental rabbit model of atherosclerosis.

Previous studies have demonstrated a strong correlation between the extent of atherosclerosis and its rate of progression with risk[4]. IVUS-derived plaque burden has also been shown to be an independent predictor of cardiac events[5]. IVUS has also been used to demonstrate an association between positive vascular remodelling and larger plaque areas with unstable clinical presentations[6].

In this study, serial 40MHz IVUS was utilised to image vessel walls and assess endothelium vasomotor reactivity to investigate the relationship between progressive endothelial dysfunction and atherosclerosis development in the rabbit abdominal aortic model. The quantification of endothelial function can then be used to determine risk of acute coronary events and provide further insights into clinical management of atherosclerosis.

METHODS

All procedures were approved by the University of Adelaide Animal Ethics Committee and the Institute of Medical and Veterinary Science (IMVS) Animal Ethics Committee (M-2011-031; 17/11). Atherosclerotic lesions were induced in rabbit abdominal aortas through a combination of a high cholesterol diet (0.2% supplemented, Glen Forest Stock Feed, Western Australia) and balloon denudation of the endothelium in male New Zealand White rabbits (n=26, weight 3-3.5kg) as described previously[7,8]. Animals were divided into 3 cohorts; 3 month (n=10), 6 month (n=8) and 9 month (n=8).

IVUS Imaging protocol

IVUS imaging and endothelial function assessment of the rabbit abdominal aorta was performed using the iLab imaging console and 40MHz Atlantis SR Pro catheters (Boston Scientific, Natick, MA, USA) at baseline and 3 months (n=10), 6 months (n=8) and 9 months (n=8) of disease progression. Anaesthesia was induced with 25mg/kg Ketamine (Ketamine Hydrochloride, Fort Dodge Animal Health, Fort Dodge, USA) and maintained with 1% Isoflurane in 4L/min O_2 (Isoflurane, Bomac Animal Health, NSW, Australia). The femoral artery was identified and cannulated with a 24 gauge cannula through which a 0.014” guidewire was introduced and advanced to the aortic arch. The IVUS catheter was guided via fluoroscopy (Phillips BV-24) to the lowest branch of the renal artery and IVUS catheter placement was confirmed by manual IVUS imaging. Automatic pullbacks were performed (0. 5mm/s) for a length of 75mm.

IVUS assessment of endothelial function

Endothelial function was assessed by incremental infusions of the endothelial-dependent vasodilator Acetylcholine (Ach; 0.05 [LOW], 0.5 Intermediate [INT], 2.5 [HIGH] µg/kg/min; Miochol-E Acetylcholine chloride, Bausch & Lomb, Auckland, New Zealand) followed by endothelial-independent Glyceryl Trinitrate (GTN; 3µg/kg/min; DBL Glyceryl Trinitrate Concentrate Injection, Hospira, Victoria, Australia). ACh and GTN were delivered via the marginal ear vein using a Gemini PC-2 infusion pump (IMED Corporation, San Diego, CA).

IVUS Image analysis

Generated IVUS images were transferred to an external hard disk drive for offline analysis using echoPlaque v3.0.53 (Indec Medical Systems, Santa Clara, USA). Cross sectional IVUS images representing end diastole (ED) were analysed at every 30 frames (0.5mm) for a 15mm segment of aorta per animal.

The leading edge of the lumen and the external elastic membrane (EEM) were manually traced. Vessel wall area (VWA) as a marker of atherosclerosis was defined as the area occupied between these limits. Plaque burden [% atheroma volume (PAV)] was calculated as the proportion of the entire vessel CSA occupied by atherosclerotic plaque.

$$PAV = \sum [(EEM_{area} - Lumen_{area}) / \sum EEM_{area}] \times 100$$

To calculate vasomotor responses following ACh and GTN infusions, the luminal contours were measured following each pullback and were reported as a %Δ from baseline.

Statistical analysis

For the analysis of vessel parameters (lumen CSA, vessel CSA, VWA, PAV) and vasomotor responses to ACh and GTN at multiple time points, a one-way ANOVA model with post hoc Tukey multi-comparison test was applied. All values are expressed as mean ± standard deviation, with a p value of <0.05 considered to be statistically significant. All statistical analysis was performed with GraphPad Prism v6.03 (GraphPad Software, San Diego, CA).

RESULTS

Atherosclerotic lesions were induced in 26 animals using a combination of a high cholesterol diet and balloon denudation of the abdominal aorta. IVUS imaging and endothelial function assessments were performed without complications. The typical duration of the endothelial function tests were 10-12 minutes with the entire procedure taking approximately 20-30 minutes.

Weights

There was an initial significant increase in weight from baseline to 3 months (3.37±0.18kg and 3.67±0.28kg respectively; $p<0.01$). There was no significant difference in weight at 6 months 3.55±0.24kg ($p=0.45$) however there was a significant increase in weight at 9 months compared to baseline (3.76±0.39kg ; $p<0.005$; Figure 1).

Cholesterol diet

The mean baseline serum cholesterol was 0.4±0.16mmol/L. There was a significant increase 3 months later 1.11±0.32mmol/L ($p<0.001$). There was a significant decrease at 6 months 0.78±0.15mmol/L ($p<0.02$) however serum cholesterol remained significantly elevated compared with baseline ($p<0.007$). There was no significant difference in serum cholesterol levels observed at 9 months 0.8±0.19mmol/L ($p=0.99$; Figure 2).

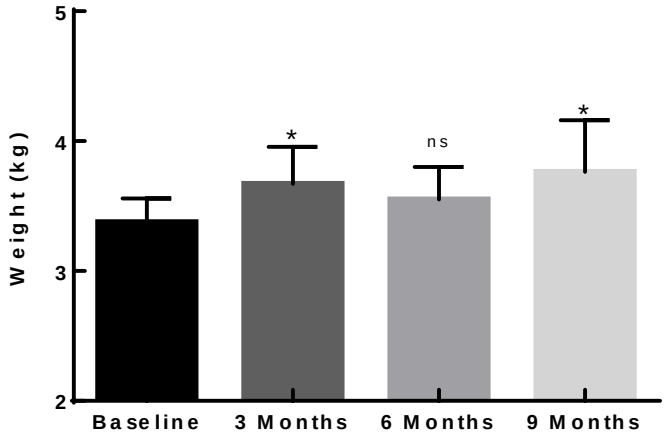

Figure 1. Recorded animal weights across all time points.

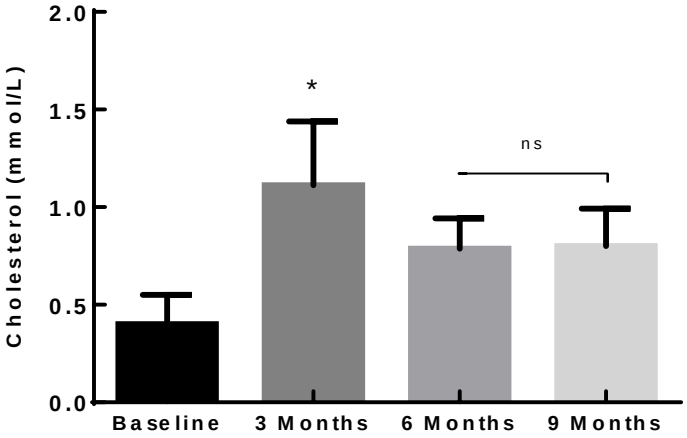

Figure 2. Serum cholesterol across all time points.

Vascular Remodelling

There was a small but significant increase in lumen CSA from baseline and 3 months (7.91±0.46mm^2 vs. 8.73±0.42mm^2; $p<0.05$). There was no significant difference in lumen CSA between 3 months and 6months (8.95±0.71mm^2; $p=0.98$) and between 6 months and 9 months (8.99±0.97mm^2; $p=0.21$; Figure 3a).*

There was no significant difference between vessel CSA from baseline and 3 months (9.72±0.57mm^2 vs. 10.51±0.47mm^2; $p=0.66$). There was also no significant difference between 3 months and 6months (12.06±1.59mm^2; $p=0.19$) however there was a significant increase in vessel CSA between baseline and 6 months ($p<0.01$). There was no significant difference in vessel CSA between 6 months and 9 months (12.83±1.91mm^2; $p=0.2$) however there was a significant increase in vessel CSA between 3 months and 9 months ($p<0.019$; Figure 3b).*

There was no significant difference in VWA between baseline and 3 months (1.69±0.28mm^2 vs. 1.77±0.12mm^2; $p=0.66$) however there was a significant increase between 3 months and 6 months (3.18±0.94mm^2; $p<0.0005$) and a greater increase between 6 months and 9 months (4.16±0.69mm^2; $p<0.01$; Figure 3c).*

There was no significant difference in percent atheroma volume (PAV) between baseline and 3month (18.47±0.92% vs. 16.93±0.99%; $p=0.54$). There was a significant increase between 3 months and 6 months (27.85±2.96%; $p<0.0001$) and a further increase between 6 months and 9 months (32.53±3.24%; $p<0.0007$; Figure 3d).*

* Table 2.

	Baseline **(n=10)**	**3 Months** **(n=10)**	**6 Months** **(n=8)**	**9 Months** **(n=8)**
Lumen CSA (mm^2)	7.91 ± 0.46	8.73 ± 0.42	8.95 ± 0.71	8.99 ± 0.97
Vessel CSA (mm^2)	9.72 ± 0.57	10.51 ± 0.47	12.06 ± 1.59	12.83 ± 1.91
VWA (mm^2)	1.69 ± 0.28	1.77 ± 0.12	3.18 ± 0.94	4.16 ± 0.69
PAV (%)	18.47 ± 0.92	16.93 ± 0.99	27.85 ± 2.96	32.53 ± 3.24

Table 1. Serial analysis of atherosclerosis progression and vessel remodelling. CSA = cross sectional area, VWA = vessel wall area, PAV = percentage atheroma volume.

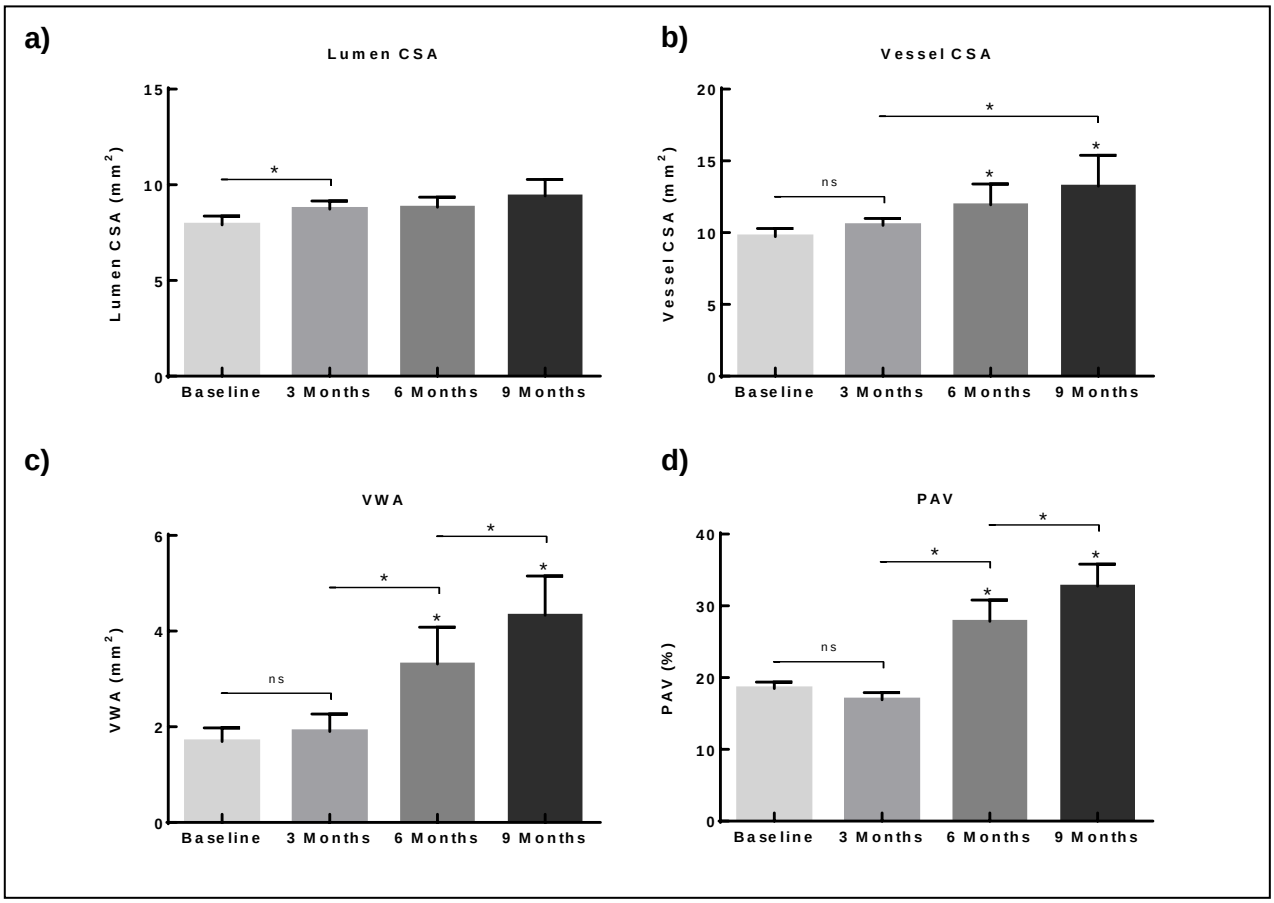

Figure 3. Serial analysis of atherosclerosis progression and vessel remodelling. a) Lumen CSA, b) Vessel CSA, c) VWA = vessel wall area, d) PAV = % Atheroma volume. ns = not significant ($p>0.05$).

Endothelial function

Infusion of ACh in disease-free animals at baseline resulted in dose-dependent vasodilation of the abdominal aorta (7.61±1.47% [low], 10.69±2.25% [int], 12.48±3.56% [high]).*

An attenuated ACh vasodilator response was observed at 3-month disease progression (3.25±1.78% [low], 7.15±3.12% [int], 10.48±3.68% [high]) with significantly reduced responses to low ($p<0.0001$) and intermediate dose ($p<0.0001$) ACh.*

At 6 months, low-dose ACh infusion resulted in minimal vasodilation (0.69±1.5% [low]) and paradoxical vasoconstriction was observed at both mid and high dose infusions (-5.33±3.11% [mid], -8.42±3.96% [high]). Dose-dependent vasoconstriction in response to ACh infusion was observed at 9-month disease progression (-4.64±2.11% [low], -9.255±2.433% [mid], -15.49±2.36% [high]).*

The vasodilatory response to GTN was preserved across all time-points 17.20±3.34% [baseline] 14.28±2.67% [3 months] 16.17±3.06% [6 months] 15.94±3.99% [9 months].*

* Table 2

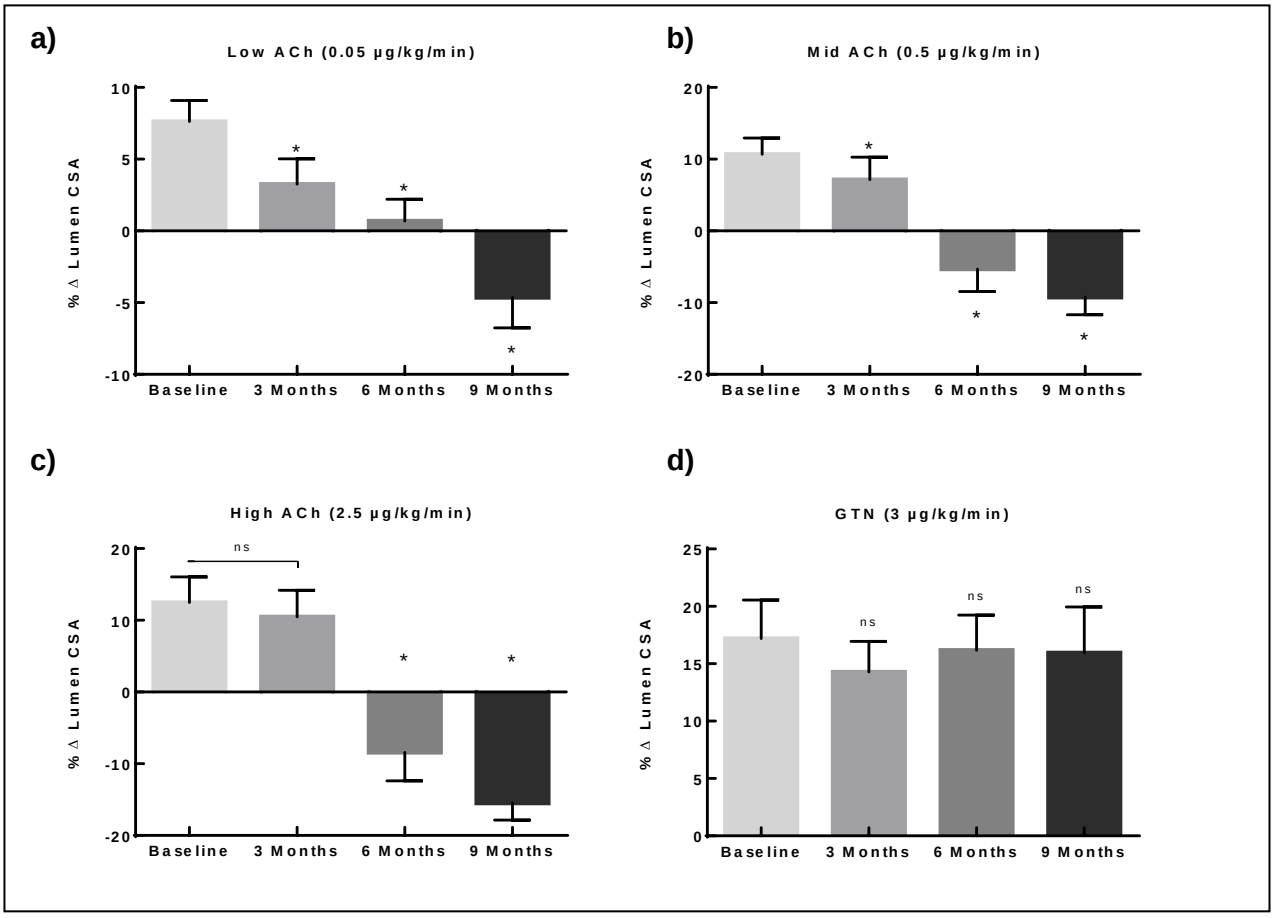

Figure 4. Serial analysis of endothelial function. Vasomotor responses were measured over time against a) Low ACh 0.05 µg/kg/min, b) Mid ACh 0.5 µg/kg/min, c) High ACh 2.5 µg/kg/min, d) GTN 3 µg/kg/min. ns = not significant ($p>0.05$).

	Baseline (n=10)	**3 Months (n=10)**	**6 Months (n=8)**	**9 Months (n=8)**
Low Ach (0.05 µg/kg/min)	7.61 ± 1.47%	3.25 ± 1.78%	0.69 ± 1.5%	-4.64 ± 2.11%
Int ACh (0.5 µg/kg/min)	10.69 ± 2.25%	7.15 ± 3.12%	-5.33 ± 3.11%	-9.255 ± 2.433%
High ACh (2.5 µg/kg/min)	12.48 ± 3.56%	10.48 ± 3.68%	-8.42 ± 3.96%	-15.49 ± 2.36%
GTN (3 µg/kg/min)	17.20 ± 3.34%	14.28 ± 2.67%	16.17 ± 3.06%	15.94 ± 3.99%

Table 2. Endothelial function assessment. 40MHz IVUS derived luminal CSA in response to ACh and GTN across all time-points.

DISCUSSION

Endothelial dysfunction is considered to be a key factor in the initiation and development of atherosclerosis. This study utilised serial 40MHz IVUS imaging to systematically assess the in-vivo relationship between endothelial function and vascular remodelling during the progression of atherosclerosis in the rabbit aorta, to assess the correlation between endothelial function and regional plaque burden progression over time.

The combination of balloon denudation of the aorta and high cholesterol diet stimulates the progression of atherosclerosis in the rabbit aorta in a process similar to positive remodelling observed in the early stages of human atherosclerotic progression[9]. A progressive increase in atherosclerotic burden is evident by increases in vessel wall area and PAV, without compromise or lumen narrowing for the duration of the study (Figure 3). The increasing vessel wall allows for increased plaque burden without causing luminal stenosis. Angiographic analysis would most likely reveal no evidence to suggest atherosclerosis in these animals, as inferred from a relatively consistent lumen CSA over the 9-month duration of the study. Positive remodelling of the rabbit aorta has previously been described[8] and we have demonstrated this process with the associated changes in endothelial function over time.

Endothelial function assessment has previously been performed non-invasively by transcutaneous ultrasound in the rabbit model[10,11]. This method however is limited by poor image resolution, it can assess changes in luminal diameter, but not provide accurate structural composition of the vessel wall. In contrast, IVUS provides both in-vivo functional assessment of endothelial function and structural information by providing high-resolution imaging of the vessel wall.

Initial clinical studies by Ludmer *et al*[12] had provided mechanistic associations between endothelial dysfunction and atherogenesis. Endothelial dysfunction was thought to occur prior to intimal lesion formation in an experimental rabbit model[13]. It has since been shown that endothelial dysfunction in conjunction with the presence of cardiovascular risk factors precedes atheroma formation[2,14]. Endothelial dysfunction may also be involved in stimulating plaque progression, instability and increases the propensity to rupture[15,16].

In the current study, endothelial dysfunction was initially observed at the initial follow-up at 3months to be an attenuated response to ACh compared to baseline results (Figure 4). This change in endothelial response preceded any significant structural changes in vessel wall area. Endothelial dysfunction progression was proportional to increasing plaque burden throughout the study.

Whilst plaque in the rabbit model remains stable[17] thus somewhat reducing its clinical relevance in investigating the association between endothelial dysfunction and plaque vulnerability, this study demonstrates that endothelial dysfunction precedes structural changes in the rabbit aorta. This in conjunction with the occurrence of positive remodelling therefore makes it a good experimental model for early clinical atherosclerosis development.

CONCLUSION

This study provides serial analysis of the association between endothelial function and progressive atherosclerosis in the rabbit aorta. IVUS analysis documented that progressive endothelial dysfunction occurs with increasing plaque burden. We also observed that the rabbit aorta undergoes remodelling analogous to positive remodelling observed clinically in early atherosclerosis.

REFERENCES

1. Landmesser U, Hornig B, Drexler H. Endothelial Function: A Critical Determinant in Atherosclerosis. Circulation 2004;27:11-33.

2. Celermajer D, Sorensen K, Bull C, Robinson J, Deanfield J. Endothelium-Dependent Dilation in the Systemic Arteries of Asymptomatic Subjects Relates to Coronary Risk Factors and their Interaction. Journal of the American College of Cardiology 1994.

3. Schächinger V, Britten M, Zeiher A. Prognostic Impact of Coronary Vasodilator Dysfunction on Adverse Long-Term Outcome of Coronary Heart Disease. Circulation 2000;101:1899-906.

4. Lorenz M, Markus K, Bots M, Rosvall M, Sitzer M. Prediction of Clinical Cardiovascular Events with Carotid Intima-Media Thickness: A Systematic Review and Meta-Analysis. Circulation 2007;115:459-67.

5. Nicholls S, Hsu A, Wolski K, et al. Intravascular Ultrasound-Derived Measures of Coronary Atherosclerotic Plaque Burden and Clinical Outcomes. Journal of the American College of Cardiology 2010.

6. Shoenhagen P, Ziada K, Kapadia S, Crowe T, Nissen S, Tuzcu E. Extent and Direction of Arterial Remodelling in Stable Versus Unstable Coronary Syndromes. Circulation 1999;101:598-603.

7. Skinner M, Yuan C, Mitsumori L, et al. Serial Magnetic Resonance Imaging of Experimental Atherosclerosis Detects Lesion Fine Structure, Progression and Complications In Vivo. Nature 1995;1:69-73.

8. Worthley S, Helft G, Fuster V, et al. Serial In Vivo MRI Documents Aretrial Remodeling in Experimental Atherosclerosis. Circulation 2000;101:586-9.

9. Glagov S, Weinsberg E, Zarins C, Stankunavicius R, Kolettis G. Compensatory Enlargement of Human Atherosclerotic Coronary Arteries. New England Journal of Medicine 1987;316:1371-5.

10. Drolet M, Plante E, Battistini B, Couet J, Arenault M. Early Endothelial Dysfunction in Cholesterol-Fed Rabbits: A Non-Invasive In Vivo Ultrasound Study. Cardiovascular Ultrasound 2004;1:1-8.

11. Hiss K, Steioff K, Loehn M, Ruetten H. Transcutaneous Vascular Ultrasound in Hypercholesterolaemic Rabbits: A New Method to Evaluate Endothelial Function. Laboratory Animals 2006;40:80-6.

12. Ludmer P, Selwyn A, Shook T, et al. Paradoxical Vasoconstriction Induced by Acetylcholine in Atherosclerotic Coronary Arteries. New England Journal of Medicine 1986;17:1046-51.

13. Mano T, Masuyama T, Yamamoto K, et al. Endothelial Dysfunction in the Early Stage of Atherosclerosis Precedes Appearance of Intimal Lesions Assessable with Intravascular Ultrasound. American Heart Journal 1996.

14. Zeiher A, Drexler H, Wollschläger H, Just H. Modulation of Coronary Vasomotor Tone in Humans. Progressive Endothelial Dysfunction with Different Early Stages of Coronary Atherosclerosis. Circulation 1991;83:391-401.

15. Lerman A, Zeiher A. Endothelial Function: Cardiac Events. Circulation 2005;111:363-8.

16. Bogaty P, Hackett D, Davies G, Maseri A. Vasoreactivity of the Culprit Lesion in Unstable Angina. Circulation 1994;90:5-11.

17. Abela G, Picon P, Friedl S, et al. Triggering of Plaque Disruption and Arterial Thrombosis in an Atherosclerotic Rabbit Model. Circulation 1995;91:776-84.

Chapter 6:

METHODOLOGY FOR NON-INVASIVE ENDOTHELIAL FUNCTION ASSESSMENT OF THE RABBIT AORTA USING 1.5T MRI

TABLE OF CONTENTS

INTRODUCTION

The normal endothelium exerts a vasoprotective effect including the control of thrombosis and thrombolysis, inhibition of inflammatory responses by mediating platelet and leukocyte interactions with the vessel wall and the regulation of vascular tone and growth by regulation of the underlying smooth muscle cells[1]. These processes are largely mediated by the endothelium derived nitric oxide (NO)[2].

Endothelial dysfunction is a characteristic feature of patients at risk for coronary atherosclerosis. Endothelial dysfunction results in increased endothelial permeability, platelet aggregation, leukocyte adhesion and cytokine production[1]. Endothelial dysfunction is associated with a decreased production or bioavailability of NO and therefore the impairment of NO-mediated vasomotor and anti-thrombotic effects[3]. Endothelial dysfunction is a systemic process that has been shown to be an independent predictor of major cardiac events[4]. Therefore the quantification of endothelial function may be used to determine risk and improve patient outcomes.

Quantification of endothelial-dependent vasomotion in response to pharmacological or physiological stimuli has been the most widely used end point for assessment of endothelial function[5]. Endothelial function of the coronary circulation can be assessed invasively by infusion of ACh and quantification of vasomotion with quantitative coronary angiography[6,7] or with Intravascular Ultrasound (IVUS)[8]. The assessment is based on the findings of Furchgott and Zawadzki[9,10], that ACh induces vascular smooth muscle to release NO from vessels with an intact endothelium, resulting in vasodilatation, but causes vasoconstriction

in subjects with endothelial dysfunction, as a result of a direct muscarinic smooth muscle vasoconstrictor effect[5,6].

Non-invasive assessment of endothelial function is currently limited to the peripheral circulation[11], such as flow mediated dilation (FMD) which utilises ultrasound to measure the diameter of the brachial artery before and after increasing shear stress induced by reactive hyperaemia[12].

The non-invasive assessment of vasodilation in response to endothelial dependent and independent stimuli allows serial analysis of endothelial function and eliminates the risk inherent from invasive procedures. It would allow multiple time-points to be assessed allowing for dynamic changes to be identified. Magnetic Resonance Imaging (MRI) is a non-invasive technique which is capable of providing both functional and structural information of atherosclerotic vessels.

We have designed a novel method using 1.5T MRI to perform serial non-invasive endothelial function assessment in the rabbit aortic model of atherosclerosis, which has previously been utilised in MRI studies[13,14]. We assessed changes in luminal CSA in response to Acetylcholine and GTN at baseline and 3 months following atherosclerosis initiation by balloon denudation of the aorta and high cholesterol feeding. The results were compared to those obtained with 40MHz IVUS as the gold standard.

METHODS

All procedures were accepted by the University of Adelaide Animal Ethics Committee and the Institute of Medical and Veterinary Science (IMVS) Animal Ethics Committee. Male New Zealand White rabbits (n=20, 12 weeks, 3-3.5kg) on an atherogenic diet (0.2% cholesterol) were used, these animals were part of an ongoing study. All 20 animals underwent endothelial function assessment with IVUS and MRI at baseline prior to initiating atherosclerosis by balloon denudation of the abdominal aorta. Endothelial function was then reassessed with IVUS and MRI 3 months later in 15 animals.

Ear vein cannulation

To allow infusion of vasoactive drugs for both IVUS and MRI tests the marginal ear vein was cannulated. A 24 gauge Jelco cannula was used to cannulate the marginal ear vein. To assist cannulation the ear was immersed in warm water.

IVUS Imaging protocol

IVUS imaging of the abdominal aorta was performed using the iLab imaging console and the 40 MHz Atlantis SR Pro catheters (Boston Scientific, Natick, MA, USA). Anaesthesia was induced with 25mg/kg Ketamine (Ketamine Hydrochloride, Fort Dodge Animal Health, Fort Dodge, USA) and maintained with 1% Isoflurane in 4L/min O_2 (Isoflurane, Bomac Animal Health, NSW, Australia). The femoral artery was identified by and cannulated with a 24 gauge Jelco through which a 0.014” guidewire was introduced and advanced to the aortic arch. The

IVUS catheter was guided via fluoroscopy (Phillips BV-24) to the lowest branch of the renal artery, IVUS catheter placement was confirmed by manual imaging. Automatic pullbacks were performed (0. 5mm/s) for a length 75mm.

IVUS assessment of endothelial function

Immediately following baseline IVUS imaging, ACh (0.5µg/kg/min) was infused via the marginal ear vein for 2 minutes to reach steady state and was continued whilst an automated pullback was performed (0.5mm/s) from the renal arteries to the iliac bifurcation. This was repeated for GTN infusions (3µg/kg/min) (DBL Glyceryl Trinitrate Concentrate Injection, Hospira, Victoria, Australia). ACh and GTN were delivered using a Gemini PC-2 (IMED Corporation, San Diego, CA) infusion pump.

IVUS Image analysis

The IVUS images were transferred to PC for offline analysis using echoPlaque v3.0.53 (Indec Medical Systems, Santa Clara, USA). The renal artery branches were identified from which the corresponding sections of aorta to MRI were identified. Cross sectional IVUS images representing end diastole (ED) were selected and luminal contours were manually traced to determine luminal cross-sectional area (CSA). Vasomotor responses in response to ACh and GTN were reported as a %Δ from baseline.

MRI Imaging protocol

MRI imaging was performed using a 1.5T Siemens MAGNETOM Sonata system and a human knee coil (Siemens Medical Solutions, Erlangen, Germany). The rabbits were placed in the supine position in the isocentre of the scanner; anaesthesia was maintained with 1% Isoflurane in 4L/min O_2 (Isoflurane, Bomac Animal Health, NSW, Australia) delivered via nosecone. The thorax was shaved and cleaned with ethanol before attaching ECG electrodes. A 3 lead ECG was obtained before connecting the knee coil. A foam block was positioned between the rabbit and the knee coil, this allowed optimum contact of the ECG electrodes and also reduced respiratory motion artefacts. All MRI images were free breathing, ECG-gated acquisitions.

Axial Time of Flight (TOF) Maximum Intensity Projection (MIP) sequences were performed in both coronal and transverse slices to localise the aorta and the renal arteries (Figure 1). These images were obtained to plan the following sequences.

Prospectively gated (alternate R waves) FLASH (Fast Low Angle Shot) cine sequences were used to generate diagnostic quality images. The imaging parameters used were: Field of view (140x96mm), Phase FOV (68.8%) Slice thickness (6mm), TR (32ms), TE (4.9ms), Flip Angle (30^0), Average (3), Base resolution (256), Phase resolution (80%) Matrix (141x256), Voxel (0.7x0.5x6mm). These sequences were performed 10mm below the lowest renal artery at 5 positions that were 6mm apart.

MRI assessment of endothelial function

After acquiring baseline images, ACh (0.5µg/kg/min) was infused for 2mins to reach steady state prior to imaging. The infusion was continued for the duration of the scan. GTN (3µg/kg/min) was then infused for 2mins and the sequences repeated. Each imaging sequence performed took ~10mins (dependent on the quality of ECG signal). ACh and GTN were delivered using a Gemini PC-2 (IMED Corporation, San Diego, CA) infusion pump from the MRI control room, via an infusion set connected to extension tubing that was passed through the waveguide into the MRI room and connected to the ear vein cannula. Prior to connecting the infusion line to the rabbit the ear vein cannula was flushed with saline using a MR safe syringe to ensure vessel patency.

MRI Image analysis

The MRI images were transferred to PC for offline analysis using QMass 7.2 (Medis Medical Imaging Systems, Leiden, Netherlands). For each position along the aorta the phase representing end diastole (ED) was selected and luminal contours were manually traced to determine luminal cross-sectional area (CSA). Vasomotor responses in response to ACh and GTN were reported as a %Δ from baseline.

Intra-inter observer variability

To assess intra-observer variability of both IVUS and MRI measurements a subset of the data was analysed on two separate occasions at least one month apart. To assess inter-observer variability of both IVUS and MRI measurements a subset of the data was analysed by another observer (AC).

Statistical analysis

Values are expressed as mean ± standard deviation. Paired t-tests were used to compare IVUS and MRI measurements at baseline and 3 months. Intra- and inter-observer agreements were assessed using linear regression and intraclass correlation coefficients (ICC). Bland-Altman analysis was conducted with mean bias, standard deviation and 95% limits of agreement calculated. A p value of <0.05 was considered statistically significant. Statistical analysis was performed with GraphPad Prism 6.03 (Graph Pad Software Inc, San Diego, CA) and SPSS 20 (SPSS Inc, Chicago, IL, USA).

RESULTS

Baseline imaging and endothelial function assessment was successfully performed on 20 animals using both IVUS and MRI systems. Imaging and endothelial function assessments were successfully repeated on 15 animals 3 months following atherosclerosis initiation by balloon denudation and high cholesterol feeding.

Endothelial function

At baseline the mean lumen CSA measured by IVUS and MRI was 7.98±1.85mm^2 and 8.20 ±1.02mm^2 respectively. Following the infusion of ACh the lumen CSA increased to 8.7±0.88mm^2 (IVUS) and 8.62±0.91 mm^2 (MRI). ACh induced a significant vasodilation from baseline 8.8% ($p<0.0001$) (IVUS), 8.0% ($p<0.0011$) (MRI). Following the infusion of GTN the lumen CSA increased to 9.24±0.91 mm^2 (IVUS) and 9.11±0.77 mm^2 (MRI). GTN induced further vasodilation of 15.84% ($p<0.009$) (IVUS) and 14.24% ($p<0.0038$) (MRI).

At 3 months disease progression the mean lumen CSA at baseline measured by IVUS and MRI was 8.04±1.04mm^2 and 8.27±1.55mm^2 respectively. There was no significant difference between baseline lumen CSA measured at baseline and 3 months ($p=0.915$) (IVUS), ($p=0.69$) (MRI).

Following the infusion of ACh the lumen CSA increased to 8.34±1.9mm^2 (IVUS) and 8.4±0.16 mm^2 (MRI). ACh induced an attenuated vasodilatory response which was not significantly different from baseline 5.19% ($p=0.14$) (IVUS), 2.81% ($p=0.5$) (MRI). Following the infusion of GTN the lumen CSA increased to 9.31±1.32 mm^2 (IVUS) and 9.6±1.62 mm^2 (MRI). GTN induced significant

vasodilation of 20.57% ($p<0.04$) (IVUS) and 19.01% ($p<0.03$) (MRI). There was no significant difference observed between the response to GTN at baseline and 3 months ($p=0.84$) (IVUS), ($p=0.24$) (MRI).

	Baseline (n=20)			**3 Month Atherosclerosis (n=15)**		
Infusion	IVUS CSA mm^2	MRI CSA mm^2	p value	IVUS CSA mm^2	MRI CSA mm^2	p value
BL	8.04±1.04	8.03 ±1.02	NS 0.86	7.98±1.85	8.27±1.55	NS 0.09
ACh	8.70±0.88	8.62±0.91	NS 0.35	8.34±1.9	8.40±1.6	NS 0.68
GTN	9.24±0.91	9.11±0.77	NS 0.17	9.31±1.32	9.60±1.62	NS 0.15

Table 1. Comparison of aortic lumen CSA measured by IVUS and MRI in animals at baseline and following 3 months disease progression. p values of paired t-test analysis between IVUS and MRI (NS = not significant $p>0.05$).

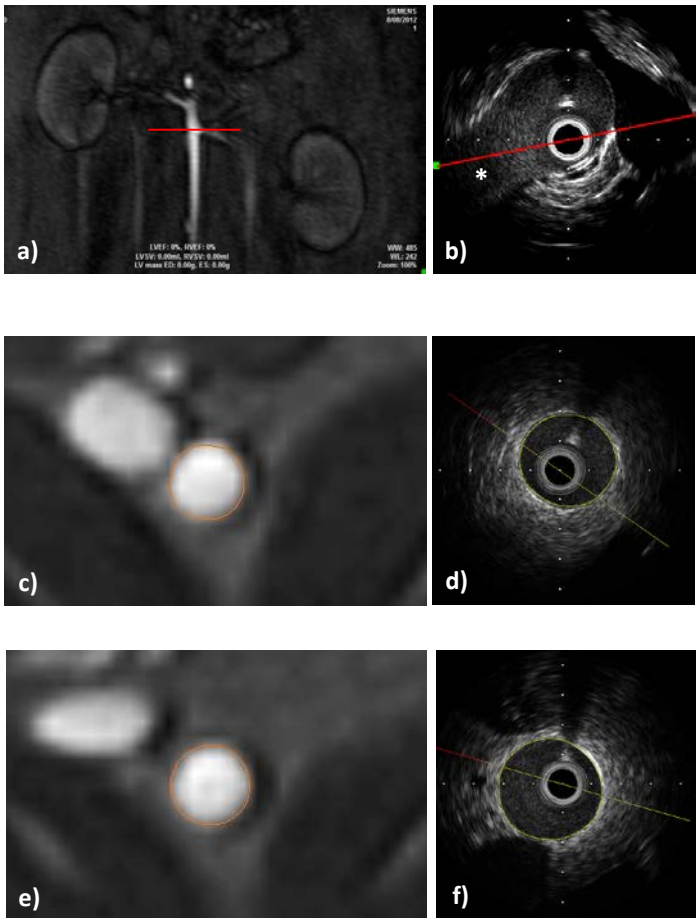

Figure 1. 1.5T MRI and 40MHz IVUS images (a, b) co-registration of MRI and IVUS images, a) coronal localiser sequence, red line indicates the renal artery b) the corresponding IVUS image * indicates the renal artery branching into to abdominal aorta. (c, d) corresponding MRI and IVUS images at baseline and (e, f) following GTN infusions.

Correlation between IVUS and MRI

The reported lumen CSA at baseline and following infusion of ACh and GTN at both baseline and 3 month time-points were very similar for both IVUS and MRI (Table 1). There were no significant differences between IVUS and MRI reported CSA at any points (Table 1). Correlation between IVUS and MRI at baseline was very strong in baseline animals (r^2 =0.94, ICC = 0.97, p<0.0001) and strong following ACh and GTN infusions (r^2=0.86, ICC = 0.92, p<0.0001), (r^2= 0.82, ICC = 0.89, p<0.0001) respectively. Bland-Altman analysis supported the high level of agreement and revealed a trend that IVUS reported slightly greater lumen CSA than MRI (Figure 2).

At the 3 month follow up the correlation between IVUS and MRI at baseline and following ACh infusions remained very strong (r^2 = 0.94, ICC = 0.95, p<0.0001) (r^2 = 0.94, ICC = 0.95, p<0.0001) respectively and strong following GTN infusions (r^2=0.8, ICC = 0.86, p<0.0001). Bland-Altman analysis supported the high level of agreement and revealed a trend that MRI reported slightly greater lumen CSA than IVUS (Figure 3).

Intra-inter observer variability

Intra-observer agreement was excellent for IVUS (r^2=0.9, ICC=0.98, p<0.0001) and very good for MRI (r^2=0.84, ICC=0.91, p<0.0001) measurements. Bland-Altman analysis supported the high level of intra-observer agreement for both IVUS and MRI measurements (Figure 4).

Inter-observer agreement was very good for both IVUS (r^2=0.86, ICC=0.94, $p<0.0001$) and MRI (r^2=0.84, ICC=0.91, $p<0.0001$) measurements. Bland-Altman analysis supported the high level of inter-observer agreement and revealed a trend that one observer reported slightly greater lumen CSA in both IVUS and MRI measurements (Figure 5).

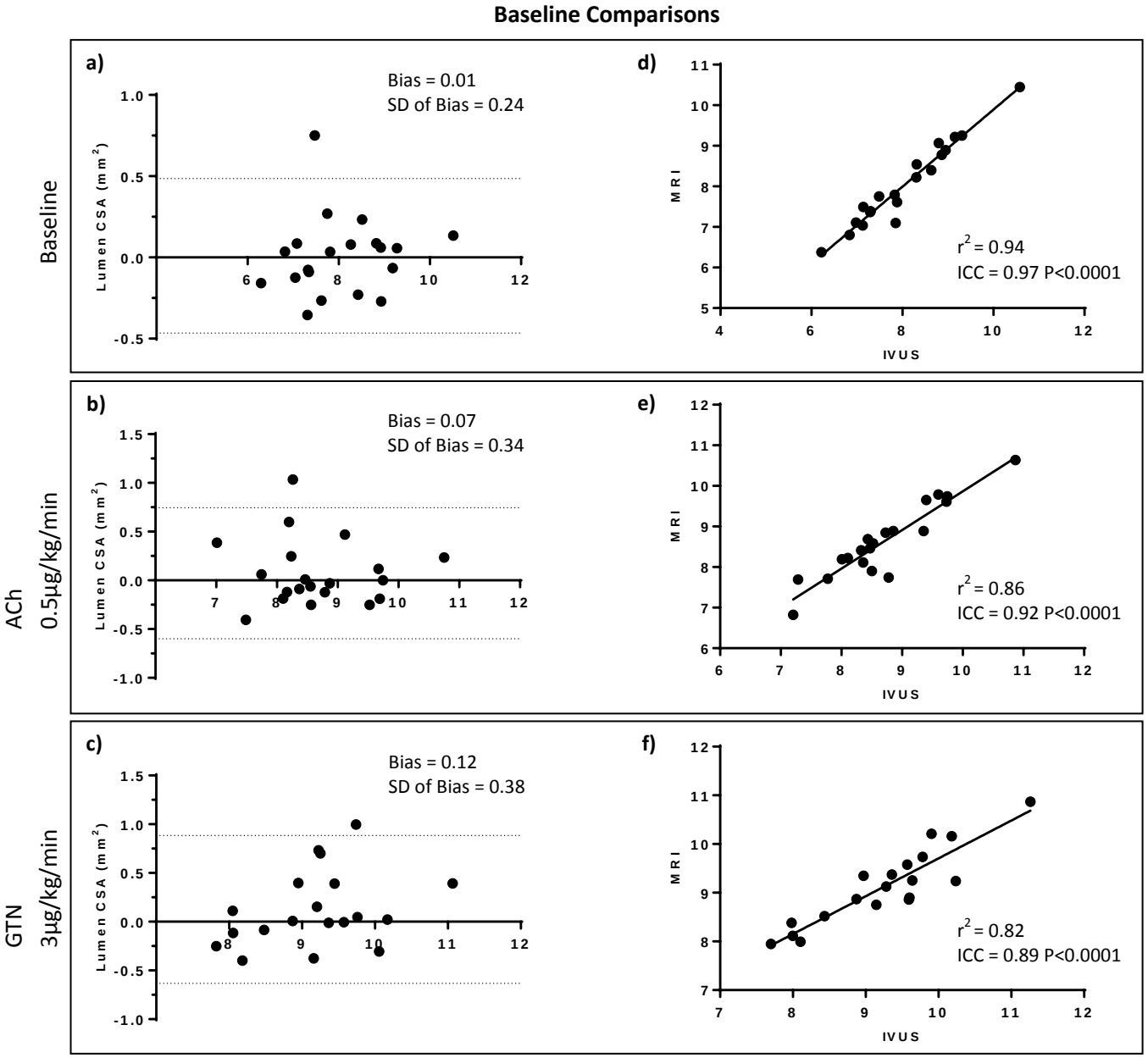

Figure 2.Correlation between MRI and IVUS measurements at baseline and following infusions of Acetylcholine and GTN in disease free animals. Linear correlation chart with regression line (d, e, f) with correlation r^2 value and intraclass correlation coefficient (ICC) and corresponding Bland-Altman plots (a, b, c) with 95% limits of agreement displayed.

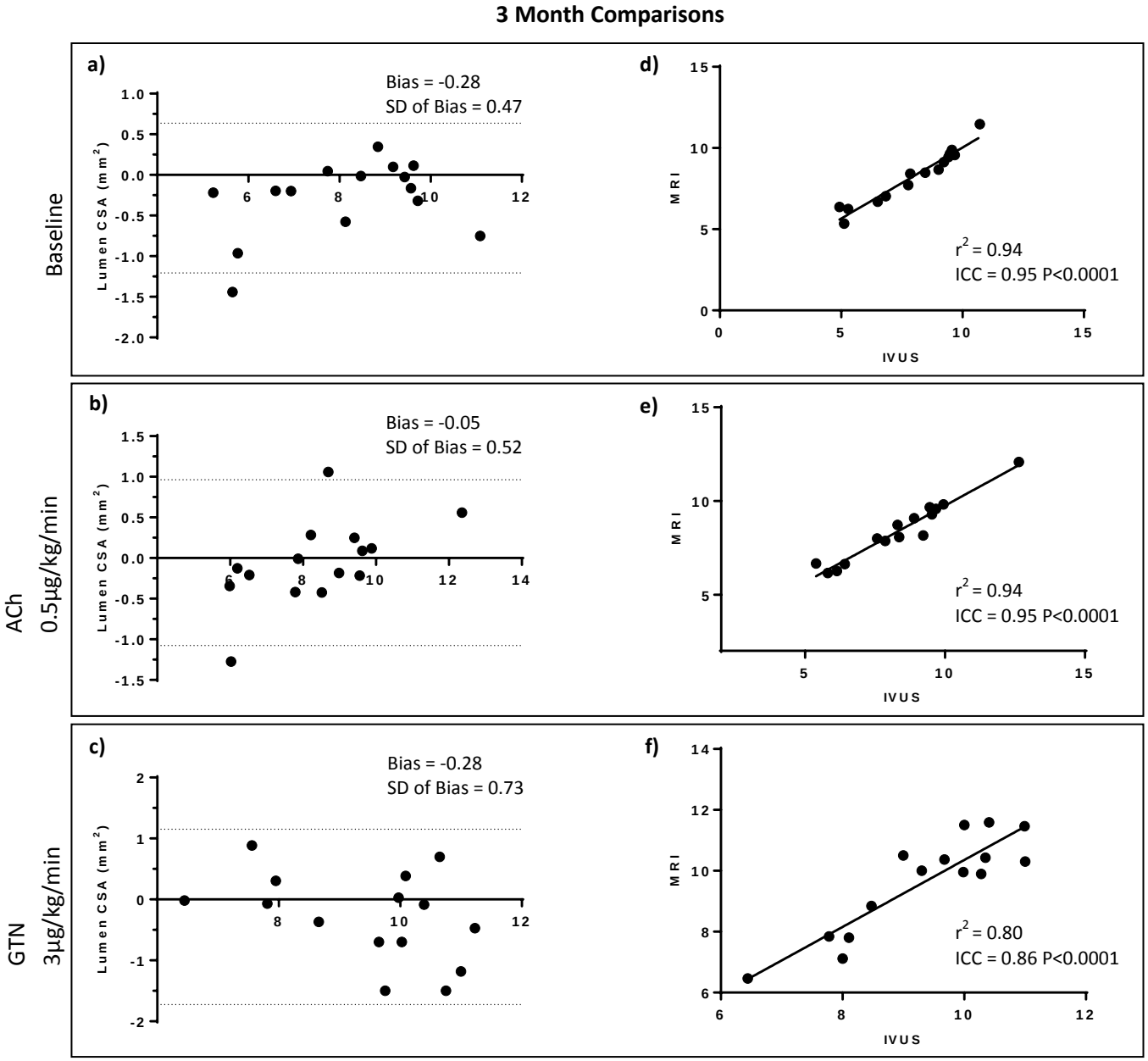

Figure 3. Correlation between MRI and IVUS measurements at baseline and following infusions of Acetylcholine and GTN 3 months disease progression. Linear correlation chart with regression line (d, e, f) with correlation r^2 value and intraclass correlation coefficient (ICC) and corresponding Bland-Altman plots (a, b, c) with 95% limits of agreement displayed.

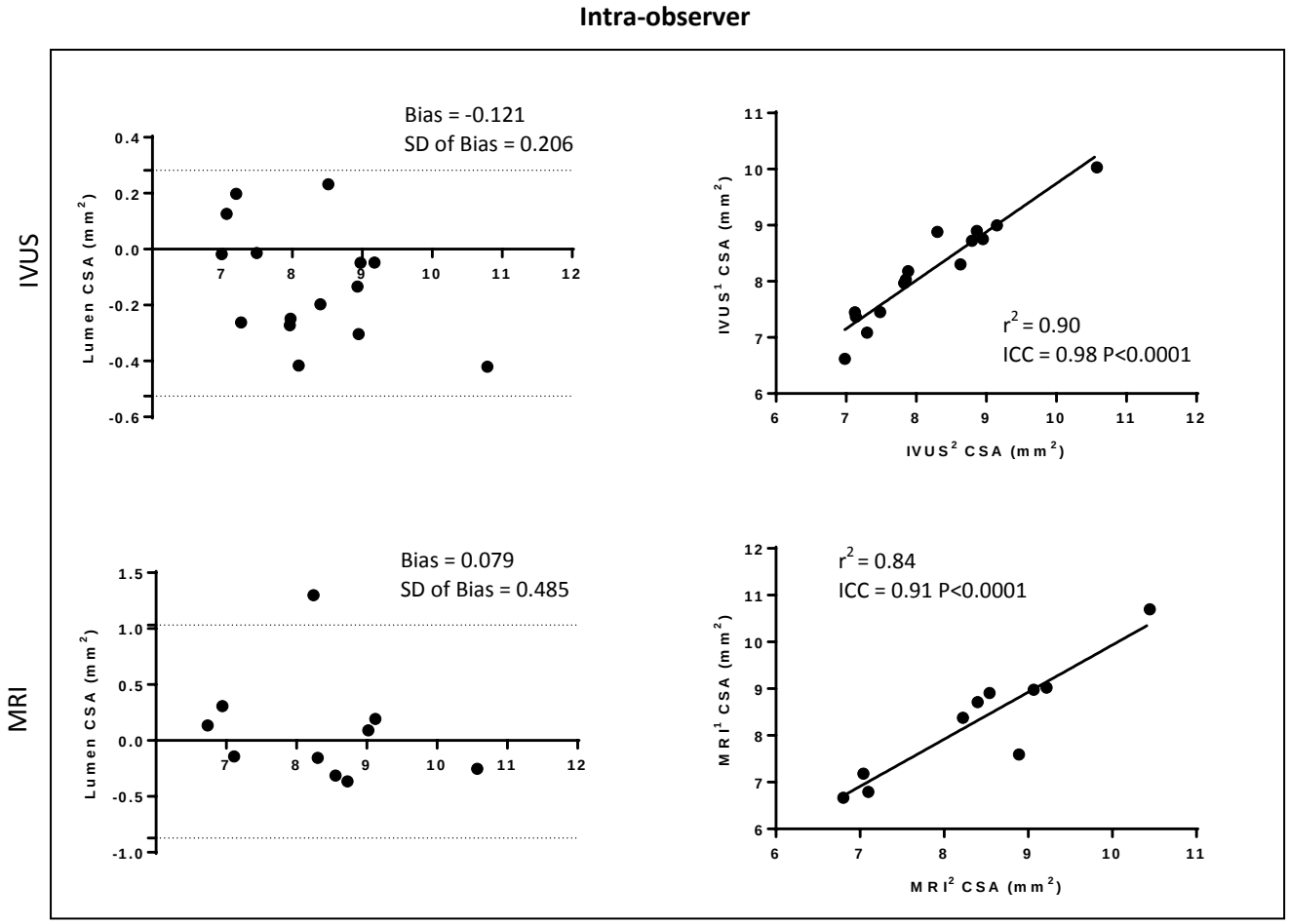

Figure 4. Intra-observer variability for IVUS and MRI. Linear correlation chart with regression line (b, c) with correlation r^2 value and intraclass correlation coefficient (ICC) and corresponding Bland-Altman plots (a, b,) with 95% limits of agreement displayed.

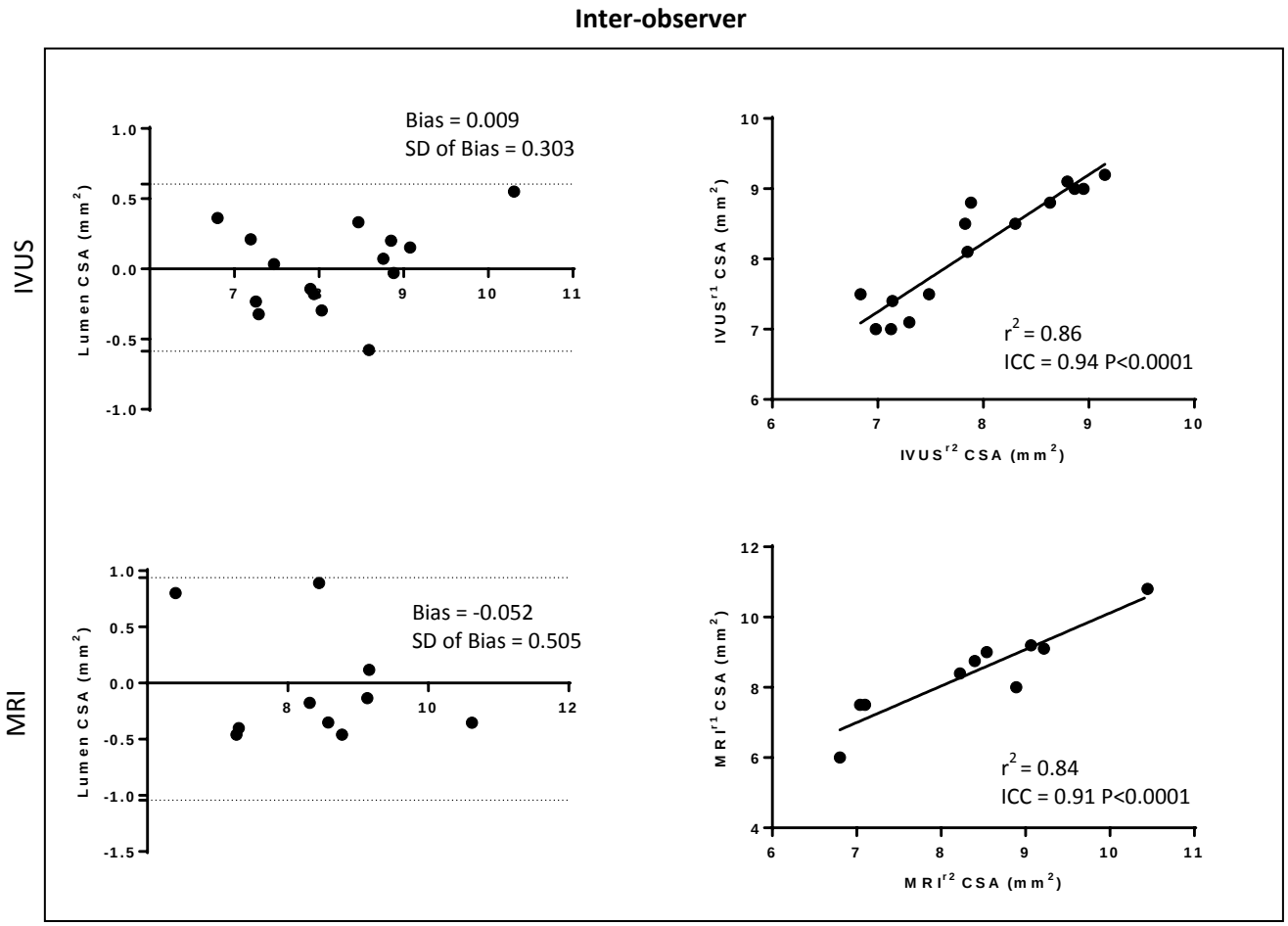

Figure 5. Inter-observer variability for IVUS and MRI. Linear correlation chart with regression line (b, c) with correlation r^2 value and intraclass correlation coefficient (ICC) and corresponding Bland-Altman plots (a, b,) with 95% limits of agreement displayed.

DISCUSSION

In this study we have utilised a 1.5T MRI scanner to develop a non-invasive endothelial function test in the rabbit aortic model of atherosclerosis. The endothelial function test was replicated using 40MHz IVUS as a comparison. We believe this is the first time that MRI has been utilised as a tool to assess endothelial function in the rabbit model. The comparisons between IVUS and MRI were made in disease free animals and repeated 3 months following initiation of atherosclerosis by balloon denudation of the aorta and high cholesterol feeding.

The high levels of reproducibility for both inter/intra observer assessment of MRI vasomotion indicates that it is a reliable method for performing non-invasive endothelial assessments in the rabbit aorta. This suggests that the method is as accurate as the invasive IVUS method in assessing vasomotor responses in small calibre vessels. The high levels of agreement were preserved at the 3 month follow up which indicates that the MRI methodology is robust enough to be used in a diseased state.

Using MRI as a non-invasive technique for assessing endothelial function allows researchers to observe the dynamic progression/regression of the disease in the same animal. MRI unlike other non-invasive methods for assessing endothelial function such as ultrasound is limited to only functional measurements due to its lower resolution as MRI can also analyse the morphology of the vessel wall, providing both structural and functional data. The potential of MRI to combine these two factors in a serial fashion will provide greater insight into the atherosclerosis progression and monitor therapeutic interventions.

This study only included one dose of ACh for the MRI protocol, however when performing endothelial function assessments a dose response is generated, compared to a protocol for another study using IVUS to assess endothelial function we include 3 incremental dosages of ACh in addition to the GTN. The study has shown that MRI was able to detect small changes with accuracy comparable to IVUS and the method could be adapted to include other doses.

CONCLUSION

We have developed a reliable method for non-invasive endothelial function testing using a 1.5T MRI scanner. By using the renal artery as a fiduciary marker these can be perform serially allowing comparison of the same positions of the aorta over time. MRI is a viable non-invasive modality for assessing luminal CSA changes in very small calibre vessels in response to vasoactive drugs.

REFERENCES

1. Davignon J, Ganz P. Role of Endothelial Dysfunction in Atherosclerosis. Circulation 2004;109:27-32.

2. Luscher T, Barton M. Biology of the Endothelium. Clinical Cardiology 1997;20:3-10.

3. Verma S, Anderson T. Fundamentals of Endothelail Function for the Clinical Cardiologist. Circulation 2011;105:546-9.

4. Schächinger V, Britten M, Zeiher A. Prognostic Impact of Coronary Vasodilator Dysfunction on Adverse Long-Term Outcome of Coronary Heart Disease. Circulation 2000;101:1899-906.

5. Deanfield J, Halcox J, Rabelink T. Endothelial Function and Dysfunction: Testing and Clinical Relevance. Circulation 2007;115:1285-95.

6. Ludmer P, Selwyn A, Shook T, et al. Paradoxical Vasoconstriction Induced by Acetylcholine in Atherosclerotic Coronary Arteries. New England Journal of Medicine 1986;17:1046-51.

7. Cox D, Vita J, Treasure C, et al. Atherosclerosis Impairs Flow-Mediated Dilation of Coronary Arteries in Humans. Circulation 1989;80:458-65.

8. Mills R, Billet J, Nichols W. Endothelial Dysfunction Early After Heart Transplantation. Assessment with Intravascular Ultrasound and Doppler. Circulation 1992;86:1171-4.

9. Furchgott R. Endothelium-Derived Relaxing Factor: Discovery, Early Studies, and Identification as Nitric Oxide. Bioscience Reports 1998;19:235-51.

10. Furchgott R, Zawadzki J. The Obligatory Role of Endothelial Cells in the Relaxation of Arterial Smooth Muscle by Acetylcholine. Nature 1980;288:373-6.

11. Tousoulis D, Antoniades C, Stefanadis C. Evaluating Endothelial Function in Humans: A Guide to Invasive and Non-Invasive Techniques. Heart 2005;91:553-8.

12. Anderson T, Uehata A, Gerhard M, et al. Close Relation of Endothelial Function in the Human Coronary and Peripheral Circulations. Journal of the American College of Cardiology 1995;26:1235-41.

Chapter 7:

SERIAL QUANTIFICATION OF ATHEROSCLEROSIS WITH 1.5T MRI COMPARED TO 40MHz IVUS

TABLE OF CONTENTS

INTRODUCTION

Serial imaging of coronary arteries allows for the monitoring of plaque progression and the possibility of identifying vulnerable plaque prior to developing acute coronary syndrome (ACS). There is a need for an imaging modality that is safe, non-invasive or minimally invasive, accurate and reproducible that would allow for multiple imaging of the same segment of coronary artery over time. Currently there is no one imaging modality that meets all these criteria[1].

Intravascular Ultrasound (IVUS) has established itself as the gold standard of vascular imaging[2]. IVUS imaging provides a high resolution tomographic imaging of the vessel wall and lumen. However it is an invasive imaging modality and has limited usefulness for serial imaging[3].

MRI is a non-invasive imaging platform that provides excellent soft-tissue contrast, visualisation of blood and vessel wall. MRI has the ability to assess coronary lumen and plaque burden and composition. MRI is currently used clinically for assessment of carotid atherosclerosis [4,5]. In this study we compared non-invasive 1.5T MRI against 40MHz IVUS for the serial quantification of atherosclerosis in the experimental rabbit model of atherosclerosis.

METHODS

All procedures were approved by the University of Adelaide Animal Ethics Committee and the Institute of Medical and Veterinary Science (IMVS) Animal Ethics Committee (M-2011-031; 17/11). New Zealand White rabbits (n=30) fed an atherogenic diet (0.2% cholesterol) that were part of an ongoing study were used. All animals underwent imaging of the abdominal aorta with 40MHz IVUS and 1.5T MRI at baseline and 3, 6, 9 month disease progression.

IVUS Imaging protocol

IVUS imaging and endothelial function assessment of the rabbit abdominal aorta was performed using the iLab imaging console and 40MHz Atlantis SR Pro catheters (Boston Scientific, Natick, MA, USA) at baseline and 3 months (n=10), 6 months (n=8) and 9 months (n=8) of disease progression. Anaesthesia was induced with 25mg/kg Ketamine (Ketamine Hydrochloride, Fort Dodge Animal Health, Fort Dodge, USA) and maintained with 1% Isoflurane in 4L/min O_2 (Isoflurane, Bomac Animal Health, NSW, Australia). The femoral artery was identified and cannulated with a 24 gauge cannula through which a 0.014” guidewire was introduced and advanced to the aortic arch. The IVUS catheter was guided via fluoroscopy (Phillips BV-24) to the lowest branch of the renal artery and IVUS catheter placement was confirmed by manual imaging. Automatic pullbacks were performed (0. 5mm/s) for a length 75cm.

MRI Imaging protocol

MRI imaging was performed using a 1.5T Siemens MAGNETOM Sonata system and a human knee coil (Siemens Medical Solutions, Erlangen, Germany). The rabbits were placed in the supine position in the isocentre of the scanner; anaesthesia was maintained with Isoflurane (1% in 4L/min O_2) delivered via nosecone for the duration of the scan.

ECG independent Proton Density Weighted (PDW) sequences with fat saturation were performed. 20 sequential axial images were generated every 5mm from the renal arteries. The imaging sequence parameters were: TR (2000ms), TE (11ms), Slice Thickness (3mm), Field of view (9x9cm), Matrix (256x256), Echo train length (9), Flip angle (180^o), Average (4).

MRI Image analysis

The MRI images were transferred to hard disk drive for offline analysis using QMass 7.2 (Medis Medical Imaging Systems, Leiden, Netherlands). For each position along the aorta a phase representing end diastole (ED) was selected and luminal and vessel contours were manually traced to determine areas. Vessel wall area (VWA) was defined as the area occupied between luminal and EEM contours.

IVUS Image analysis

IVUS images were transferred to hard disk drive for offline analysis using echoPlaque 3 (Indec Medical Systems, Santa Clara, USA). The renal artery branches were identified from which the corresponding sections of aorta to MRI were identified.

Frames representing end diastole (ED) were selected and luminal contours were manually traced to determine luminal cross-sectional area (CSA). The leading edge of the lumen and external elastic membrane (EEM) were traced by manual planimetry. Vessel wall area (VWA) was defined as the area occupied between luminal and EEM contours.

Statistical analysis

Values are expressed as mean ± standard deviation. Groups were compared using paired t-tests, correlation between IVUS and MRI measurements. Intra- and inter-observer agreements were assessed using linear regression and intraclass correlation coefficients (ICC). Bland-Altman analysis was conducted with mean bias, standard deviation and 95% limits of agreement calculated. A p value of <0.05 was considered statistically significant. Statistical analysis was performed with GraphPad Prism 6.03 (Graph Pad Software Inc, San Diego, CA) and SPSS 20 (SPSS Inc, Chicago, IL, USA).

RESULTS

Serial imaging of the abdominal aorta was successfully performed on 30 animals using both 40 MHz IVUS and 1.5T MRI systems. Imaging was performed at baseline and then 3, 6, 9 months following atherosclerosis initiation by balloon denudation and high cholesterol feeding.

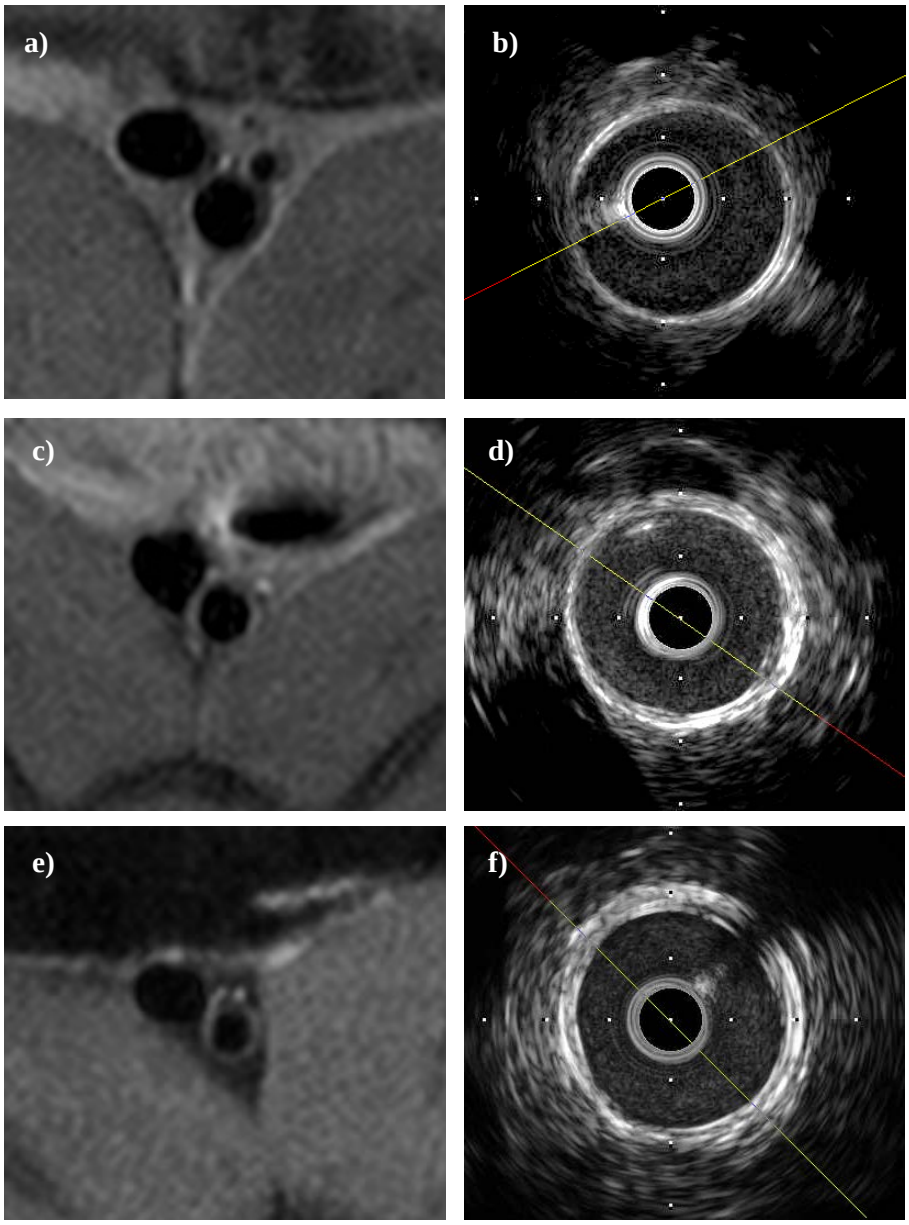

Figure 1. Comparison of 1.5T MRI and 40MHz IVUS images. (a,b) 3 Months. (c,d) 6 Months. (e,f) 9 Months

Baseline	IVUS	MRI	p-value
Lumen (mm^2)	7.83±0.66	7.79±0.83	0.8
Vessel (mm^2)	9.41±0.93	9.81±1.13	$p<0.05$
VWA (mm^2)	1.78±0.47	2.05±0.51	$p<0.02$

Table 1. MRI and IVUS comparisons at Baseline. There was no significant difference between lumen CSA reported by (p=0.8). There was a small but significant difference between IVUS and MRI reported values for both vessel CSA ($p<0.05$) and VWA ($p<0.02$). (n=10)

3 Months	IVUS	MRI	p-value
Lumen (mm^2)	8.65±1.11	8.86±0.83	0.22
Vessel (mm^2)	10.59±0.77	10.87±1.58	0.41
VWA (mm^2)	1.85±0.15	2.28±0.28	0.12

Table 2. MRI and IVUS comparisons at 3 Months. There was no significant difference between Lumen CSA (p=0.22), Vessel CSA (p=0.41) or VWA (p=0.12). (n=10)

6 Months	IVUS	MRI	p-value
Lumen (mm^2)	8.97±0.38	8.87±0.42	0.22
Vessel (mm^2)	12.28±0.85	12.33±1.36	0.86
VWA (mm^2)	3.30±0.74	3.29±0.7	0.59

Table 3. MRI and IVUS comparisons at 6 Months. There was no significant difference between Lumen CSA (p=0.22), Vessel CSA (p=0.86) or VWA (p=0.59). (n=10)

9 Months	IVUS	MRI	p-value
Lumen (mm^2)	9.04±0.98	9.27±1.15	0.12
Vessel (mm^2)	12.91±1.8	13.64±1.34	0.06
VWA (mm^2)	4.48±0.36	4.82±0.53	0.21

Table 4. MRI and IVUS comparisons at 9 Months. There was no significant difference between Lumen CSA (p=0.12), Vessel CSA (p=0.06) or VWA (p=0.21). (n=10)

Pooled comparisons

IVUS and MRI data was pooled across all time-points for analysis (Table 5). There was no significant difference between lumen CSA reported by IVUS 8.61±0.95mm^2 and MRI 8.6±1.10mm^2 (p=0.75). There was no significant difference between vessel CSA reported by IVUS 11.27±1.83 mm^2 and MRI 11.65±2.0mm^2 (p=0.39). There was no significant difference between VWA reported by IVUS 2.77±1.23mm^{2}and MRI 3.12±1.26mm^2 (p=0.22). Correlations between IVUS and MRI reported values were very strong for lumen CSA (r^2 =0.81, ICC = 0.9, p<0.0001), vessel CSA (r^2 =0.81, ICC = 0.89, p<0.0001) and VWA (r^2 =0.81, ICC = 0.93, p<0.0001) (Figure 5). Bland-Altman analysis supported the high level of agreement and revealed a trend that MRI reported slightly greater vessel CSA and subsequently VWA values than IVUS.

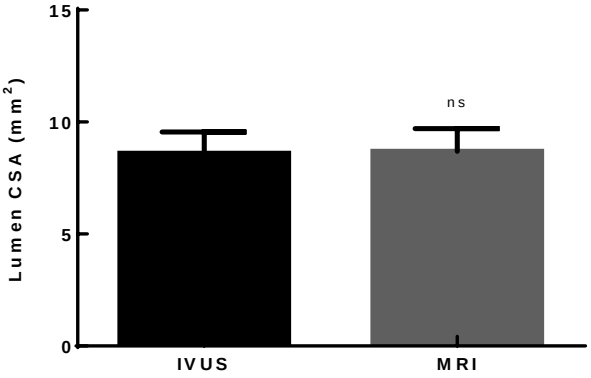

Figure 2. Mean lumen CSA measured by IVUS and MRI.

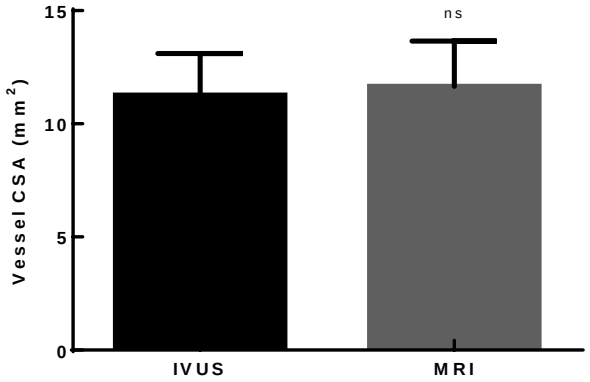

Figure 3. Mean vessel CSA measured by IVUS and MRI.

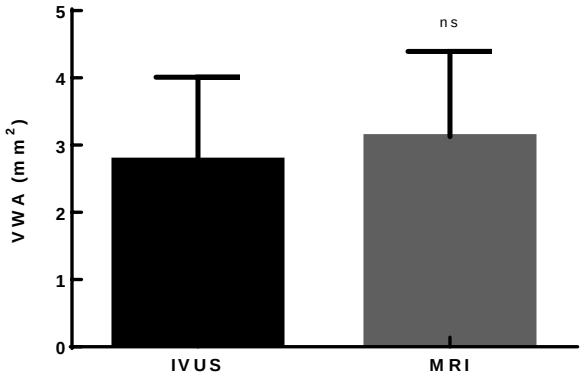

Figure 4. Mean PAV measured by IVUS and MRI.

	IVUS	MRI	p-value
Lumen (mm^2)	8.61±0.95	8.6±1.10	0.75
Vessel (mm^2)	11.27±1.83	11.65±2.0	0.39
VWA (mm^2)	2.77±1.23	3.12±1.26	0.22

Table 5. Comparison of pooled IVUS and MRI derived measurements. Data pooled across all time-points. There was no significant difference between Lumen CSA (p=0.75), Vessel CSA (p=0.39) or VWA (p=0.22). (n=30)

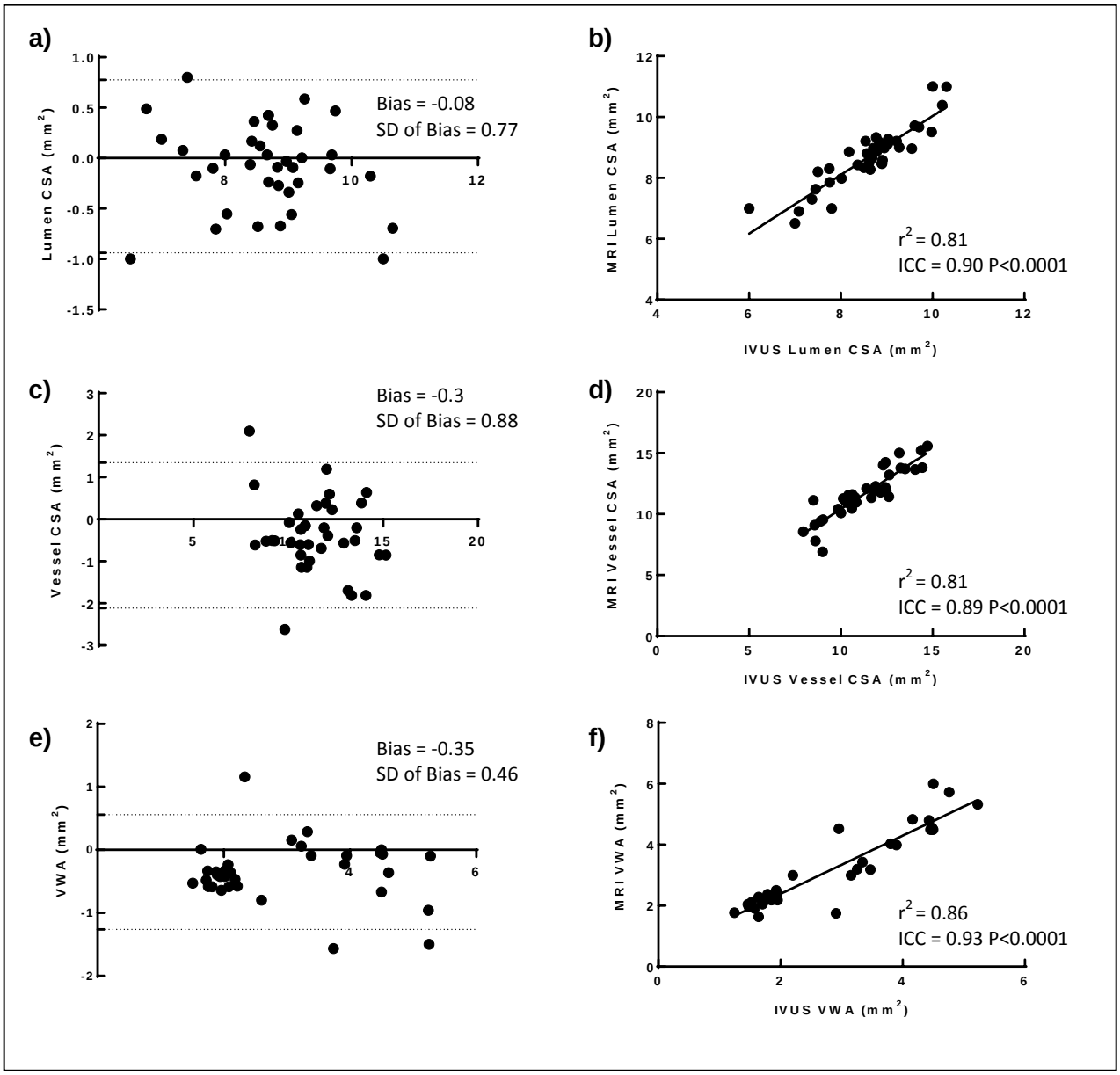

Figure 5. Correlation between pooled MRI and IVUS measurements. Linear correlation chart with regression line with correlation r^2 value and intraclass correlation coefficient (ICC) and corresponding Bland-Altman plots with 95% limits of agreement displayed. (a,b) Lumen CSA, (c,d) Vessel, (e,f) VWA.

Intra-inter observer variability

Intra-observer agreement was excellent for IVUS (r^2=0.9, ICC=0.98, p<0.0001) and very good for MRI (r^2=0.80, ICC=0.88, p<0.001). Inter-observer agreement was very good for both IVUS (r^2=0.86, ICC=0.94, p<0.0001) and MRI (r^2=0.84, ICC=0.90, p<0.0001).

DISCUSSION

MRI and IVUS both offer the potential of in-vivo monitoring of the same lesion over time. This study was performed to compare the usefulness of IVUS and MRI for the serial quantification of atherosclerotic lesions in the rabbit model of disease

Utilising a similar animal model to this current student Yuan et al[6], using a custom designed volume phased array coil, reported that PDW weighted images have the highest overall contrast between tissue components and provided optimum differentiation between vessel wall, lumen and background, compared to T1 and T2 weighted images. Manninen et al[7] performed a similar study imaging the rabbit carotid artery with 30MHz IVUS and 1.5T MRI utilising T1 and T2 weighted spin echo sequences. This was a relatively small study (n=7) and only involved one imaging time-point (5 weeks). They reported comparable measurements of mean plaque area and thickness between IVUS and MRI. Similarly Chiesa et al [8] utilised a 2T and scanner and weighted T1 spin echo sequences and reported an excellent correlation ($r=0.969$, $p<0.0014$) between MRI and 30MHz IVUS. These studies however only provide comparison against IVUS at one time-point.

MRI has been utilised to serially image plaque composition in the rabbit model. Skinner et al[9] study focused on comparing plaque components to histology rather than accuracy of measurements using two-dimensional TOF MRI to serially monitor the progression of rabbit abdominal aortic plaques 9-16 months. A similar study was performed by Helft[10] to document changes in plaque size and composition in response to dietary modification. Worthley et al[11] utilised MRI to serially monitor arterial remodelling. These studies made comparisons against histology and not against other imaging platforms. In this study we did not

compare IVUS or MRI against histological measurements this was due to the immersion fixation method and as a result would have undergone significant shrinkage.

A small but significant difference in vessel and VWA measurements was observed at baseline (Table 1.). This may be attributed to an overestimation of the vessel contour when performing MRI analysis as there was no significant difference observed in luminal measurements at the same time-point. No significant difference was observed at the 3 month follow up.

MRI allows for more imaging time-points than invasive, not introducing variables and lower risk to animals (such as complications during procedure and post-operative infection). In our IVUS experience it was possible to interrogate the same vessel following a 3months interval; however it could not be performed in every case and had a greater difficulty with more complications.

CONCLUSION

MRI quantification of atherosclerotic burden correlated well with IVUS across all time-points. MRI is a feasible non-invasive alternative for imaging atherosclerosis in the experimental rabbit model.

REFERENCES

1. Celermajer D, Sorensen K, Gooch V, et al. Non-Invasive Detection of Endothelial Dysfunction in Children and Adults at Risk of Atherosclerosis. The Lancet 1992;340:1111-5.

2. Nissen S. Application of Intravascular Ultrasound to Characterize Coronary Artery Disease and Assess the Progression or Regression of Atherosclerosis. The American Journal of Cardiology 2002;89:24-31.

3. Nicholls S, Sipahi I, Schoenhagen P, Crowe T, Tuzcu E, Nissen S. Application of Intravascular Ultrasound in Anti-Atherosclerotic Drug Development. Nature REviews Drug Discovery 2006;5:458-92.

4. Cai J, Hatsukami T, Ferguson M, Small R, Polissar N, Yuan C. Classification of Human Carotid Atherosclerotic Lesions with In Vivo Multicontrast Magnetic Resonance Imaging. Circulation 2002;106:1368-73.

5. Yuan C, Kerwin W, Ferguson M, et al. Contrast-Enhanced High Resolution MRI for Atherosclerotic Carotid Artery Tissue Characterisation. Journal of Magnetic Resonance Imaging 2002;15:62-7.

6. Yuan C, Skinner M, Kaneko E, et al. Magnetic Resonance Imaging to Study Lesions of Atherosclerosis in the Hyperlipidemic Rabbit Aorta. Magnetic Resonance Imaging 1996;14:93-102.

7. Manninen H, Vanninen R, Laitinen M, et al. Intravascular Ultrasound and Magnetic Resonance Imaging in the Assessmnet of Atherosclerotic Lesions in Rabbit Aorta: Correlation to Histopathologic Findings. Investigative Radiology 1998;33:464-71.

8. Chiesa G, Rigamonti E, Monteggia E, et al. Evaluation of A Soft Atherosclerotic Lesion in the Rabbit Aorta by an Invasive IVUS Method Versus a Non-Invasive MRI Technology. Atherosclerosis 2004;174:25-33.

9. Skinner M, Yuan C, Mitsumori L, et al. Serial Magnetic Resonance Imaging of Experimental Atherosclerosis Detects Lesion Fine Structure, Progression and Complications In Vivo. Nature 1995;1:69-73.

10. Helft G, Worthely S, Fuster V, et al. Progression and Regression of Atherosclerotic Lesions: Monitoring with Serial Noninvasive Magnetic Resonance Imaging. Circulation 2002;105:993-8.

11. Worthley S, Helft G, Fuster V, et al. Serial In Vivo MRI Documents Aretrial Remodeling in Experimental Atherosclerosis. Circulation 2000;101:586-9.

Chapter 8:

DISCUSSION

In this thesis we have investigated the application of IVUS and MRI for serial imaging of atherosclerotic plaque burden and assessment of endothelial function. The studies generally utilised the rabbit hypercholesterolaemia balloon denudation model of atherosclerosis, which has previously been utilised for MRI and IVUS studies.

The studies performed in this thesis aimed to:

- Compare the variation in measurements obtained with mechanical and phased-array catheters in both an in-vivo and in-vitro setting.
- Investigate the accuracies of VH-IVUS and iMap in quantifying individual plaque components.
- Investigate the relationship between the progression of atherosclerosis and endothelial dysfunction.
- Assess the feasibility of MRI as a non-invasive imaging alternative to IVUS in both the assessment of plaque quantification and the progression of endothelial dysfunction.

In chapter 3 we compared the accuracy of mechanical and phased array IVUS catheters. A custom built phantom was constructed to assess in-vitro accuracy as well as imaging the rabbit aorta to provide a head to head in-vivo comparison. All three catheters utilised in the in-vitro study overestimated the known phantom CSA. In-vivo the 20MHz phased-array catheters reported higher vessel CSA than the 40MHz mechanical catheters this has implications for serial clinical studies where both systems could be utilised.

In chapter 4 we utilised two state-of-the-art plaque characterisation platforms, VH-IVUS and iMap. This study was the first to compare these two systems directly in-vivo in addition to comparisons against histology. The results of this study supported finding from previous studies about the inaccuracies of these platforms. We demonstrated that both systems had reported consistently significantly different values for every individual plaque component. Our analysis revealed a poor correlation between iMap and histology reported values for fibrotic and lipidic areas, these being the only two values where a non-significant difference was found.

In chapter 5 we utilised serial IVUS imaging over a period of 9 months to document the progression of atherosclerosis and the subsequent changes in endothelial function. The results revealed the rabbit aorta undergoes remodelling analogous to positive remodelling observed clinically in early atherosclerosis. It also revealed the relationship between progressive endothelial dysfunction with increasing plaque burden.

In chapter 6 we explored the application of non-invasive MRI this time however we investigated the use of MRI as a tool to investigate endothelial function. We developed a procedure using white-blood cine imaging and a similar infusion protocol used in our IVUS analysis. The methodology was applied to animals at baseline and 3 months post atherosclerosis induction. MRI was able to detect these small changes in vasomotor responses in the small calibre rabbit abdominal aorta.

In chapter 7 we investigated the feasibility of non-invasive MRI imaging of serial plaque quantification compared against the gold standard of IVUS. This study followed previous studies that have investigated the application of MRI in quantifying atherosclerosis in the experimental rabbit model. However this study was the first to draw comparisons between MRI and IVUS at a number of time-points, instead of relying on comparisons against histologically derived measurements.

The studies performed in this thesis compared invasive and non-invasive imaging platforms for the analysis of atherosclerosis and the endothelial function. We have demonstrated that 1.5T MRI is a feasible alternative to IVUS in this experimental model of atherosclerosis for the imaging of plaque burden and the assessment of endothelial function. We have shown that plaque characterisation systems VH-IVUS and iMap are not currently reliable as an experimental research tool.

Future directions resulting from this study could possibly include further comparisons between VH-IVUS and iMap in a clinical setting. The comparison between the two and against histology has not yet been performed; this could be achieved by the imaging of coronary artery in a diseased heart in patients who are undergoing cardiac transplant. Other comparisons could be investigated with the application of other plaque characterisation platforms such as NIRS.